Modeling and Experimental Behavior Studies on Tin Whiskers

By

Zekun Wang

A dissertation submitted to the Graduate Faculty of
Auburn University
in partial fulfillment of the
requirements for the Degree of
Doctor of Philosophy

Auburn, Alabama
December 11, 2021

Keywords: tin whiskers, in-layer strain, material diffusion,
deposition isolation, reliability

Copyright 2021 by Zekun Wang

Approved by

George T. Flowers, Chair, Professor of Mechanical Engineering
Michael Bozack, Co-Chair, Professor of Physics
Jeffrey C. Suhling, Professor of Mechanical Engineering
Dan Marghitu, Professor of Mechanical Engineering

Abstract

The spontaneous growth of tin whiskers can occur under room temperature conditions. However, under more extreme external conditions (e.g., high temperature, high humidity, or thermal cycling), the rate of such growth tends to accelerate, longer whisker lengths, resulting in a larger possibility to decrease the reliability of electronic devices. Most research has not focused on internal conditions, such as the microstructure and internal stress distribution. Researchers have gained knowledge on factors that drive the tin whisker growth rate, but there is no general consensus on the internal mechanisms and key factors of whisker growth.

Here, it is proposed to study the behavior of whisker formation from tin depositions on silicon substrates with different dimensions and applied stress. A model for the whisker growth mechanism is presented, which applies the influence of internal stress release and atomics diffusion in a finite element formation, based on the existing DRX model for tin whisker growth. The process of whisker formation of samples under controlled possible influencing factors is studied with the goal of developing a deeper understanding of the critical factors that drive whisker growth. In the experiments, reasonable controls on background Ar pressure, sputtering duration, thermal cycling temperature, and duties will be applied, and the comparison and analysis between the computational and experimental results will be made. The expected experimental results will serve to validate and provide insight to enhance the model's predictive capability. The resulting model for whisker growth will illustrate

whisker growth mechanisms using a DRX-based model, and provide insight into the influence of internal stress among metal layers, which would in turn provide input to the manufacturing process of electronics devices for the decrease whisker occurrences in future uses.

Further, with TEM meshed grids, we confine volume of deposition material in both thickness and areal dimensions. On limited depositions, the whisker production is reduced by more than 86% comparing to controlling specimens without volume limitation. The experimental results also reveal the existence of volume threshold, below which whisker incubation is completely ceased. Such suppression effect of whiskering is also speculated to be governed by the spacings induced during deposition, which are considered as a powerful method to drain large amount of in-layer stress and affected the whiskering process.

Acknowledgements

I would like to express my highly respect and thanks to my advisors, Dr. George T. Flowers and Michael Bozack, for both the academic guidance, encouragement and support during the past four years. Without their patience, this thesis would never be accomplished. I am deeply grateful for the time, help, and effort from my committee members: Jeffrey C. Suhling, and Dr. Dan Marghitu.

I gratefully appreciate the whole personnel from the Leach Science Center of Auburn University for the great helps with all experimental affairs related to my research.

Table of Contents

1. Chapter 1. 12

1.1. The Definition of Whiskers 12

1.2. The History of Whisking Problem 13

1.3. The Lead-Free Movement 17

1.4. Recorded Failures Caused by Sn Whiskers 18

1.5. Factors Governing the Whiskering 20

1.6. Model Description of Whisker Process 29

1.7. Goals of the Study 32

1.8. Technical Details During the Study 34

1.9. Unique Features in This Study 37

1.10. Reference 39

Chapter 2. 50

2.1 Abstract 50

2.2 Introduction 51

2.3 Model Description 53

2.3.1 Geometry 54

2.3.2 Equation Derivation 56

2.3.3 Boundary Conditions 61

2.3.4 Input Parameters 62

2.3.5 Model Calibration 63

2.4 Simulation Results and Discussion 64

2.4.1 Simulation results 64

2.4.2 Sensitivity analysis on material properties parameters 64

2.4.3 Uncertainty analysis on two key inputs 66

2.4.4 Elements in the constant $\varepsilon bias'$ 67

2.5 Conclusion 70

2.6 Reference 72

Chapter 3. 97

3.1 Abstract 97

3.2 Introduction 98

3.3 Experimental ... 100
3.4 Results ... 102
3.5 Discussion ... 104
3.5.1 Different whisker density behaviors between deposited Sn volume and areal dimension ... 104
3.5.2 Effects of Sn layer thickness on whisker shapes and volumes ... 106
3.5.3 Factors governing the whisker density from small deposition areas ... 109
3.5.4 Occurrence of DRX grains within smaller deposition areas ... 113
3.5.5 Suppression prediction to whisker occurrence in limited areas ... 116
3.5.6 Perspectives from the DRX Model of Whisker Production ... 117
3.6 Conclusion ... 121
3.7 Reference ... 122
Chapter 4. ... 147
4.1 Introduction ... 147
4.2 Experimental ... 148
4.3 Results ... 150
4.4 Discussion ... 154
4.4.1 Whisker production governed by confined deposited areas ... 154
4.4.2 Whisker production behaviors under Sn deposition confined with various thicknesses ... 158
4.4.3 Characteristics of incubated whiskers in confined deposition areas ... 159
4.5 CONCLUSION ... 162
4.6 Reference ... 163
Chapter 5. ... 177
1.11. Summary of Results ... 177
1.12. Future Works ... 184

List of Tables

Table 1 Numerical constants with input values and definitions........................... 81

Table 2 Symbols with definitions in this model... 82

Table 3. Experimental data of Sn/Si samples from previous studies and related simulation results 83

Table 4 Simulation errors from output_0 and output_1.86 to reference results .. 84

Table 5 Test values for incubation environment parameters................................ 85

Table 6 Constants involved for uncertainty and test results................................ 86

Table 7 Statistics data of fitting lines for Figure 6e and 6f................................. 87

Table 8 Methods to calculate εcr 88

Table 9 Performance of model simulation on different humidity........................ 89

Table 10 Multiple methods for critical strain calculation 90

Table 11 Aperture Opening Dimensions 130

Table 12 Sn Whisker Density vs. Deposited Size and Incubation Condition 131

Table 13 $\boldsymbol{cs, f}$ VALUE ESTIMATION 132

Table 14 OFFSET VALUE CALCULATIONS 133

Table 15 Coefficient of thermal expansion (CTE) differences of Sn on multiple substrates, adapted from [21] 134

List of Figures

Figure 1. Analytical concept diagram for whisker formation mechanism on Sn/Si specimens. Red marks concepts not taken into consideration, and yellow marks concepts estimated without quantitative analysis in this model. Specially, the "IMC expansion" is ignored in the in-layer generation section, due to no existence of IMC between the material combination of Sn and Si. 91

Figure 2 Geometrical sketches for the whisker sites studied in this model. The whisker is modeled as a cylinder associated with the whisker grain, and the whisker site is the area surrounding the grain, extending to the midpoint of neighboring spacing. 92

Figure 3 Sketches illustrating the stress patterns at different stages of whisker growth: (a) before; (b) after; and (c) cease of whisker growth. The spatially uniformity leads to the even stress across the site in (a) and (c), and with the stress release effect of whisker ever since its growth at $t0$, the peak stress in (b) is smaller than that before $t0$..93

Figure 4 The comparison plots between model output and historical experimental data with value of $\boldsymbol{\varepsilon bias'}$ equals to (a) 0; and (b) 1.86*10-3. Linear fitting lines present as solid red lines associated 95% confidence bands with y-intervals fixed at 0. 1:1 reference line is illustrated as dashed line in both figures. Statistics data of linear fitting lines are shown in Table IV. With calibration on $\varepsilon bias'$ to a satisfying value, model output is in good agreement with experimental data. 94

Figure 5 Sensitivity test results on parameters $\boldsymbol{kG}$, $\Delta\boldsymbol{h}$, $\boldsymbol{m}$, $\boldsymbol{\varepsilon 0p}$, $\boldsymbol{\sigma 0}$, $\boldsymbol{\delta}$, $\boldsymbol{D0}$, $\boldsymbol{Qgb}$ and $\boldsymbol{Qcr}$, are plotted from (a) to (i), respectively. Ranges of y-axis are set same in all figures for illustration convenience. Test statistics is presented in Table V. The tests claim that the model is more sensitive to kG and Δh than the other parameters tested where slight linearities are present, directing to higher governing effect of grain size and depleted step height of site in film thickness on whisker length. 95

Figure 6 Monte-Carlo simulations on the two key input parameters: film thickness $\boldsymbol{h}$ and whisker density $\boldsymbol{N}$. a. plots the output of 10,000 points simulation vs h, and **b.** for and N as red circles, with 9 constants varying in certain range as Table VI listed. Linear and polynomial fitting lines are plotted in solid blue lines. Statistical data of fitting lines are listed in Table VII. The sub figure in **b.** illustrates the amplified plots in the range of 150k/cm^2 to 225k/cm^2, where the polynomial fitting line begins to present obvious fluctuation................96

Figure 7 a) Photograph of a specimen, with TEM apertured grids and fixtures just detached. The dark areas are covered with TEM grids and fixtures during sputtering, and the light areas are sputtered with Sn with or without grids. b) A magnified view of the 23 x 23 mm grid pattern. 135

Figure 8 Argon gas pressure in the magnetron sputtering system to produce intrinsic net compressive and tensile stress in deposited films [22]. For Sn

(red line, 118.7 atomic weight), an Ar pressure < 7 mTorr produces compressive Sn films and tensile Sn films are produced by Ar pressures > 9 mTorr. 136
Figure 9 Thermal cycle profile for whisker growth acceleration. The cycle had a 2-hour ramp followed by 4 hours of dwell. The upper dwell is held at 125oC; the lower dwell is held at -40oC. The total time for one cycle is 12 hours. 137
Figure 10 Sn whisker density vs. deposited size per the three incubation conditions. Due to the rapid transition to zero whisker growth < 23 mm deposition size, the linear least squares fit to data included data only > the 23 mm and not including the point at 10,000 mm (control specimen; no aperture). The R2 fitting value was > 0.9 for the three incubation conditions and the relative slopes of the fitted lines were: 1.8, 24.9, and 60.3. 138
Figure 11 SEM photos of whiskers incubated from various deposition areas. a) A combined hillock and needle whisker from 19 mm2 area; b) A "toothpaste-like" whisker from a 90 mm2 area; c) A traditional "needle-like" whisker from a 153 mm2 area, shown to bridge two neighboring deposition areas. 140
Figure 12 A series of SEM photos showing whiskers over successively larger deposited areas. a) 11 mm x 11 mm; b) 23 mm x 23 mm; c) 46 mm x 3000 mm strip; d) 54 mm x 54 mm; e) 113 mm x 113 mm; f) 153 mm x 153 mm. Figure(a) shows areas with no whiskers. The white dots are grains on the Sn surface, which are too small and not considered as whiskers. The needle whiskers seen in the photos above are 0, 0, 0, 1, 2 and 4, respectively. The needle whiskers in (f) are hard to distinguish, which is due to: (1) they are all thinner than those seen in (d) and (e); and (2) the scale is relatively large. The average density of needle whiskers increases with the dimension of limited areas increases. 141
Figure 13 Increasingly higher magnification SEM images of a whisker found on a 54 mm x 54 mm limited area. The needle whisker proceeds from a hillock whisker. 142
Figure 14 (a) A squared-limited Sn deposition layer, with m and n represents the width and length of this layer. (b) A section seperated from layer in (a) horizontally, with n as the length and p as the width. (b) A section seperated from layer in (a) vertically, with m as the length and have the same width p as the section in (b). With the same amount of stress release in both (b) and (c) at the two edges, their different numbers of high-whisker-likelihood grains result in different final whisker decrease effects. 143
Figure 15 Schematic diagrams illustrating whisker growth process in DRX mechanism: (a) strain energy is built up in dislocation structures; (b) a DRX grain initiates growth; (c) the DRX grain continues growth; (d) with grain boundary pinning, the DRX grain initiates expansion vertically, resulting in whisker growth. 144
Figure 16 Schematic diagrams illustrating growth process of a hillock whisker in

DRX mechanism: (a) a small whisker is growing with the DRX grain expanding; (b) the uneven stress acting on boundaries of DRX grain, allowing lateral growth of the DRX grain; (c) the whisker is a hillock when the process (b) occurs for multiple time until it slows with the loss of strain energy... 145
Figure 17 Schematic diagrams illustrate that the existence of void areas provides extra spaces for DRX grains to expand with the loss of strain energy. The expansion of limited areas is shown in an exaggerated manner to illustrate the energy release effect of void areas. Void areas are not observed to become significantly getting narrower than originally sputtered, due to two facts: (1) the volume change caused by limited areas expansion is small comparing to the whole volume of the limited area; (2) due to the small thickness of the Sn layer, the margin line of limited area is blur to define (Figure 6), so the movement of the margin line is hard to observe. 146
Figure 18 Argon gas pressure in the magnetron sputtering system to produce intrinsic net compressive and tensile stress in deposited films [22]. For Sn (red line, 118.7 atomic weight), an Ar pressure < 7 mTorr produces compressive Sn films and tensile Sn films are produced by Ar pressures > 9 mTorr. 169
Figure 19 Thermal cycle profile for whisker growth acceleration. The cycle had a 2-hour ramp followed by 4 hours of dwell. The upper dwell is held at 125oC; the lower dwell is held at -40oC. The total time for one cycle is 12 hours. 170
Figure 20 Whisker density v.s. Sn deposition volume 171
Figure 21 Whisker density v.s. areal dimensions of Sn deposition regarding different thicknesses. Strong linearities have been observed on whisker densities with areal dimension varies. 172
Figure 22 Whisker density v.s. Sn deposition thickness regarding different areal dimensions The whisker densities increase at low thicknesses (<0.2um), and become stable on thicker ones (>0.2um), which applies to all the areal dimensions tested. The governing effect of thickness is weaker than areal dimension, and the maximum thresholds are much easier to reach. 173
Figure 23 Whisker densities incubated from the control group where depositions are not confined during sputtering (can be treated as 1cm areal dimension). With same incubation methods, the unconfined specimens produce whiskers at least 6x to confined ones. 174
Figure 24 Schematic diagrams illustrating the deposition structure creep towards void areas, during which stress and strain are released. 175
Figure 25 Schematic diagrams illustrating the deposition structure creep towards void areas. 176

List of Symbols

Young's modulus	E
Poisson’s ratio	ν
Boltzmann’s constant	k
CTE mismatch between Sn and Si	$\Delta\alpha$
Sn atomic volume	Ω
Nominal yield stress of Sn	σ_0
Grain size constant	k_G
Grain boundary width	δ
Stress exponent for power-law creep	m
Characteristics strain rate for power-law creep	$\dot{\varepsilon}_0^p$
Activation energy for power-law creep	Q_{cr}
Activation energy for grain boundary diffusion	Q_{gb}
Pre-exponential coefficient for grain boundary diffusion	D_0
Step height of whisker site	Δh
Average whisker radius	a
Half of average whisker spacing	b
Whisker density	N
Average whisker length	L
Incubation duration	t
Temperature	T
Elastic Strain	ε_e
Creep Strain	ε_c
Diffusion Strain	ε_d
Strain caused by DRX grain expansion	ε_{rec}
Strain caused by CTE mismatch between deposition and substrate	$\varepsilon_{thermal\ expansion}$
Rate of Creep Strain	$\dot{\varepsilon}_c$
Strain bias	ε_{bias}
Effective diffusivity	D_{eff}
Grain boundary self-diffusivity	D_{gb}
Deposition film thickness	h
Grain size	G

1. Chapter 1.

The Role of Whiskers in Reliability

1.1. The Definition of Whiskers

Metallic whiskers are single crystal filamentary eruptions arising from metal surfaces or finishes, and a single whisker can be formed as joint of multiple single crystalline filaments. Most whiskers observed are cylindrical in shape, with average diameters (equal to the grain size where it erupts from) varying around one micron. Under certain environmental conditions, a whisker can grow to several millimeters. The growth directions of whiskers are not controllable, and whiskers themselves can also be straight, kinked, or even curved. The formation material of metal whiskers comes from the growing films or finishes, which endows them high malleability and conductivity. These metal characteristics, associated with the length whiskers can grow, and the unpredictability in direction, has shaped whiskers to be one of the major concerns of reliability issue in modern electronics and devices, just as the role whiskers are first reported in early 1940s by Western Electric and Bell Labs. Besides these straight and needle-like ones, multiple other types of eruptions are also observed, which are quite different in the appearance. These are commonly referred as extrusions, hillocks, flowers, toothpastes and volcanos. However, they attract fewer academic interests when compared with the longer whiskers due to the weaker ability conducting circuits failures in morphology.

Besides Tin (Sn), other materials are also found associated with whiskering problem, such as cadmium, zinc, indium, gold, lead, aluminum, etc. The dominant role of Sn in soldering and finishing for electronic components today makes itself the most serious whiskering material, leading to the fact that most of the work concerning whiskering problems focused on tin (Sn) whiskers.

1.2. The History of Whisking Problem

In the early 1940s, the formation of metallic whisker was first be witnessed and reported, which arose the interest of study. The first circuit short occurred in 1946, where a cadmium whisker grew long enough from electroplated film to connect the neighboring capacitor in electronic components [1]. Later, Bell Telephone Corporation reported several failures caused by Cd whiskers formation on channel filters which maintained frequency bands in multi-channel phone transmission lines in 1948. Followed these failures, Bell Telephone Corporation initialed a series of long-term investigations on the topic of whisker formation, as reported by Compton et al. in 1951 [2], and revealed the spontaneous occurrence of whiskers. The formation of whiskers was not limited on Cd electroplating due to the reported of similar crystal formation from electroplated zinc, Sn, silver and even on Al casting alloy. The summary of these investigations provided by Compton et al. worked as the first guide for later research on whiskering problem.

Due to the favorable combination of low cost, solderability, contact resistance, and corrosion resistance, the Sn and Sn-alloy electroplating had become the major

plating choice for electronic components, much of the following research since the Compton's work in 1951 turned their interests on electroplated Sn and Sn-alloys on various substrates. Arnold unveiled the beneficial whisker mitigation effect during the alloying process of Sn plating with Pb in 1959 [3]. He stated that whiskering would rarely occur on Sn-Pb alloys under ordinary environment but be highly encouraged when subjected to high compressive stresses. Affected by this work, Pb was introduced as the co-deposition into the Sn electroplating process in the predominant mitigation strategy for Sn plating in the US electronics industry for the next 50 years. Later, in 1964, the contribution of Pb in ceasing whiskers was reinforced by Pitt and Henning [4], where whisker growth were witnessed occurring from hot-dipped Sn and 50%Sn-50%Pb deposited on copper (Cu) and steel substrates in the clamped-pressure environments. They also revealed the decreasing trend of whisker densities with increasing Pb content.

Britton of the Tin Research Institute (the International Tin Research Institute (ITRI) Ltd. nowadays) in collaboration with Bell Labs reported a review article in 1974, stating that a minimum thickness of 8μm (either matte or bright) would probably maintain most safe and suitable purposes avoiding the whiskering hazard [5]. They also claimed that 1% content of Pb in Sn was sufficient to prevent whiskers, but a larger developed Pb content would be encouraged, which again recommended the Sn-Pb alloy as the best alloy of choice.

Later, a series of publications by Dunn from the European Space Agency suggested to exclude Sn, Cd, Zn, etc. from the surface choices, which were prone to

induce stress and results in whisker growth [6], [7], and strongly recommended, a Sn-Pb alloy of 60Sn/40Pb as the finishes alternatively. These papers were the first to clear state getting rid of pure Sn from plating for critical applications, such as spacecraft. However, multiple major manufacturers refused to take these suggestions unless mandated or regulatory position was taken, which was proven unfortunate by the occurrences of several significant Sn-whisker-related reliability failures in US Air Force equipment

Nordwall et al. discussed about the whiskers growing case from Sn-plated hybrid circuits reported by the US military in 1986, where whisker pieces broke off from the root and fall between neighboring circuitry to cause intermittent operation on a 12-years-old radar systems [8], [9]. Analytic report mentioned the maximum length of numerous bridging whiskers to be more than 2.5 mm. In 1989, Corbid examined the Sn usage in miniature electronic packages [10]. He denied the prevention of reflowing (melting solder during circuit assembly) onto whiskering problem as previously claimed in earlier studies. The prevention function of reflowing remains vague until nowadays.

The whisker incubating effect was first studied in 1990, when Cunningham and Donahue from the Raytheon Company published a study to compare the whisker growth scheme from Sn and Sn-Pb alloy depositions subjected to mechanical stresses and increasing environmental temperatures [11]. The experimental results reached the combination ratio of 60Sn-40Pb to minimize the whisker density production, combined with an increasing temperature with Pb-Sn. Later, such combination was

first applied to alleviate whiskering problem, as stated in a 1993 work by Diehl from Burndy Connector Corporation [12]. As a connector company, Burndy Connector Corporation concerned more on the elevated reliability of Pb-Sn soldering and finishing. Diehl found that the addition of Pb was necessary for Sn electroplating to cease from producing Sn whiskers, which was adopted subsequently by Burndy Corporation onto all of Sn plated connector productions.

In ultrafine pitch circuits, whisker problem was first reported by Ishii et al. in 1999 [13], [14]. The ultrafine circuits could reach a minimum width of 50 μm in a pitch then, associated with lead-frame spacing of less than 20 μm or less between the neighboring circuits.

Whisker problems became severe with the miniaturization and wide application of electronic devices. Since the beginning of the 21st century, multiple electronic companies subsequently reported the whisker-induced relay failures in both commercial and military facilities after the service for more than eight years [15]. The finishes were originally settled on concrete Sn-Pb, but due to the relatively high cost, finishes had been gradually switched to pure Sn ever since 1983.

The reported failures were observed on multiple key industries, immediately forcing the initiation of one total field replacement action. In 2002, in name of the Government-Industry Data Exchange Program (GIDEP), Khuri from the Department of the Navy issued an Agency Action Notice to the electronics industry on Sn whiskers [16], stating the potential risks associated with the use of pure Sn-plated finished on electronic assemblies and should be avoided at all costs. This notice

recommended the usage of Sn-Pb solders as the substitution. However, the application of Pb-involved solders was soon ceased by the following mandated regulations, and the whiskering problem arose again afterwards.

1.3. The Lead-Free Movement

As discussed in the above section, since the late 1940s when Sn associated alloy were chosen as the material for soldering and finishing use for electronic systems, Sn had soon become the most popular due to its multiple material characteristics. However, there have been numerous severe incidents reported in electronic circuits (in spite of Cd) ever since the application of Sn, and the threaten of Sn would elevate with the increase of service time. In the beginnings of 21st century, according to the previous studies on the alleviating effect on whisker of Pb-involved alloy, government immediately announced a notice to recommend the Pb-Sn alloy to take the place of pure Sn in electronic circuits. The elevating advances in electronic area led to the exponential sales growth in consumer electronics such as computers and cell phones. Along with such sales growth, the disposing of electrical units is also elevating. The widely usage of Pb-Sn alloy in this field resulted in millions of Pb-containing circuit boards from disposed electronics dumped into landfills. The Pb in the buried electronics could easily migrate into soil and municipal water supplies, and the polluted water and food would finally result in harmful threaten to people's health.

By July 2006, the European Union legislation announced "Restriction of the use of Certain Hazardous Substances (RoHS) in Electrical and Electronic Equipment",

which regulated the elimination of Pb (less than 0.1 wt%) from electronic devices [17]. The most economical and direct methods of complying with the RoHS was to eliminate the usage of Sn-Pb alloy and turned back to pure Sn again [7], [18]. Such replacement arose the requirement of high confidence in pure Sn contented circuits. Therefore, Sn whiskers returned as the major reliability problem to electronic systems once again, which has further been exacerbated by the continuous increasing industry demands for minimizer and faster devices, with higher packaging densities and smaller circuit dimensions.

1.4. Recorded Failures Caused by Sn Whiskers

Whiskers can affect the circuits and lead electronic device failures through multiple ways. Among them, the short circuit caused by Sn whisker bridging the closed circuits and elements is the most common one. Typically, a maximum current of ~ 10 mA can be conducted through whiskers before melting down, and they can maintain such the bridging effect permanently if the current is less than this threshold value. If the current got greater than the threshold, whiskers would melt and result in an intermittent short. Besides the physical short circuits, whiskers can threaten devices in the form of a plasma: Very high levels of current and voltage can vaporize whiskers into a conductive plasma of metal ions, which is capable to conducting currents as high as hundreds of amperes, and leads to catastrophic situations. The current arcs can usually be sustained for several seconds before interrupted by the circuit protection devices. Richardson and Lasley (1992) reported that with the air pressure reduced, the

power requirement for a whisker-induced metal vapor arc to initiate and sustain is also reduced [19]. Further, needle whiskers are usually growing in small diameter but long length, and such morphology makes the occurrences of fracture. When a fracture occurs, whisker portions would fall onto neighboring circuits and elements where whiskers may not grow from, and lead to unpredictable interfere.

Clearly, whiskers can lead to device failures in multiple ways including but not limited to ones discussed above, and the easy growing characteristics of whiskers makes them common on numerous electronic elements. Several cases with whiskers observed are summarized and illustrated by NASA, with photos shown whiskering growing long enough to be observed by naked eyes [20]. Sn whiskers are found from pure Sn-plated connector pins, from matte Sn-plated microcircuit leads, from the exterior and interior surface of Sn-plated electromagnetic relays. Alloys are also found creating numerous whiskers, such as whiskers from Sn-coated Ni terminals on ceramic chip capacitors [20]. The methods observed that whisker connecting is also various: terminal-to-terminal, terminal-to-header, case-to-another component, and even whisker-to-whisker.

As discussed, whiskers are easy to grow from pure Sn coating and Sn-contented alloys, and are claimed to be responsible for multiple failures in critical and uncritical applications, including but not limited to heart pacemakers, space capsules, missile control systems, satellites, medical devices, aircraft radar, nuclear and electrical power plants.

1.5. Factors Governing the Whiskering

The threaten of whiskering problem to electronic elements and circuits has been revealed for decades, and researchers have conducted multiple experiments and studies, eager to reach the formation mechanism of whiskering and then can cease the growth of whiskers. There is still no general mechanism which can quantitatively predict the whisker production from depositions, but multiple theoretical explanations have been published to deal with the formation and growth of whiskers. There are several commonly agreed variables that influence whisker formation. Most researchers agree that in-layer stress beneath the Sn film surface is the fundamental contribution to whisker growth [21], where both the intrinsic and extrinsic stress are involved. Intrinsic stress is distributed with associated texture (crystallographic orientation or grain size) [22]–[24], and extrinsic stress usually originates from the mechanical processes onto the specimens such se forming, bending, thermal expansion (induced by coefficients of thermal expansion mismatch), chemical reactions (intermetallic compound formation) between the Sn-film and the substrate material, impurities introduced during film deposition, plating chemistry (bright tin), and/or material diffusion flux along the substrate material and tin film. Multiple factors from the material incubation environment have been proven able to governing the in-layer stress.

It is commonly accepted that compressive stress contributes to whisker formation, while tensile stress retards it. However, the direct applied stress does not always determine the compressive/tensile of the in-layer stress, because multiple other factors

grouped into several categories are conveniently involved, such as plating chemistry and process, deposit characteristics, substrates, and environment.

The first process for a deposition film is the plating, where the plating chemistry affects the deposition during film depositing, and attributes many study concerns. Pure Sn is the most commonly used finishing and soldering material where whiskers have been observed incubated from in numerous cases, but other Sn alloys (such as Sn-Cu and Sn-Bi) also possess the ability to generate whiskers. Even the most rare whisker-producing material, Pb-Sn, also has been observed incubating whiskers under suitable environmental conditions [25]. Besides, the usage of "brighteners" during plating can also affect the whiskering problem [26], [27]. In all, "bright" Sn deposition are proven more prone to whisker formation and growth than "matte" Sn films, which are Sn films maintaining larger grain sizes (typically of 1 μm or greater) and lower internal stress with the carbon content lower than 0.050%. As a comparison, the bright Sn films possess high internal stresses but smaller grain sizes (0.5 to 0.8 μm) with the carbon content varying from 0.2 to 1.0% [28]. The impurities introduced during plating bath may strengthen the whisker formation. Though the impurities playing as the primary culprits is still uncertain, Cu and C impurities had been proven inducing compressive stress into the depositions [29]–[31]. Other factors involved in the plating process such as current density [32], [33], bath temperature [34], and degree of bath agitation during the plating process [35], [36] also influence whisker formation by affecting the in-layer stress.

Following the deposition, the deposited film characteristics takes the place in

whisker formation. Growth of whiskers are affected by the grain shapes and sizes with crystal orientation of the deposition, and typically, smaller grain size induced higher in-layer stress [37], [38]. Besides, the grain size and shape also affect the grain boundaries, and in turn influence whiskers through such means. A larger grain size of deposited Sn films usually reduces the total length of grain boundaries, and gradually decrease the internal material diffusion rate in the deposition. Fewer grain boundaries also lead to fewer occurrence and position for non-uniform intermetallic compound (IMC) growth, alleviating the stress induced by IMC expansion, which is caused by the migration of the free substrate atoms into the deposition film. The Sn atoms diffusion along the grain boundaries to the root of whiskers is one supplying methods to whisker growth from the deposition surface, where the grain boundary diffusion plays the predominant role [39], [40]. The pinning effect of grain boundaries fixed them within films, limiting the diffusion rate not larger than the available flux of vacancies with the film. The film thickness affects the whiskering problem other than through diffusion. Sn films thicker than 7 μm could provide enough volumes and alleviate the overall stress, resulting in a longer incubation duration for whiskers [41], [42].

Besides the expansion of IMC atoms, there are still multiple process and reactions considered as the potential stress sources to stimulate whisker growth. Among them, the dynamic recrystallization (DRX) attracts the most concerns, which numerous researchers have considered as the major driving force for whisker growth [43], [44]. The DRX is an enhancement recrystallization process of static recrystallization. The

static recrystallization occurs when the strain energy of defected structures decreases without further deformation at the same time, while the DRX process is caused by the simultaneous occurrence of deformation [45]. The creep deformation, resulting from the in-layer compressive stress, initiates the DRX process and provides the material diffusion to maintain the growth of DRX grain [46]. In DRX theories, the contribution of compressive stress to whisker growth is not explicitly through the bulk movement of material, but through generating the inelastic deformation, increasing the strain energy and finally initiating DRX as a result. Theoretically, the DRX process occurs with the defects building up. The slow strain rate usually results in a high possibility of deformation, associated with the occurrences of recrystallization (strain energy loss), as well as the DRX, for that the building-up of strain energy makes the initialization of DRX process either sooner or, at a lower temperature than of static recrystallization. As soon as the strain energy built up to exceed a certain limit, the DRX process proceeds with the nucleation of new DRX grains, with grain size smaller than the original ones in most cases. The crystal dislocations builds up at boundaries of these recently created DRX grains. As a result of dislocations, these new-created grains become new initiation sites for possible whisker growth. The growth of whiskers is a serial comprising process of deformation from the strain energy building up, initiation of new grain and then the expansion of DRX grain. After the initiation of nucleation in these DRX grains, the in-layer compressive stress drives the material transport mechanism to maintain such deformation, and also creates dislocations at grain boundaries and in turn raise the strain energy to the

locations at new grains initiations as a result.

Another model proposed by Smetana, the growth mechanism is slightly different. He proposed that the atoms at the root of the whisker are at lower energy levels than the surrounding areas, which initiates the movement of Sn atoms without consuming extra energy from higher energy state [48]. During this process, recrystallization is necessary, as well as the vacancies at the root of the whisker grain boundary to ensure the concrete movement of Sn atoms. After recrystallization, grain boundaries are created with oblique angles, resulting in lower stress on the grain boundaries than on the vertical grain boundaries. These different stress allocations create the stress gradient beneath the deposition surface. With a portion of grain boundaries at high vacancy sites with low degreed of atom density, they act as sinks for vacancies. Due to the stress gradient, diffused Sn atoms are driven into the grain boundaries with oblique angles. During such process, the occurrence of dislocations may cause movement of grain boundaries along the directions of boundaries, which is the sources of creep strain. With Sn atoms diffusing into the grain boundaries, a portion of atoms in the grain boundaries will move into the whisker grain. Such injection of atoms from boundaries into grains results in the grain expansion, and the vertical part (directed upward) is the growth of whisker. Such growth process of whiskers are of course governed by pinned grain boundaries, resulting the different morphologies, striations and growing angels of the final whiskers.

Other than the DRX process which has been discussed as one of the major sources of whisker growth, oxidation of deposition material also affects the whisker growth.

Oxidation occurs as soon as the material is deposited. Multiple works have proven that the localized breaches in the surface of Sn oxidation layer can provide a path that vacancies could diffuse from ambient gas into the deposition within a limited duration [49]–[51]. The free atoms in the film can move along those unpinned grain boundaries under compressive stress. And atoms reaching any nucleation sites can begin to grow at the site, resulting the formation of whiskers [50].

There are still other methods that oxidation contributes to whiskers. The reported of non-uniform Sn oxides implies the existence of holes in the oxide or regions with weaker oxidation locations, so that whiskers can penetrate through the Sn oxidation layer [52]. Besides, oxidation can induce stress into the layer. During the diffusion of oxygen into the deposition film, oxygen atoms combine with Sn atoms to form SnO or SnO_2. Such process comes with the volume change of atoms, and can induce extra stress into the film. The stress introduced by such process is often considered playing more important roles in thinner films than thicker ones, given that thicker films possess larger volumes to dissipate the induced stress, while the amount of stress is maintained to a certain level regarding to the thickness of oxidation layers instead of deposition layers. In all, the effect of oxygen on whiskering is controversial and has not been well understood. Multiple theories have been established to explain its role in whisker growth. Tu believed that the existence of surface oxidation layer is necessary for whisker formation [53], while Moon et al. claimed that it has minimal effect [54].

Unlike the oxidation layer which stays above the deposition films, the substrate

under them is great governing whiskering problem. Different substrate materials affect whiskers growing from depositions differently in multiple ways. Certain deposition and substrate combinations have been studied to form IMC while other combinations not. For the Sn/Cu combination, Cu_6Sn_5 is the dominant IMC which can be found on almost each Sn depositions with Cu as the substrates at ambient room temperature [31], [55]. The IMC layer is usually formed by Cu atoms diffused into Sn deposition film through grain boundaries. Though experiments have proven that the growth rate of Cu_6Sn_5 is accelerated with increasing temperature, they are more threatening at room temperature, for that the diffusivity through the grain boundary is higher than bulk diffusion near room temperature, and in turn create limited Cu migration routes. Such process leads to the formation of highly irregular Cu-Sn IMC, inducing localized, compressively stressed to neighboring regions within the Sn film. However, the diffusion within bulk is increased with elevated temperatures, resulting in less stress due to the IMC is formed more uniform.

Molar volume difference is another source of film stress and can affect whiskers. The volume of one Cu_6Sn_5 is larger than six parts of Cu atoms with five parts of Sn atoms (10.6 cm^3 /mol), leading to compressive stress induced into the deposition film [56], [57]. Further, a complicated way exists for IMC to affect the in-layer stress: through the formation of a neighboring intermetallic layer of Cu_3Sn with temperature elevated. Cu_3Sn possesses a molar volume lower than Cu_6Sn_5 (8.6 cm^3 /mol), but affect the stress amount in the deposition film [58].

Time is consumed for whiskers to grow, during which they will be largely

affected by the incubation environment of the specimen. Each factor in the storage conditions has been found possessing influence onto growth of whiskers, including but not limit to the temperature, thermal cycling, humidity, pressure, external stress, and current flow / electric bias. Due to the CTE mismatches, environmental temperatures and, especially, temperature cycling. Zhang et al. (2004) reported that thermal cycling can increase the growth rate of whiskers [59], while Brusse et al. (2002) denied the effect of thermal cycling [60], [61].

The heat treatment processes, including annealing, fusing, and reflow, can also affect the whisker growth rate. Annealing is a process of heating and cooling, intending to soften metals and reduce the fragility. For deposition films, annealing performed within 24 hours of plating can help mitigating whiskers due to irregular IMC growth, and Dittes and Olberndorff (2003) have suggested Pb/Cu frames to be heated to 150°C for 1 hour directly after plating, which can form a less irregular but more continuous IMC layer, resulting in less compressive stress [62]. Elevated temperature can shift the rain boundaries of Sn layer, and form larger grains and fewer grain boundaries [63]. Regulated IMC layer results in continuous diffusion barriers for IMC expansion, which decrease the formation rate of irregular IMC caused by the diffusivity along the grain boundary at ambient conditions [64].

The Fusing and reflow act similarly, because both melt and resolidify plating deposition under the slow decreasing temperature. The fusing is a reflow process that is usually completed by dipping deposition surface in a hot environment. Glazunova (1963) reported that the fusing procedure completed shortly after deposition would

mitigate whisker formation, and such effect would be reduced when IMC layers were formed [65]. Unlike fusing, reflow, as a part of the printed circuit board assembling process, is not playing the same role influencing the whisker mitigation practice. On the contrary, whiskers are reported increased during the reflow without flux [66], [67].

The role of relative humidity is quite complex in whisker formation. Multiple reports claim that humidity is not a factor direct governing the whiskers while others reported encouraged whisker growing rate under high humidity (≥85% RH) [58], [68], [69]. Conventionally, stress is introduced by humidity through the diffusion of oxygen from the surface into the film [69], and different humidity results in changes of deposition oxide film thickness, affecting the in-layer stress [58]. Besides, Su et al. (2006) claimed that high relative humidity also increases the diffusivity along the grain boundary or on surface of deposition films, leading to stress increase due to the corrosion process [68]. Whiskers incubated from corrosion caused by water condensation or water droplet exposure was also been reported [70]. Localized corrosion on deposition surface results in non-uniform oxide growth, imposes different stress states at different locations on the deposition film. Such difference in stress state decides the occurrence of whiskers in the corroded regions and growth of them after removal of the condensed moisture.

The final factor we discussed here is electric field or voltage bias, which were reported governing whisker growth in multiple methods. Hilty et al (2005) observed bending of whiskers as a result of electrostatic attraction, which increases the possibility of whisker shorts [71]. Multiple studies also reported the acceleration

phenomenon of electrical currents on Sn whisker growth [72], [73].

As a summary, multiple factors have been reported play certain roles in the whisker growth process in any given system and environment. However, quantitative descriptions between these factors and whisker growth have not been revealed yet. In spite of this fact, After the RoHS regulations prohibited the usage of lead in electrical products, electronic researchers and industries have made numerous attempts to develop whisker prevention and mitigation methods. The National Institute of Standards and Technology was one of those first agencies specifying whisker mitigation practices through the reduction of in-layer compressive stress induced by IMC formation. To specify major factors in whiskering process, a series of accelerated experiments, such as high temperature, humidity and thermal cycling, were also embarked for tin whiskers. During the time when the industries continued their march on Pb-free electronics, the necessary to ensure the reliability of tin soldering and coating was emphasized, and a set of industrial test procedures were then established to monitor and improve whisker reliability exposure in July 2004 by NEMI [74]. However, these documents provided only guidelines to possibly reduce the threaten of whiskering but did not specify the methods to eliminate whisker-related failures.

1.6. Model Description of Whisker Process

As discussed, the whiskering process of deposition films have been proven governed by numerous factors through complex ways and processes, while no quantitative relationships of these factors were established. Besides, there are still

other problems lying in the process of whisker study.

One of the complications of whisker studying process is the issue of time. In some cases, whiskers were observed growing within days, but several years or even decades were taken before they finally grew long enough to threaten the reliability of electronic systems. Now it is commonly known that the incubation period, that distinguishes whiskers from other surface plating threatens including nodules or dendrites, which are similar in morphology to whiskers but occur immediately on the surface after deposition. One obstacle of experiments on whisker growth observation is that, to complete any meaningful experiment, a comparatively long time periods is necessary for whiskers to be incubated. The long time period for whisker growth implies that electronic systems with Sn soldering and plating which functions fine for many years still remain threat of reliability. Dunn from the European Space Agency suggested that surfaces susceptible to whisker growth should be excluded from spacecraft design [6]. However, not all satellite manufacturers took these suggestions, and over a decade later, in 1990, multiple failure cases of commercial spacecrafts reported due to the Sn whisker problems. Besides, the U.S. military were aware of the potential problems of Sn whiskers on failed circuits in 12-year-old radar systems, and observed whiskers up to 2.5 mm in length incubated from Sn-deposited lids of hybrid circuits [8]. Another incident was that whiskers were found arising after a long period of dormancy in 10-year-old relays of General Electric. Studies on whiskers measured the growth rate of whiskers varying from 0.03 to 9 mm/yr, with high unpredictability [15], and the rate was essentially linear which went to zero at some point in time. The

wide variation range in whisker growth rate results in giant difficulties in whisker study. With such variation, one would never know how long to whiskers can grow, how fast whiskers are incubated, and when whiskers stop growing.

Other contributing complications include that fact that the incomplete group of factors which can govern the whiskering process, and the inaccurate variables reporting of known factors when study is published. Besides, current test methods may not correlate whisker growth to experimental conditions, and whisker growth cannot be predicted in other environments or for longer durations. Therefore, a mechanism model which can describe whisker formation quantitatively is necessary for long-term field exposures under different environment.

Models have always been pursued by researchers which are designed to quantify the threaten of whiskers to electronic components and circuits, no matter they are theoretical or empirical. However, the numerous factors governing the whiskering process have largely elevate the complexity of models. Later, ever since the consensus that in-layer stress was the major contributor to whisker growth, convincible mechanisms were improved by researchers to theoretically depicting the growing process of whiskers, associated with the quantifying of in-layer stress. Followed by these whisker growing mechanisms, mathematical models were developed based on the physical theory and in-situ experimental. The models proposed by Tu (1994) [75] and Hutchinson et al (2004) [76] revealed the role of mass diffusion between whisker sites and attributed it to the long-range gradient of in-layer stress, which also proposed that the stress field contributing to whisker growth in a steady-state was determined

by the spacings between whiskers. By proposing a strain generation mechanism within the deposition film, Buchovecky et al (2009) extended the model to involve the dynamic balance between IMC formation strain and whisker-induced relaxation phenomenon [77]. Their simulation results indicated that, the diffusion range and whisker growth rate was rather determined by the strain rate applied other than the whisker spacing. Later, the stress relaxation measurement suggested that the plasticity in deposition films could be characterized by power-law creep [78]–[83]. Buchovecky (2010) proposed an analytic model concentrating on the whisker growing process in the presence of power-law creep (as the plasticity). Basing on these works, Pei et al. (2015) established a model to simulate the stress allocation strategy within whisker sites with the premise of pure stress-balanced [84].

Models established has been validated for most external stress-driven whisker growth phenomenon. However, there still exist several processes which have been revealed greatly governing the stress amount and allocation within the deposition film but not been involved in any of the models. Among them, the DRX is the major one. With lack of enough quantitative description and experimental data, the DRX process cannot be predicted on occurrence or quantitively derived with certain given material and environmental parameters. Therefore, there are still some improvement models can make to describe whiskering problem more accurately.

1.7. Goals of the Study

One of our goals in this work is to develop a theoretical model to quantitatively

describe the whisker formation from the strain integration within whisker sites under certain experimental conditions. Multiple factors discussed being able to govern the whiskering process will be involved into the model, with determined expression on the relationship between them and strain. The volume change resulting from strain will be assumed to contribute to whisker eruption fully, and a final average whisker length will be estimated from such volume change.

Further, material diffusion is one of the major sources which provide continuous stress to deposition layer and results in whisker growing long enough to short circuits after years or decades as discussed above. In order to cease the whisker growth within long period, it might be a perfect practice to minimize the effect of diffusion in whisker growing period and observe results. Unfortunately, many factors in the incubation environment have been proven being able to govern the diffusion process, while currently the whiskering process cannot be isolated from the influence of these factors. As a result, to study the effect of diffusion on whiskering, we need to take another method instead of simply controlling environmental parameters.

Here comes the other goal of this study: trying to isolate the effect of diffusion in whiskering process. Long range diffusion has been reported by Woodrow (2006) [85], which was validated as a large portion of the whole diffusion process. If we can cease such material diffusion, whisker growth should be affected a lot, and we may quantify the importance of the role diffusion playing in the whiskering problem. In this study, we achieve such applying gaps as physical barriers on deposition films. We establish comprehensive experiment on Sn/Si specimens using sputtering methods, and

collected whisker growth strategies controlling the effect diffusion range of Sn materials which builds up the whiskers.

1.8. Technical Details During the Study

Sputtering will be the deposition method we apply in this study. Sputtering at high Ar background pressure increase the number of Sn/Ar atom interactions during the travel of Sn atom from sputter target to substrate, leaving the deposited Sn atoms with low kinetic energy, and producing a film with low packing density. Atoms from such a film are deposited far apart, creating attraction net force between neighboring atoms, which provides a shrink trend of the film produces concave curvature in the center of substrate. On the contrary, with less energy loss of atoms during sputtering, a low Ar background pressure results in the deposited atoms with high kinetic energy, leaving atoms packed tight. Atoms from such a film exerts a force of repulsion against neighboring ones due to electron orbitals possibly overlapped. The films is produced with a resultant convex curvature in the substrate. Such characteristic of sputtering allowing researchers to govern the compressive, tensile or zero stress to the deposition films.

Compressive in-layer stress, taken as major source of whisker growth, is assumed contributing to the strain within the whisker sites in this model. Given that sputtering will be the major method in this study for Sn deposition, we need to induce compressive in-layer stress during sputtering. Hoffman and Thornton (1989) studied

sputtering deposition of many different metal films though argon (Ar) plasma, and reached a simple system to introduce various amounts of intrinsic film stress by adjusting the background Ar gas pressure in sputtering system [86]. For Sn films, a background Ar pressure ranging from 1~6 mTorr results in compressive intrinsic stress. Tensile and even "zero" stress can also be produced, related to 10~100mTorr and a fairly narrow range of 7-9 mTorr, respectively.

The next challenge in this study is the limited whisker statistics available to count whisker numbers and measure lengths. For simplicity and time maintenance, SEM is applied in this study for whisker observation and measurement, with the incident electron beam of SEM perpendicular to film surface. However, the single-angle observation of SEM will inevitably foreshorten the length of protruding whisker in some cases. In this study, we apply a common whisker measuring technique [87]: the length of a whisker is measured as the straight distance from the emergence point of the whisker to the distant point on the whisker. To complete such measurements, a SEM need to be equipped with a moveable and rotatable stage in three dimensions.

With a known tilt, the measurement is completed by two images taken before and after rotating the SEM stage [88]. Then the whisker length L_{ab} can be calculated using the following equation:

$$L_{ab} = \sqrt{\frac{{L_{cd}}^2 + {L_{ce}}^2 - 2L_{cd}L_{ce}cos\theta}{sin^2\theta} + (L_{cd}tan\beta)^2}$$

where L_{cd} represents the length of whisker projection on the axis which is perpendicular to rotation axis in Plane 1, L_{ce} represents the length of whisker projection on the axis which is perpendicular to rotation axis in Plane 2, θ represents

the rotating angle between Plane 1 and 2, and β represents the angle L_{cd} between and L_{ad} in Plane 1.

Whisker density is the other term need to be examined as carefully as whisker length. Density is usually gathered by uniting the whisker numbers counted in a limited range. There are various whisker counting approaches applied in numerous studies. Some studies incorporated whisker numbers from massive, high-volume specimens, while others applied well-controlled experimental environments with fewer specimens. Besides, several improvements have also been made during the studies of whiskering problem. Whiskers have been reported able to grow millimeters in length which can even be observed with naked eyes, but most of whiskers are as short as a couple microns long, optical microscopes are necessary for whisker statistics collecting. The microscopes are limited with depth resolution that most optical microscopes can lead to false identifications of whiskers, where an SEM is ideal for whisker statistics collecting cases. Further, techniques of distinguishing whiskers from debris on the deposition surface through any microscopic is also necessary during the comparison of whisker statistics from study to study. In some cases, only crystal eruptions exceeding a given length (such as 10 μm or greater) were taken as whiskers and counted.

The battle in statistics issue will never comes to an end in whisker studies, and researchers keep ensuring the significances in their studies. In most cases, the studies of whisker length requires a significant number of whiskers with length measured. For the measurement of whisker length from a single SEM image, a percentage error

($\%E$) is defined in this study that

$$\%E = (1 - cos\alpha) \times 100\%$$

where α is the angle between the whisker and deposition surface. In the study of Panashchensko (2009), such error associated with the measurement method mentioned above varied from 4% to 31% [88].

In our study, whiskers are produced from laboratory specimens within reasonable incubation periods in well-controlled environments, and statistics of numerous whisker are collected. We applied a SEM for observation on any crystal eruptions with length ranging from 2 µm and greater which are counted as whiskers. Whisker density are measured by whisker numbers manually counting through the SEM over ten 100 µm x 100 µm areas which are randomly picked from the deposition surface. Whiskers counted are also measured length from a single view.

1.9. Unique Features in This Study

Following are the key features which have studied able to govern the experimental strategy:

- We develop an analytic model basing on the theory of in-layer compressive stress, and predict the average whisker length growing from deposition surface as the result of accumulated strain within a whisker site.
- We take most mentioned factors governing the whiskering process into the model as controllable parameters.
- We accept DRX process as another major source of compressive strain for

deposition films.

- We apply reproducible methods for whisker growing within a reasonable duration through magnetron sputtering techniques.
- We introduce certain stress (tensile, compressive or zero) into the films according to the study of Hoffman and Thornton (1989) to investigate the role of net film stress [89].
- We eliminate the interfacial stress theoretically induced by IMC by choosing certain deposition and substrate material combination.
- We apply experimental data from multiple previous reports and studies to calibrate the model output, pursuing good agreement between simulation output and recorded experimental results.
- We specify 6 parameters from all the material-related parameters through conducting sensitivity test on them, respectively.
- We present the linearity and polynomial relationship of deposition film thickness and whisker density onto average whisker length, respectively.
- We minimize the effect of material diffusion beneath deposition surface by isolating films into small defined ones.

Further, to better understand the role of long-range material diffusion playing in whiskering process, there are some more unique features we apply, which are listed as follows:

- We apply the TEM grids to isolate deposition film into small defined ones to barrier long-range diffusion.

- To better describe the effect of diffusion, we apply different incubation methods to observe whisker growing schemes with different defined diffusion ranges.

1.10. Reference

[1] H. L. Cobb, “Cadmium whiskers,” *Mon. Rev Am Electroplat. Soc*, vol. 33, no. 28, pp. 28–30, 1946.

[2] K. G. Compton, A. Mendizza, and S. M. Arnold, “Filamentary growths on metal surfaces–‘whiskers,’” *Corrosion*, vol. 7, no. 10, pp. 327–334, 1951.

[3] S. M. Arnold, “The growth of metal whiskers on electrical components,” 1959.

[4] C. H. Pitt and R. G. Henning, “Pressure-induced growth of metal whiskers,” *J. Appl. Phys.*, vol. 35, no. 2, pp. 459–460, 1964.

[5] S. C. Britton, “Spontaneous growth of whiskers on tin coatings: 20 years of observation,” *Trans. IMF*, vol. 52, no. 1, pp. 95–102, 1974.

[6] B. D. Dunn, “Metallurgy and reliability in spacecraft electronics,” *Met. Mater.*, vol. 34, pp. 32–40, 1975.

[7] B. D. Dunn, “Whisker formation on electronic materials,” *Circuit World*, 1976.

[8] B. D. Nordwall, “Air force links radar problems to growth of tin whiskers,” *Aviat. Week Space Technol.*, pp. 65–70, 1986.

[9] J. Capitano and J. Devaney, “Reliability improvement by removing electrical interrupts in equipment which result in retest–OK, Can’t Duplicate, No Defect Found,” in *IEEE 1986 National Aerospace and Electronics Conference-NAECON*, 1986, vol. 4.

[10] L. Corbid, “Constraints on the use of tin plate in miniature electronic circuits,” in *Proceedings 3rd International SAMPE Electronics Conference*, 1989, pp. 773–779.

[11] K. M. Cunningham and M. P. Donahue, “Tin whiskers: Mechanism of growth and prevention.,” in *4. International SAMPE Electronics Conference*, 1990, pp. 569–575.

[12] R. P. Diehl, “Significant characteristics of tin and tin-lead contact electrodeposits for electronic connectors,” *Met Finish*, vol. 91, no. 4, pp. 37–42, 1993.

[13] M. Ishii, T. Kataoka, and H. Kurihara, “Whisker Problem in the Ultra-fine Pitch Circuits, R&D Center Mitsui Mining & Smelting Co,” *Ltd IMAPS Proceeding*, p. 379, 1999.

[14] M. Ishii, T. Kataoka, and H. Kruihara, “Whisker problem in ultra-fine pitch circuits,” in *Proceedings of the 12th European Microelectronics and Packaging Conference*, 1999, pp. 379–385.

[15] C. Stevens, “Relay failures induced by the growth of tin whiskers. A Case Study,” in *IEEE Boston Reliability Chapter 38th Annual Spring Reliability Symposium*, 2001, pp. 1–6.

[16] J. Khuri, “Agency action notice,” *Gov.-Ind. Data Exch. Program GIDEP*, 2002.

[17] “National regulation: enforcement services,” *GOV.UK*. https://www.gov.uk/guidance/national-regulation-enforcement-services (accessed Sep. 07, 2021).

[18] C. Xu, Y. Zhang, C. Fan, J. Abys, L. Hopkins, and F. Stevie, “Understanding whisker phenomenon: The driving force for whisker formation,” *CircuiTree(USA)*,

vol. 15, no. 5, p. 10, 2002.

[19] J. H. Richardson and B. R. Lasley, “Tin whisker initiated vacuum metal arcing in spacecraft electronics,” in *1992 Government Microcircuit Applications Conference*, 1992, vol. 18, pp. 119–122.

[20] J. Brusse, “A discussion of the significance of metal whisker formation to the high Reliability community,” *QSS Group Inc NASA Goddard*, 2003.

[21] K.-N. Tu, C. Chen, and A. T. Wu, “Stress analysis of spontaneous Sn whisker growth,” in *Lead-Free Electronic Solders*, Springer, 2006, pp. 269–281.

[22] S. Lal and T. D. Moyer, “Role of intrinsic stresses in the phenomena of tin whiskers in electrical connectors,” *IEEE Trans. Electron. Packag. Manuf.*, vol. 28, no. 1, pp. 63–74, 2005.

[23] C. L. Rodekohr *et al.*, “Correlation of intrinsic thin film stress evolution and imc growth with whisker growth,” in *2011 IEEE 57th Holm Conference on Electrical Contacts (Holm)*, 2011, pp. 1–7.

[24] W. Nakao, M. Ono, S.-K. Lee, K. Takahashi, and K. Ando, “Critical crack-healing condition for SiC whisker reinforced alumina under stress,” *J. Eur. Ceram. Soc.*, vol. 25, no. 16, pp. 3649–3655, 2005.

[25] E. Chason, N. Jadhav, W. L. Chan, L. Reinbold, and K. S. Kumar, “Whisker formation in Sn and Pb–Sn coatings: Role of intermetallic growth, stress evolution, and plastic deformation processes,” *Appl. Phys. Lett.*, vol. 92, no. 17, p. 171901, 2008.

[26] K. Fujiwara and R. Kawanaka, “Observation of the tin whisker by micro-Auger

electron spectroscopy," *J. Appl. Phys.*, vol. 51, no. 12, pp. 6231–6232, 1980.

[27] U. Lindborg, "Observations on the growth of whisker crystals from zinc electroplate," *Metall. Trans. A*, vol. 6, no. 8, p. 1581, 1975.

[28] J. L. Agilent *et al.*, "iNEMI Recommendations on Lead-Free Finishes for Components Used in High-Reliability Products Version 4 (12-1-06)".

[29] D. A. Pinsky, "The role of dissolved hydrogen and other trace impurities on propensity of tin deposits to grow whiskers," *Microelectron. Reliab.*, vol. 48, no. 5, pp. 675–681, 2008.

[30] R. Kawanaka, K. Fujiwara, S. Nango, and T. Hasegawa, "Influence of impurities on the growth of tin whiskers," *Jpn. J. Appl. Phys.*, vol. 22, no. 6R, p. 917, 1983.

[31] M. E. Williams and G. R. Stafford, "Whisker & Hillock Formation on Sn, Sn-Cu and Sn-Pb Electrodeposits WJ Boettinger*, CE Johnson, LA Bendersky, K.-W. Moon".

[32] Y. W. Lin, Y.-S. Lai, Y. L. Lin, C.-T. Tu, and C. R. Kao, "Tin whisker growth induced by high electron current density," *J. Electron. Mater.*, vol. 37, no. 1, pp. 17–22, 2008.

[33] I. Matsubara, H. Tanigawa, T. Ogura, H. Yamashita, M. Kinoshita, and T. Kawai, "Preparation and critical current density of Bi2Sr2Ca2Cu3O10+ x superconducting whiskers," *Appl. Phys. Lett.*, vol. 57, no. 23, pp. 2490–2491, 1990.

[34] X. Zhang, L. Xu, S. Du, W. Han, J. Han, and C. Liu, "Thermal shock behavior of SiC-whisker-reinforced diboride ultrahigh-temperature ceramics," *Scr. Mater.*, vol. 59, no. 1, pp. 55–58, 2008.

[35] C. T. J. Low, R. G. A. Wills, and F. C. Walsh, "Electrodeposition of composite coatings containing nanoparticles in a metal deposit," *Surf. Coat. Technol.*, vol. 201, no. 1–2, pp. 371–383, 2006.

[36] R. Walker and C. T. Walker, "New explanation for the brightness of electrodeposits produced by ultrasound," *Ultrasonics*, vol. 13, no. 2, pp. 79–82, 1975.

[37] J.-H. Zhao, P. Su, M. Ding, S. Chopin, and P. S. Ho, "Microstructure-based stress modeling of tin whisker growth," *IEEE Trans. Electron. Packag. Manuf.*, vol. 29, no. 4, pp. 265–273, 2006.

[38] W. J. Choi, G. Galyon, K.-N. Tu, and T. Y. Lee, "The structure and kinetics of tin-whisker formation and growth on high tin content finishes," in *Handbook of Lead-free Solder Technology for Microelectronic Assemblies*, CRC Press, 2004, pp. 868–931.

[39] H. Wang and G. S. Fischman, "Role of liquid droplet surface diffusion in the vapor-liquid-solid whisker growth mechanism," *J. Appl. Phys.*, vol. 76, no. 3, pp. 1557–1562, 1994.

[40] V. Ruth and J. P. Hirth, "Kinetics of diffusion-controlled whisker growth," *J. Chem. Phys.*, vol. 41, no. 10, pp. 3139–3149, 1964.

[41] J. Cheng, F. Yang, P. T. Vianco, B. Zhang, and J. C. Li, "Optimum thickness of Sn film for whisker growth," *J. Electron. Mater.*, vol. 40, no. 10, pp. 2069–2075, 2011.

[42] A. Kosinova, D. Wang, P. Schaaf, A. Sharma, L. Klinger, and E. Rabkin, "Whiskers growth in thin passivated Au films," *Acta Mater.*, vol. 149, pp. 154–163, 2018.

[43] X. Z. Ma *et al.*, "TiB whiskers stimulated the dynamic recrystallization behavior," *J. Alloys Compd.*, vol. 812, p. 152152, 2020.

[44] A. Skwarek, B. Illés, T. Hurtony, D. Bušek, and K. Dušek, "Effect of Recrystallization on β to α-Sn Allotropic Transition in 99.3 Sn–0.7 Cu wt.% Solder Alloy Inoculated with InSb," *Materials*, vol. 13, no. 4, p. 968, 2020.

[45] P. T. Vianco and J. A. Rejent, "Dynamic recrystallization (DRX) as the mechanism for Sn whisker development. Part I: A model," *J. Electron. Mater.*, vol. 38, no. 9, pp. 1815–1825, 2009.

[46] I. Boguslavsky and P. Bush, "Recrystallization principles applied to whisker growth in tin," in *Proc. 2003 APEX Conf*, 2003, pp. S12-4.

[47] P. T. Vianco, M. K. Neilsen, J. A. Rejent, and R. P. Grant, "Validation of the dynamic recrystallization (DRX) mechanism for whisker and hillock growth on Sn thin films," *J. Electron. Mater.*, vol. 44, no. 10, pp. 4012–4034, 2015.

[48] J. Smetana, "Theory of tin whisker growth: 'The end game,'" *IEEE Trans. Electron. Packag. Manuf.*, vol. 30, no. 1, pp. 11–22, 2007.

[49] D. Pu *et al.*, "Oxidation and thermal cycling behavior of c-AlPO4 and SiC whisker co-modified mullite deposited on SiC-C/SiC composites," *Surf. Coat. Technol.*, vol. 400, p. 126201, 2020.

[50] H.-E. Kim and A. J. Moorhead, "Oxidation behaviour and effects of oxidation on the strength of SiC-whisker reinforced alumina," *J. Mater. Sci.*, vol. 29, no. 6, pp. 1656–1661, 1994.

[51] L. M. Dorogin, M. V. Dorogov, S. Vlassov, A. A. Vikarchuk, and A. E. Romanov,

Whisker Growth and Cavity Formation at the Microscale. Rev. Adv. Mater. Tech, 2020.

[52] K. Suganuma *et al.*, "Sn whisker growth during thermal cycling," *Acta Mater.*, vol. 59, no. 19, pp. 7255–7267, 2011.

[53] K.-N. Tu, *Electronic thin-film reliability*. Cambridge University Press, 2010.

[54] K.-W. Moon *et al.*, "Observed correlation of Sn oxide film to Sn whisker growth in Sn-Cu electrodeposit for Pb-free solders," *J. Electron. Mater.*, vol. 34, no. 9, pp. L31–L33, 2005.

[55] P. Oberndorff, J. Klerk, M. Dittes, and P. Crema, "Whisker formation on Sn-plated components," 2004.

[56] E. Chason, N. Jadhav, and F. Pei, "Effect of layer properties on stress evolution, intermetallic volume, and density during tin whisker formation," *JOM*, vol. 63, no. 10, pp. 62–68, 2011.

[57] N. Jadhav, E. J. Buchovecky, L. Reinbold, S. Kumar, A. F. Bower, and E. Chason, "Understanding the correlation between intermetallic growth, stress evolution, and Sn whisker nucleation," *IEEE Trans. Electron. Packag. Manuf.*, vol. 33, no. 3, pp. 183–192, 2010.

[58] S.-H. Na, M.-R. Lee, H.-S. Park, H.-K. Kim, and S.-J. Suh, "Effect of a high-temperature pre-bake treatment on whisker formation under various thermal and humidity conditions for electrodeposited tin films on copper substrates," *Met. Mater. Int.*, vol. 20, no. 2, pp. 367–373, 2014.

[59] Y. Zhang, C. Fan, C. Xu, O. Khaselev, and J. Abys, "Tin whisker growth: substrate

effect understanding CTE mismatch and IMC formation," *CircuiTree*, vol. 17, no. 6, pp. 70–73, 2004.

[60] J. Brusse, "Tin whisker observations on pure tin-plated ceramic chip capacitors," in *Proc. AESF SUR/FIN*, 2002, pp. 45–61.

[61] J. Brusse, G. Ewell, and J. Siplon, "Tin whiskers: Attributes and mitigation," *Carts Eur.*, vol. 16, 2002.

[62] M. Dittes, P. Obemdorff, and L. Petit, "Tin whisker formation-results, test methods and countermeasures," in *53rd Electronic Components and Technology Conference, 2003. Proceedings.*, 2003, pp. 822–826.

[63] P. Oberndorff, "Intermetallic formation in relation to tin whiskers," 2003.

[64] P. Oberndorff, M. Dittes, and P. Crema, "Whisker formation on Sn plating," 2004.

[65] V. K. Glazunova, "An investigation of the conditions of spontaneous growth of filiform crystals on electrolytic coatings," *Zhurnal Prikl. Khimii*, vol. 36, no. 3, pp. 543–550, 1963.

[66] B. Rickett, G. Flowers, S. Gale, and J. Suhling, "Potential for whisker formation in lead-free electroplated connector finishes," in *Proceedings SMTA International Conference, Chicago, IL*, 2004, pp. 707–716.

[67] J. W. Osenbach *et al.*, "Sn whiskers: material, design, processing, and post-plate reflow effects and development of an overall phenomenological theory," *IEEE Trans. Electron. Packag. Manuf.*, vol. 28, no. 1, pp. 36–62, 2005.

[68] P. Su, J. Howell, and S. Chopin, "A statistical study of Sn whisker population and growth during elevated temperature and humidity tests," *IEEE Trans. Electron.*

Packag. Manuf., vol. 29, no. 4, pp. 246–251, 2006.

[69] P. Oberndorff, M. Dittes, P. Crema, P. Su, and E. Yu, "Humidity effects on Sn whisker formation," *IEEE Trans. Electron. Packag. Manuf.*, vol. 29, no. 4, pp. 239–245, 2006.

[70] J. W. Osenbach, R. L. Shook, B. T. Vaccaro, B. D. Potteiger, A. Amin, and P. Ruengsinsub, "Lead free packaging and Sn-whiskers," in *2004 Proceedings. 54th Electronic Components and Technology Conference (IEEE Cat. No. 04CH37546)*, 2004, vol. 2, pp. 1314–1324.

[71] R. D. Hilty, N. E. Corman, and H. Herrmann, "Electrostatic fields and current-flow impact on whisker growth," *IEEE Trans. Electron. Packag. Manuf.*, vol. 28, no. 1, pp. 75–84, 2005.

[72] Y. Fukuda, M. Osterman, and M. Pecht, "The impact of electrical current, mechanical bending, and thermal annealing on tin whisker growth," *Microelectron. Reliab.*, vol. 47, no. 1, pp. 88–92, 2007.

[73] S.-H. Liu, C. Chen, P. C. Liu, and T. Chou, "Tin whisker growth driven by electrical currents," *J. Appl. Phys.*, vol. 95, no. 12, pp. 7742–7747, 2004.

[74] J. Smetana, "NEMI tin whisker user group–tin whisker acceptance test requirements," in *Report of NEMI Tin Whisker Workshop, Las Vegas, NV*, 2004, pp. 1–2.

[75] K.-N. Tu, "Irreversible processes of spontaneous whisker growth in bimetallic Cu-Sn thin-film reactions," *Phys. Rev. B*, vol. 49, no. 3, p. 2030, 1994.

[76] W. B. Hutchinson, J. Oliver, M. Nylén, and J. Hagstroem, "Whisker growth from

tin coatings," in *Materials Science Forum*, 2004, vol. 467, pp. 465–470.

[77] E. J. Buchovecky, N. Du, and A. F. Bower, "A model of Sn whisker growth by coupled plastic flow and grain boundary diffusion," *Appl. Phys. Lett.*, vol. 94, no. 19, p. 191904, 2009.

[78] J. Junkasem, R. Rujiravanit, B. P. Grady, and P. Supaphol, "X-ray diffraction and dynamic mechanical analyses of α-chitin whisker-reinforced poly (vinyl alcohol) nanocomposite nanofibers," *Polym. Int.*, vol. 59, no. 1, pp. 85–91, 2010.

[79] J. W. Shin and E. Chason, "Stress behavior of electroplated Sn films during thermal cycling," *J. Mater. Res.*, vol. 24, no. 4, pp. 1522–1528, 2009.

[80] J. Weertman and J. E. Breen, "Creep of tin single crystals," *J. Appl. Phys.*, vol. 27, no. 10, pp. 1189–1193, 1956.

[81] M. D. Mathew, H. Yang, S. Movva, and K. L. Murty, "Creep deformation characteristics of tin and tin-based electronic solder alloys," *Metall. Mater. Trans. A*, vol. 36, no. 1, pp. 99–105, 2005.

[82] S. N. G. Chu and J. C. M. Li, "Impression creep of β-tin single crystals," *Mater. Sci. Eng.*, vol. 39, no. 1, pp. 1–10, 1979.

[83] A. R. Geranmayeh, G. Nayyeri, and R. Mahmudi, "Microstructure and impression creep behavior of lead-free Sn–5Sb solder alloy containing Bi and Ag," *Mater. Sci. Eng. A*, vol. 547, pp. 110–119, 2012.

[84] F. Pei, E. Buchovecky, A. Bower, and E. Chason, "Stress evolution and whisker growth during thermal cycling of Sn films: A comparison of analytical modeling and experiments," *Acta Mater.*, vol. 129, pp. 462–473, 2017.

[85] T. A. Woodrow and B. P. Works, "Tracer diffusion in whisker-prone tin platings," in *Proc. SMTA Int. Conf*, 2006, vol. 1, pp. 24–28.

[86] J. A. Thornton and D. W. Hoffman, "Stress-related effects in thin films," *Thin Solid Films*, vol. 171, no. 1, pp. 5–31, 1989.

[87] "MEASURING WHISKER GROWTH ON TIN AND TIN ALLOY SURFACE FINISHES | JEDEC." https://www.jedec.org/standards-documents/docs/jesd-22-a121a (accessed Sep. 15, 2021).

[88] L. Panashchenko, *Evaluation of environmental tests for tin whisker assessment*. University of Maryland, College Park, 2009.

[89] J. A. Thornton and D. W. Hoffman, "Stress-related effects in thin films," *Thin Solid Films*, vol. 171, no. 1, pp. 5–31, 1989.

Chapter 2.

A Whisker Growth model on Strain-Accumulation Theory

2.1 Abstract

Whiskering has been a re-emerging problem for the reliability of lead-free electronics. Though the in-layer strain has long been recognized as one of the major driving forces for whisker growth, the quantitative understanding on the relation between stress and Sn whiskering is still limited. To fill this technical gap, we develop an analytical model to represent the contributing of whisker formation through strain accumulation. The model predicts average whisker length through calculating the volume of Sn material reallocated by strain within a single whisker site, with multiple incubation environmental parameters and observed whisker density as input. We applied the model to analyze strain generation (via thermal expansion mismatch, external applied forces and DRX process) and strain relaxation processes (creep-law plasticity and material diffusion). The modeled average whisker length reaches good agreements with multiple previous experimental data with R2 reached 0.80 after a solid calibration. The sensitivity and uncertainty are conducted to evaluate the reliability of the model in response to the variations of external inputs, including deposition thickness and whisker density. The amount of DRX strain is estimated

from the model results. The application and limitation of model has ben theoretically analyzed and discussed.

2.2 Introduction

In-layer stress has long been recognized as the major driving force that governs whisker formation. Multiple sources have been documented that can contribute to in-layer stress, including but not limited to temperature change (thermal stress) [1]–[4], formation of intermetallic compound (IMC) at the interface of tin (Sn) and copper (Cu) layers (IMC stress) [5]–[9], formation of dynamic recrystallization (DRX) grains (DRX stress) [10]–[12], and mechanical stress [13]–[16].

To examine the in-layer stress state during whisker formation, the X-ray diffraction [17]–[20] and wafer curvature measurements [7], [8], [21], [22] have been applied for quantifying the in-layer stress of Sn deposition. However, due to the relaxation phenomenon of the dislocation-meditated plastic deformation and material diffusion at grain boundaries onto the expansion of localized IMC particles [23], the relationship between IMC growth and stress is still too complex to identify the role of each stress plays during whisker growing. To eliminate the existence of IMC stress, specimens with Sn deposition on silicon (Si) substrates were applied in the studies of whiskers [24]–[26], because no IMC existing in the combination of Sn and Si [27], [28].

Associated with the quantifying of in-layer stress, convincible mechanisms were also studied by researchers to theoretically depicting the growing process of whiskers.

Mathematical models were developed based on the physical theory and in-situ experimental. The models proposed by Tu (1994) [25] and Hutchinson et al (2004) [29] reveal the mass diffusion between whisker sites and attributed it to the long-range gradient of in-layer stress; they also proposed that the stress field contributing to whisker growth in a steady-state is determined by the spacings between whiskers. Buchovecky et al (2009) extended the model to involve the balance between IMC formation strain and whisker-induced relaxation phenomenon by proposing a strain generation mechanism within the deposition film [30]. Their simulation results indicated that, instead of whisker spacing, the diffusion range and whisker growth rate was rather determined by the strain rate applied. Then, the stress relaxation measurement suggested that the plasticity in deposition films could be characterized by power-law creep [17], [31]–[35]. Further, Buchovecky (2010) proposed an analytic model concentrating on the whisker growing process in the presence of power-law creep (as the plasticity). Based on these works, Pei et al. (2015) [36] established a model to simulate the stress allocation strategy within whisker sites with the premise of pure stress-balanced.

However, the effect of DRX process during whiskering formation were absent in the models mentioned above. DRX is an eruption and generation process of new crystallites during the course of hot deformation, which can highly govern the flow behavior during deformation. With such characteristic, in-layer stress originated from DRX process is induced to deposition films, and has made DRX process another major source of whisker formation. Yoo et al. (1997) reported the significant role the DRX

stress plays in the formation of SiC whiskers, and the strain rate introduced by thermal change and/or external applied stress can lead the total in-layer strain rate exceeding the required threshold to initial DRX process [37]. Vianco et al. (2015) proposed a DRX-related mechanism, attributing the different formation process of needle and hillock whiskers to the different microstructure beneath deposition surface [38], and experimentally validated the trigger effect of strain rate to the occurrence of whiskers with different morphologies [38], [39].

Promoted by the absence of stress originated from DRX process in models, we propose an analytic model to predict the average whisker length with external incubation environmental and internal material constants as input. We apply a constant named "biased strain" to represent the existence of unpredictable and unknown elements into the whisker growth process. We evaluate the simulated results of the model against the data collected through a literature survey. We discussed the mechanism of strain sources contributing to whisker growth.

2.3 Model Description

The predictive model for whisker formation proposed in this study is based on the theory of stress-driven mechanism for whisker growth, driven by multiple environmental inputs, including external stress, and thermal change stress (Figure 1). The major component of the model explicitly quantified in-layer generation, which involves material diffusion, crystal dislocation and DRX (Figure 1). In this model, a strain calculation equation is derived to predict the resultant whisker volume).

2.3.1 Geometry

The model is validated by assuming an alignment of whisker sites on the Sn layer (referred to as whisker grains), originating from models of Tu [25] and Hutchinson et al. [29] (Figure 2). With the alignment, average spacing of between each neighboring pair of whiskers is defined *2b*, which is in agreement with the whisker density *(N)*, where *N* is considered as an input value from experimental results. Therefore, the value of *b* is determined as:

$$b = \sqrt{\frac{1}{N\pi}} \tag{1}$$

We assume that each whisker site is centered at a circle zone, where all the stress and displacement only contribute to the growth of the whisker from the center grain (Figure 2). Grains are considered as a unit cell in this model. Each whisker, associated with the grain, is modeled as a cylinder with radius *a*, extending throughout the thickness of the Sn film to the whisker tip. The thickness of Sn film is noted as *h*, and the length from the deposition surface to whisker tip is noted as *l*. Factors governing the nucleation process is not taken into consideration in this model, and we assumed a maximum nucleation rate when whiskers grains began to expand.

Given the axially symmetric geometry of the model (Figure 2), the stress and strain within the whisker zone can be expressed in a cylindrical coordinate. The flux of diffusion materials and stress are considered being uniform regarding the layer depth. Thus, the variable *r* ($a \le r \le b$) is the only independent variable governing the stress

model. Therefore, we can quantify a biaxial-symmetric planar state in one whisker site:

$$\begin{cases} \sigma_{rz} = \sigma_{\theta z} = \sigma_{r\theta} = 0 \\ \sigma_{rr} = \sigma_{\theta\theta} \equiv \sigma_r(r) \\ \sigma_{zz} = \sigma_z(r,\theta) = \sigma_z \end{cases} \tag{2}$$

σ_{rr}, $\sigma_{\theta\theta}$ and σ_{zz} represent stress in cylindrical coordinates. In many works, external load has been applied onto Sn layers [10], [13], [40]–[42], which can be represented into the model through σ_{zz} component. Due to the uniformity assumption of in-layer stress, σ_{rr} and $\sigma_{\theta\theta}$ can be taken as variables with only radial dependence, and multiple θ-independent stress sources can be involved in the model though these two components, including the thermal expansion mismatch originated from different coefficients of thermal expansion (ΔCTE) between depositions and substrates [3], [4], [21], [36], [43], and expansion of intermetallic compound and single crystal growth [5], [7], [42], [44], [45], etc. However, due to the micro size of the model (micrometers), most stress source would not variate much within a whisker site, so the $\sigma_z(r,\theta)$ can be taken as a constant σ_z.

The concept of critical strain for whisker is induced into this model. Critical strain is defined as the minimum strain as the grain boundary that stimulate the growth of whiskers [10], [11]. When the strain at the boundary rises over ε_{cr}, all the material diffusing through grain boundaries is assumed to be incorporated to whisker formation and can be counted as an available feedstock for whisker growth. We are assumed that all resistance to material diffusion under layer surface only exist at grain boundaries, and the diffusion of materials on the surface is resisted by a passivating layer, which is consistent with the experimental observations [42], [46].

2.3.2 Equation Derivation

In this model, Sn layer is considered as anisotropic continuum, and can accommodate both elastic and plastic deformation, as well as material diffusion driven by in-layer stress. The Si substrate is considered thick and rigid, restricting vertical displacement. Meanwhile, the characteristics of whisker zone are universal to all zones, resulting in no displacement at any boundaries, and the total in-zone planal strain components must equal to zero all the time. These fundamental hierarchal requirements result in the following strain balance equation:

$$\varepsilon_{total,r}(r,t) = \varepsilon_e + \varepsilon_p + \varepsilon_d + \varepsilon_{bias} \tag{3}$$

where ε_e represents the elastic strain, ε_p represents the plastic strain, ε_d represents strain of material diffusion, and ε_{bias} represents a value in strain to balance the theoretical and experimental results, which represents the sum of all those strain sources not involved in the first three terms. Now we will move on to establish appropriate expressions for each strain rate so that the strain rate balancing equation can be expressed as a function of stress.

Multiple sources have been tested to exert external strain to Sn films in previous studies. Regarding the fundamental isotropic prerequisites of this model, the external strain sources are finally settled on the thermal expansion mismatch, and vertical applied external stress, including the environmental gas pressure:

$$\varepsilon_e = \varepsilon_{thermal\ expansion} + \varepsilon_{applied} + \varepsilon_{pressure} \tag{4}$$

In most cases, external applied stress and gas pressure do not varying largely during incubation [13], [47], while temperature is usually applied as the controlling

parameter in many studies [3], [4], [10], [11], [48], [50]. During thermal expansion, the strain rate is corresponding to the thermal variation rate. As the Sn layer thickness is relatively thin compared to Si substrate, $\varepsilon_{thermal\ expansion}$ is corresponding to temperature changing rate:

$$\varepsilon_{thermal\ expansion} = \Delta\alpha \cdot T \tag{5}$$

where $\Delta\alpha$ is the difference of coefficients of thermal expansion ("CTE") between deposition and substrate material. The final expression for ε_e can be expressed as:

$$\varepsilon_e = \left(\sigma_{applied} + \sigma_{gas\ pressure}\right)\frac{(1+\nu)(1-2\nu)}{E\nu} + \Delta\alpha \cdot T \tag{6}$$

The expression of plastic strain ε_p is corresponding to the assumption of rate-dependent plasticity, associated with the power-law stress sensitivity for the Sn film. Referring to the experiments described in [32], [54], and the theories in [36], the plastic strain rate can be formulated as:

$$\dot{\varepsilon_{p}}_{ij} = \dot{\varepsilon}_0^p \exp\left(-\frac{Q_{cr}}{kT}\right)\left(\frac{\sigma_v}{\sigma_0}\right)^m \left(\frac{3\sigma'_{ij}}{2\sigma_e}\right) \tag{7}$$

where $\dot{\varepsilon}_0^p$, Q_{cr}, and σ_0 are material characteristic strain rate, activation energy, and stress exponent, respectively. σ_v is the von Mises stress:

$$\sigma_v = \sqrt{\frac{3}{2}\sigma'_{ij}\sigma'_{ij}} \tag{8}$$

And σ'_{ij} is the deviatoric stress which can be transferred from stress as:

$$\sigma'_{ij} = \sigma_{ij} - \frac{1}{3}\delta_{ij}\sigma_{kk} \tag{9}$$

In this model, no hardening condition is assumed, leading to a constant nominal yield stress σ_0. The stress vectors are expressed in cylinder coordinates, so $\sigma'_{rr} = \sigma'_{\theta\theta} = \sigma/3$, and $\sigma_v = |\sigma|$, resulting in the plastic strain rate to be equi-biaxial, which can be

expressed as:

$$\dot{\varepsilon_p} = \dot{\varepsilon}_0^p \exp\left(-\frac{Q_{cr}}{kT}\right)\left(\frac{|\sigma|}{\sigma_0}\right)^m \left(\frac{\sigma}{2|\sigma|}\right) \#(10)$$

The plastic strain can then be expressed in the following equations:

$$\varepsilon_p = \int_0^t \dot{\varepsilon}_0^p \exp\left(-\frac{Q_{cr}}{kT}\right)\left(\frac{|\sigma|}{\sigma_0}\right)^m \left(\frac{\sigma}{2|\sigma|}\right) dt \quad (11)$$

The in-layer diffusion is driven by chemical potential μ [55], [56], which can be shortly expressed as

$$\mu = -\Omega\sigma \quad (12)$$

where Ω represents Sn atomic volume. With this expression, the in-layer volume flux of material $\vec{J_v}$, driven by the gradient of chemical potential [57], can be written as:

$$\vec{J_v} = -\frac{D_{eff}}{kT}\nabla\mu \quad (13)$$

where D_{eff} is the effective diffusivity, and in the agreement of the grain boundary self-diffusivity D_{gb} as:

$$D_{eff} = \frac{\delta}{G} D_{gb} = D_0 \exp\left(-\frac{Q_{gb}}{kT}\right) \quad (14)$$

where δ is the boundary thickness, G is the grain size, D_0 is the pre-exponential coefficient for grain boundary diffusion, and Q_{gb} is the activation energy for grain boundary. The value of grain size G is either extracted from experimental data, from references data, or estimated with the following equation when the grain size information was absent from references:

$$G = 2a = 2k_G h^{0.5} \quad (15)$$

where k_G represents the grain size constant [58].

The in-layer volume flux of material results in the volumetric strain rate $\dot{e}_d$ in the

following form that:

$$\dot{e}_d = -\nabla \cdot \overrightarrow{J_v} \tag{16}$$

Then we can obtain the expression of the stress-strain relation in diffusion:

$$\begin{aligned} \dot{\varepsilon}_d &= \frac{1}{3}\dot{e}_d \\ &= -\frac{1}{3}\frac{D_{eff}}{kT}\nabla^2\mu \end{aligned} \tag{17}$$

The $\frac{1}{3}$ factor results from the model assumption that isotropic strain is led by material diffusion on each axis of coordinate. In this model, column coordinate is applied, and $\dot{\varepsilon}_d$ can be written as:

$$\dot{\varepsilon}_d = -\frac{1}{3}\frac{D_{eff}}{kT}\left(\frac{\partial^2\sigma}{\partial r^2} + \frac{1}{r}\frac{\partial\sigma}{\partial r}\right) \tag{18}$$

As a result, the diffusion strain ε_d is finally settled as:

$$\varepsilon_d = -\frac{1}{3}\int \frac{D_{eff}}{kT}\left(\frac{\partial^2\sigma}{\partial r^2} + \frac{1}{r}\frac{\partial\sigma}{\partial r}\right) \tag{19}$$

$$\varepsilon_d = -\frac{1}{3}\int \frac{(1+\nu)(1-2\nu)D_{eff}\Omega}{E\nu kT}\left(\frac{\partial^2\varepsilon}{\partial r^2} + \frac{1}{r}\frac{\partial\varepsilon}{\partial r}\right)dt \tag{20}$$

The total strain at any time and position of the film surface can be written as:

$$\begin{aligned} \varepsilon_{total,r}(r,t) = \left(\sigma_{applied} + \sigma_{gas\ pressure}\right)\frac{(1+\nu)(1-2\nu)}{E\nu} + \Delta\alpha \cdot T \\ + \int_0^t \dot{\varepsilon}_0^p \exp\left(-\frac{Q_{cr}}{kT}\right)\left(\frac{|\sigma|}{\sigma_0}\right)^m \left(\frac{\sigma}{2|\sigma|}\right)dt \\ -\frac{1}{3}\int \frac{(1+\nu)(1-2\nu)D_{eff}\Omega}{E\nu kT}\left(\frac{\partial^2\varepsilon}{\partial r^2} + \frac{1}{r}\frac{\partial\varepsilon}{\partial r}\right)dt + \varepsilon_{bias} \end{aligned} \tag{21}$$

Multiple studies contributed whisker growth to the volume reallocation of the deposition films. In this model, the volume reallocation amount can be estimated through the strain equation:

$$V_{d,v}(t) = \Delta h \cdot \pi(b^2 - a^2) + \int_b^a 2\pi r \cdot h \cdot \left(\varepsilon_{total,r}(r,t) - \varepsilon_{cr,w}\right) dr + 2\pi bh \cdot u_{r=b} \quad (22)$$

where h represents the deposition thickness, Δh is the thickness reduce during the incubation [25], $\varepsilon_{cr,w}$ is the critical strain for whisker formation from the deposition film, and the last term "$2\pi bh \cdot u_{r=b}$" represent the volume reallocation amount at the boundary from the outer site. Different from the material yield strain, $\varepsilon_{cr,w}$ represents the strain of the film can possess without creating lateral displacement, when vertical deformation does not take place and no whiskers start to grow. Here, we combine the ε_{bias} term in $\varepsilon_{total,r}(r,t)$ with the $-\varepsilon_{cr,w}$ term to be a new constant ε'_{bias}, where:

$$\varepsilon'_{bias} = \varepsilon_{bias} - \varepsilon_{cr,w} \quad (23)$$

Then the growth volume of the whisker at the center place of the model, can be expressed as:

$$V_{whisker}(t) = L\pi a^2 \quad (24)$$

where L represents the length of the whisker. By the geometry of the model, the whisker growth at the center consumes all the vertical deformation of the film, where

$$V_{d,v}(t) = V_{whisker}(t) \quad (25)$$

and we can have:

$$L\pi a^2 = \Delta h \cdot \pi(b^2 - a^2) + \int_b^a 2\pi r \cdot h \cdot \left(\varepsilon_{total,r}(r,t) + \varepsilon'_{bias}\right) dr + 2\pi bh \cdot u_{r=b} \quad (26)$$

Then the average whisker length can be estimated as:

$$L = \Delta h \cdot \left(\frac{b^2}{a^2} - 1\right) + \frac{2h}{a^2} \int_b^a \left(\varepsilon_{total,r}(r,t) + \varepsilon'_{bias}\right) r dr + \varepsilon_{r=b} \quad (27)$$

to complete an estimation of whisker length. Given the model describes a united whisker site on the film, the length L represents the average whisker length of grown from this film.

2.3.3 Boundary Conditions

The whisker sites described in this model are assumed to be aligned to cover the deposition film without overlapping neighboring ones. As a result, zero flux condition on the outer boundary should be imposed. Besides, whisker sites are assumed to be identical, resulting in symmetric stress and strain allocation at boundaries of whisker sites, as well as the displacement caused by strain. To hold these amounts to both sides at the boundary, we can obtain values at outer boundary ($r = b$):

$$\begin{cases} u_r(r = b) = 0 \\ \sigma(r = b) = 0 \\ \varepsilon(r = b) = 0 \end{cases} \quad (28)$$

At the inner boundary ($r = a$), the boundary conditions are different.

The time of whisker growth occurrence is defined at $t=t_0$, and the inner boundary condition is time-dependent to t_0, which can be described as follows. Before the whisker nucleated, i.e. $t < t_0$, due to the spatially uniformity assumption throughout deposition film, the strain (corresponding to stress σ') at the whisker grain ($r = a$) is same as the rest place of the deposition, without any difference in stress gradient driving diffusive material flux during this period (Figure 3a); while ever since the whisker begins to nucleate ($t > t_0$), the strain at the whisker grain is specified to be the critical value $\varepsilon_{cr,w}$ [36]:

$$\varepsilon(r = a, t \geq t_0) = \varepsilon_{cr,w} \quad (29)$$

Such boundary condition is fixed ever since the nucleation of whiskers, and a gradient in strain and stress is developed (and also in correspondent radial stress)

which provide continuous driving force to whisker growth. Such stress gradient also makes it possible to maintain the material diffusion inside the whisker site as the result of the enhanced relaxation phenomenon to the surrounding grains , and stress is accumulated at the whisker root and released during whisker growth [8], [31]. In the meantime, due to the stress release phenomenon, the whisker grows with the stress amount descending, and the strain ε'' at boundaries is also decreasing, as reported by the experimental results of Pei et al. (2017) [36] (Figure 3b). Further, with such release keeps functioning, the spatially uniform strain will finally fall to around $\varepsilon_{cr,w}$, when the whisker growth ceases (Figure 3c). The stress gradient is reduced with the stress decrease inside the whisker site, and the material flux will vanish finally when stress in the site has fallen below the critical stress, corresponding to the critical stress of whisker $\varepsilon_{cr,w}$.

The value of the $\varepsilon_{cr,w}$ is governed by multiple parameters, including deposition and substrate material constants (the existence of intermetallic, oxidation, as well as the different expansion ratio of different compound, modulus, Poisson's ratio) [8], [51], the occurrence of other phenomenon (dynamic recrystallization) [10], the working or storage conditions (temperature, humidity, gas pressure) [59], [60], etc., leading to complexity in value settlement of $\varepsilon_{cr,w}$.

2.3.4 Input Parameters

Multiple inputs are involved in the simulation. Numerous previous studies have

reported that the mechanical behavior and the material diffusivity vary significantly with respect to compositions, impurities, microstructure and textures [35], [49]–[51]. Due to the lack of experimental data and measurement, parameters $\dot{\varepsilon}_0^p$, Q_{cr}, Q_{gb}, D_0 and m are treated as fitting parameters with reference values extracted from Pei et al. (2017) which assumes the same deposition and substrate material and similar incubations [36]. The sensitivity will also be discussed in the following chapter to evaluate the variation of the parameter and the reliability of the proposed model.

2.3.5 Model Calibration

Numerical constants and the reference values applied for simulations are listed in Table 1. Other symbols mentioned in this model associated with definitions are list in Table 2.

The model simulation focuses on estimating the average whisker length at the center of whisker site through calculating the strains introduced by the environmental inputs inside the deposition film. Besides elastic, plastic and diffusion, multiple sources could contribute to in-layer strain during whiskering process, including intermetallic expansion, DRX grain expansion, etc. However, due to lack of convincing experimental data and theoretical derivation, most of these sources cannot be quantitively represented in the model theory. ε_{bias}' is defined as the strain compensation constant involved in these strain sources. The calibration result will be discussed in the following section.

2.4 Simulation Results and Discussion

2.4.1 Simulation results

To assess the performance of the whisker length model, we conducted a comparison of simulation results against experimental data from references (Table 3), where Figure 4a present the results before calibration, and Figure 4b shows the one with ε'_{bias} calibrated to be 1.86×10^{-3} (noted as "output_1.86" hereafter).

We observed a significant improvement of model performance after the calibration of parameter ε'_{bias}. The increase of Coefficient of Determination (R^2) from 0.5 (moderate condition) to 0.8 (good condition) suggest that the model can well capture the changes on ε'_{bias} in response to the variation of environmental inputs and experimental conditions. We also found that the root-mean-square deviation (RMSD) decreased from 8.6 to 6.2, and the slope of the linear fitting line of output_1.86 is approached 1.0 (increased from 0.78), showing that the calibrated parameter elevates the accuracy of model output under different conditions (Table 4).

2.4.2 Sensitivity analysis on material properties parameters

The goal of this model is to inform the selection of material combinations that can substantially help control the whiskering problem. We therefore only concentrate on the parameters related to material properties, including σ_0, k_G, δ, m, $\dot{\varepsilon}_0^p$, Q_{cr}, Q_{gb}, D_0, and Δh, that can affect the results of the model. We conducted a sensitivity

analysis with these constants varying $\pm 50\%$ around the suggested values (Figure 5 and Table 1). The environmental inputs for test are listed in Table 5.

The analysis results reveal the sensitivity between the model and each parameter, respectively (Figure 5). The results show that the model illustrate a large sensitivity in response the changes in k_G and Δh, while other parameters: Q_{cr}, Q_{gb}, D_0, σ_0, m, δ and $\dot{\varepsilon}_0^p$, show very limited sensitivity. In principle, these two parameters can directly govern the final output with respect to the others. Here, Δh is a multiplier in the mechanical deformation term, calculated as $\Delta h \cdot \left(\frac{b^2}{a^2} - 1\right)$. The influence of Δh on model output is largely governed by deposition thickness and whisker density, because both less deposition thickness and larger whisker density can minimize the volume change from strain in the whisker site (Eq. 8). The parameter k_G governs grain size a, which is the upper limit of strain integration and the radius of whisker. An increasing k_G implies narrower strain band which contributes to whisker volume, and reduces the average whisker length with increasing radius when the total volume is decreasing [53]. The influence of other parameters on the model were limited because they only have indirectly effects on the plastic and material diffusion strains. The theoretical derivation (Appendix I) suggests that plastic and diffusion can produce small but continuous strain to the deposition film, resulting in less sensitivities in this test with 30 days incubation [28], [30], [52].

Further, under extreme environment, the model output predicts high sensitivity on several constants. For example, model predicts that whiskering problem is alleviated at low temperature environment. The sensitivity of nominal yield stress σ_0 increases

largely from a relatively low level when incubation conduction changes from room temperature (27°C) to low temperature (less than -80°C): the σ_0 increases sharply from 38.9MPa at -80°C to 90.3MPa at -160 °C [54], suppressing the average whisker length to be 2.49μm (decreased by 26%).

2.4.3 Uncertainty analysis on two key inputs

Following the sensitivity analysis, we conducted Monte-Carlo simulations to evaluate the uncertainties of the model outputs induced by the key material parameters, with the variations of key inputs: film thickness (h) and whisker density (N) (Figure 6). Here, we need to clarify that whisker density determines the dimension of modeled whisker site (Eq. 1), while the whisker site size (b) and film thickness (h) are linearly related to the lateral and vertical direction in the displacement volume calculation part. Here we collect the reference range for each parameter from literatures, respectively (Table 6).

10,000-cases Monte-Carlo simulations for the two inputs h and N are then conducted (Figure 6), with the material parameters randomly selected within the suggested ranges following the Gaussian distribution (Table 6). The simulation results are plotted in Figure 6a and 6b, with linear and polynomial fittings conducted for two inputs and R^2 values approaching 1, respectively (Table 7). For easy expression on values of linear fitting parameters, the unit for N are expressed as "k/cm^2". The maximum uncertainty variations of -13.97% and +16.52% for h, and -11.71% and

+12.53% for N. We need to acknowledge that the model has a moderate uncertainty in predicting whisker length in response to the variations in h and N. Nevertheless, this uncertainty range (-13.97% to +16.52%) still falls within an acceptable level for the practical use.

2.4.4 Elements in the constant ε'_{bias}

This model defines one free parameter (ε'_{bias}) for calibration, which implicitly involving two physical elements (ε_{bias} and $\varepsilon_{cr,w}$), which require further discussions. The element ε_{bias} represents sum of the strain originated from sources other than the elasticity, plasticity and material diffusion. Besides these three strains, multiple sources engaged in whiskering process have been studied, most concentrating on intermetallic compound (IMC) expansion [1], [4], [44], [45], [55] and dynamic recrystallization (DRX) [10], [11], [37]. The expansion of IMC has long been recognized as one of the major stress sources of whisker growth. However, the existence of IMC is beyond our consideration in this model, because the model targets on Sn/Si samples aiming to eliminate the existence of IMC. Discarding the strain of IMC expansion, the model concentrates on the effect of pure environmental parameters such as humidity [56], [57], gas pressure [13], [58], external stress [31], [36], [43], and temperature [31], [59]. On the other hand, DRX is a spontaneous process occurring at any position on deposition surface where strain exceeding critical strain, and induce in-layer strain to film through resultant DRX grain expansion [10]. Obviously, the contribution of strain

by DRX cannot be ignored in the process of whisker formation.

With scant quantitative theories for DRX strain, we cannot directly calculate the value of DRX strain in deposition film. However, in this study, with the value of the sum strain ε'_{bias} estimated from experimental data in this study, we can apply the critical strain calculation methods to constrain the value for DRX strain. The parameter $\varepsilon_{cr,w}$ is defined as a strain threshold determining the occurrence of whisker eruption. Similarly, in DRX theory, a concept of critical strain ε_c is also defined as the threshold for occurrence of DRX process, and DRX strain is considered as the major strain source in these studies [10]–[12], [60], [61]. As a result, we can apply:

$$\varepsilon_{cr,w} = \varepsilon_c \tag{30}$$

Multiple methods have been summarized to calculate the ε_c (Table 8). Here, we apply the equation reported by Yang (2020) basing on the surface energy to obtain a critical strain expression [60]:

$$\varepsilon_c = \sqrt{{18h\gamma^2}/{M^2a^2}} \tag{31}$$

The detailed derivation process refers to Appendix II.

With the surface energy of β-Sn measured by Eckold et al. (2015) as 0.0535eV/Å^2 [62], associated with parameters input in this study, we obtain ε_c as $2.46 \times 10^{-5} mm/mm$.

Besides, Pei et al. applied 15MPa as the critical stress which defined the threshold of whisker growth. Similarly, applying the material theory, another value of ε_c as $4.64 \times 10^{-4} mm/mm$ is obtained as the critical strain.

Currently there is no reasonable data or method to determine the correctness

between these two values. However, with the ε'_{bias} tested as $1.86 \times 10^{-3} mm/mm$, according to the definition of ε'_{bias}, we can roughly extrapolate the strain created by DRX process. The resultant values of DRX expansion are $1.88 \times 10^{-3} mm/mm$ and $2.32 \times 10^{-3} mm/mm$, respectively. Different from plastic and diffusion strain, such values make the DRX to be distinguishing in multiple strain sources, and the elastic strain is comparable to it only when strong external stress or sharp thermal change is applied. Such conclusion re-emphasizes the major role of DRX strain plays in whiskering problem.

On the other hand, the amount of DRX strain might be slightly overestimated, because the strain still be affected by other elements, which can potentially pose indirectly effects on one or several strain-generating process, i.e., the IMC expansion (not applied on Sn/Si samples), the humidity, the oxidation and corrosion, electromigration, etc. For humidity, we should notice that all the data applied in this study are assumed or incubated under certain humidity closed to room temperature (Table 3). As reported by Oberndorff et al. (2006) and Crandall et al. (2011), whisker density and length is extremely sensitive to different humidity incubation [57], [63]. However, the simulation results of different gas pressure are incorrectly simulated while against the reported data (Table 9). This fact strongly questions the assumption that different humidity only influences the whiskering process through the gas pressure. For oxidation and corrosion, despite the Sn/Si combination, Oberndorff et al. (2006) incubated whiskers on Sn/Cu and Sn/FeNi42 samples, and observed severe oxidation and corrosion on Sn layers under high humidity, which were taken as the third majority

of whiskers besides CTE mismatch and IMC growth [57]. Unfortunately, with lack of comparable data, the strain caused by these two factors can not be well quantified in this study. Dynamic simulations for these two processes as well as the DRX and IMC expansion will significantly affect the accuracy and application of this model.

2.5 Conclusion

In the present work, the whisker growth mechanism is considered as a phenomenon of volume displacement and reallocation of deposition material. As a result of in-layer strain, deposition volume displacement is attributed to multiple internal and external causes, including severe thermal change or cycling, external force or torque, power-law creep, in-layer material diffusion, etc. The accumulated strain is examined and quantitatively studied. Prompted by these mechanistic understanding, we developed a strain-based model that established on one united whisker site, with radius-related strain being expressed during with certain incubation duration. This enables the prediction of whisker length grown at the center of the model associated with certain incubation parameters.

The major contributions of this study are summarized as follows:

(1) An analytical model is proposed based on the representation of the strain at any radius of a whisker site where the parameters of deposition displacement volume is expressed as a resultant value of strain accumulation, and the length of the whisker at the site center is predicted with incubation parameters.

(2) Experimental data for average whisker length from previous studies are

collected and organized. The key constants in the model are carefully calibrated to accommodate these experimental data. The final R^2 value of the linear fitting line of simulated vs. experimental data is 0.80, and RMSD is 6.229.

(3) A series of sensitivities test involving 6 material constants are conducted to examine the prediction variation. Two constants with large sensitivities to the model are distinguished. Different sensitivities of these constants reveals that the elastic strain plays the major role during short-time incubation.

(4) Two Monte-Carlo simulations on key input parameters (film thickness and whisker density) of the model are conducted for uncertainty test. The accepTable 5ariation ranges of -13.97% and +16.52% for h, and -11.71% and +12.53% for N are reported, which validate the reliability of the model.

(5) The output prediction of the model is examined on two key input parameters. Correlation of the two parameters to the whisker length prediction is established, plotted, and expressed in linear and polynomial form, which enables the whisker length estimation according to input values.

(6) Previous value estimations for the critical strain of whisker growth are collected and examined. These values are applied to calculate the strain induced by DRX expansion and other potential elements. The major role of DRX expansion in whiskering process is examined and emphasized with value estimated from experimental data.

2.6 Reference

[1] K. S. Kim, C. H. Yu, and J. M. Yang, “Tin whisker formation of lead-free plated leadframes,” *Microelectron. Reliab.*, vol. 46, no. 7, pp. 1080–1086, 2006.

[2] E. K. Snipes, G. T. Flowers, P. Lall, and M. J. Bozack, “Impact of thermal cycling and background gas environment on tin whiskering,” in *2014 IEEE 60th Holm Conference on Electrical Contacts (Holm)*, 2014, pp. 1–7.

[3] K. Suganuma *et al.*, “Sn whisker growth during thermal cycling,” *Acta Mater.*, vol. 59, no. 19, pp. 7255–7267, 2011.

[4] W. D. Fei, M. Hu, and C. K. Yao, “Thermal expansion and thermal mismatch stress relaxation behaviors of SiC whisker reinforced aluminum composite,” *Mater. Chem. Phys.*, vol. 77, no. 3, pp. 882–888, 2003.

[5] K. S. Kim, C. H. Yu, S. W. Han, K. C. Yang, and J. H. Kim, “Investigation of relation between intermetallic and tin whisker growths under ambient condition,” *Microelectron. Reliab.*, vol. 48, no. 1, pp. 111–118, 2008.

[6] C.-F. Yu, C.-M. Chan, and K.-C. Hsieh, “The effect of tin grain structure on whisker growth,” *Microelectron. Reliab.*, vol. 50, no. 8, pp. 1146–1151, 2010.

[7] N. Jadhav, E. J. Buchovecky, L. Reinbold, S. Kumar, A. F. Bower, and E. Chason, “Understanding the correlation between intermetallic growth, stress evolution, and Sn whisker nucleation,” *IEEE Trans. Electron. Packag. Manuf.*, vol. 33, no. 3, pp. 183–192, 2010.

[8] E. Chason, N. Jadhav, W. L. Chan, L. Reinbold, and K. S. Kumar, “Whisker formation in Sn and Pb–Sn coatings: Role of intermetallic growth, stress evolution,

and plastic deformation processes," *Appl. Phys. Lett.*, vol. 92, no. 17, p. 171901, 2008.

[9] M. T. Ahmed, M. Motalab, and J. C. Suhling, "Impact of Mechanical Property Degradation and Intermetallic Compound Formation on Electromigration-Oriented Failure of a Flip-Chip Solder Joint," *J. Electron. Mater.*, vol. 50, no. 1, pp. 233–248, 2021.

[10] P. T. Vianco and J. A. Rejent, "Dynamic recrystallization (DRX) as the mechanism for Sn whisker development. Part I: A model," *J. Electron. Mater.*, vol. 38, no. 9, pp. 1815–1825, 2009.

[11] P. EI and J. JJ, "Critical strain for dynamic recrystallization in variable strain rate hot deformation," *Isij Int.*, vol. 43, no. 5, pp. 692–700, 2003.

[12] P. T. Vianco, M. K. Neilsen, J. A. Rejent, and R. P. Grant, "Validation of the dynamic recrystallization (DRX) mechanism for whisker and hillock growth on Sn thin films," *J. Electron. Mater.*, vol. 44, no. 10, pp. 4012–4034, 2015.

[13] T. Shibutani, Q. Yu, M. Shiratori, and M. G. Pecht, "Pressure-induced tin whisker formation," *Microelectron. Reliab.*, vol. 48, no. 7, pp. 1033–1039, 2008.

[14] T. Singh and V. K. Gupta, "Analysis of steady state creep in whisker reinforced functionally graded thick cylinder subjected to internal pressure by considering residual stress," *Mech. Adv. Mater. Struct.*, vol. 21, no. 5, pp. 384–392, 2014.

[15] J. Brusse, G. Ewell, and J. Siplon, "Tin whiskers: Attributes and mitigation," *Carts Eur.*, vol. 16, 2002.

[16] U. Lindborg, "Observations on the growth of whisker crystals from zinc

electroplate," *Metall. Trans. A*, vol. 6, no. 8, p. 1581, 1975.

[17] J. Junkasem, R. Rujiravanit, B. P. Grady, and P. Supaphol, "X-ray diffraction and dynamic mechanical analyses of α-chitin whisker-reinforced poly (vinyl alcohol) nanocomposite nanofibers," *Polym. Int.*, vol. 59, no. 1, pp. 85–91, 2010.

[18] A. Abuhasan, C. Balasingh, and P. Predecki, "Residual stresses in Alumina/Silicon Carbide (Whisker) composites by X-ray diffraction," *J. Am. Ceram. Soc.*, vol. 73, no. 8, pp. 2474–2484, 1990.

[19] R. G. Schierding, "Measurement of whisker orientation in composites by x-ray diffraction," *J. Compos. Mater.*, vol. 2, no. 4, pp. 448–457, 1968.

[20] M. Sobiech, U. Welzel, E. J. Mittemeijer, W. Hügel, and A. Seekamp, "Driving force for Sn whisker growth in the system Cu–Sn," *Appl. Phys. Lett.*, vol. 93, no. 1, p. 011906, 2008.

[21] F. Pei and E. Chason, "In situ measurement of stress and whisker/hillock density during thermal cycling of Sn layers," *J. Electron. Mater.*, vol. 43, no. 1, pp. 80–87, 2014.

[22] A. E. Pedigo, C. A. Handwerker, and J. E. Blendell, "Whiskers, hillocks, and film stress evolution in electroplated Sn and Sn-Cu films," in *2008 58th Electronic Components and Technology Conference*, 2008, pp. 1498–1504.

[23] E. Buchovecky, N. Jadhav, A. F. Bower, and E. Chason, "Finite element modeling of stress evolution in Sn films due to growth of the Cu 6 Sn 5 intermetallic compound," *J. Electron. Mater.*, vol. 38, no. 12, pp. 2676–2684, 2009.

[24] M. J. Bozack, S. K. Snipes, and G. N. Flowers, "Methods for fast, reliable growth

of Sn whiskers," *Surf. Sci.*, vol. 652, pp. 355–366, 2016.

[25] K.-N. Tu, "Irreversible processes of spontaneous whisker growth in bimetallic Cu-Sn thin-film reactions," *Phys. Rev. B*, vol. 49, no. 3, p. 2030, 1994.

[26] F. Pei, A. F. Bower, and E. Chason, "Quantifying the rates of Sn whisker growth and plastic strain relaxation using thermally-induced stress," *J. Electron. Mater.*, vol. 45, no. 1, pp. 21–29, 2016.

[27] W. J. Boettinger, C. E. Johnson, L. A. Bendersky, K.-W. Moon, M. E. Williams, and G. R. Stafford, "Whisker and hillock formation on Sn, Sn–Cu and Sn–Pb electrodeposits," *Acta Mater.*, vol. 53, no. 19, pp. 5033–5050, 2005.

[28] E. Chason, N. Jadhav, F. Pei, E. Buchovecky, and A. Bower, "Growth of whiskers from Sn surfaces: Driving forces and growth mechanisms," *Prog. Surf. Sci.*, vol. 88, no. 2, pp. 103–131, 2013.

[29] W. B. Hutchinson, J. Oliver, M. Nylén, and J. Hagstroem, "Whisker growth from tin coatings," in *Materials Science Forum*, 2004, vol. 467, pp. 465–470.

[30] E. J. Buchovecky, N. Du, and A. F. Bower, "A model of Sn whisker growth by coupled plastic flow and grain boundary diffusion," *Appl. Phys. Lett.*, vol. 94, no. 19, p. 191904, 2009.

[31] J. W. Shin and E. Chason, "Stress behavior of electroplated Sn films during thermal cycling," *J. Mater. Res.*, vol. 24, no. 4, pp. 1522–1528, 2009.

[32] J. Weertman and J. E. Breen, "Creep of tin single crystals," *J. Appl. Phys.*, vol. 27, no. 10, pp. 1189–1193, 1956.

[33] M. D. Mathew, H. Yang, S. Movva, and K. L. Murty, "Creep deformation

characteristics of tin and tin-based electronic solder alloys," *Metall. Mater. Trans. A*, vol. 36, no. 1, pp. 99–105, 2005.

[34] S. N. G. Chu and J. C. M. Li, "Impression creep of β-tin single crystals," *Mater. Sci. Eng.*, vol. 39, no. 1, pp. 1–10, 1979.

[35] A. R. Geranmayeh, G. Nayyeri, and R. Mahmudi, "Microstructure and impression creep behavior of lead-free Sn–5Sb solder alloy containing Bi and Ag," *Mater. Sci. Eng. A*, vol. 547, pp. 110–119, 2012.

[36] F. Pei, E. Buchovecky, A. Bower, and E. Chason, "Stress evolution and whisker growth during thermal cycling of Sn films: A comparison of analytical modeling and experiments," *Acta Mater.*, vol. 129, pp. 462–473, 2017.

[37] Y.-C. Yoo, J.-S. Jeon, and H.-I. Lee, "The effect of SiC whiskers on the hot-deformation behavior of SiCw/AA2124 composites," *Compos. Sci. Technol.*, vol. 57, no. 6, pp. 651–654, 1997.

[38] P. T. Vianco, M. K. Neilsen, J. A. Rejent, and R. P. Grant, "Validation of the dynamic recrystallization (DRX) mechanism for whisker and hillock growth on Sn thin films," *J. Electron. Mater.*, vol. 44, no. 10, pp. 4012–4034, 2015.

[39] P. T. Vianco *et al.*, "Mitigation of Long Whisker Growth Based upon the Dynamic Recrystallization Mechanism," *J. Electron. Mater.*, vol. 49, no. 1, pp. 888–904, 2020.

[40] Y. He *et al.*, "Origin of lithium whisker formation and growth under stress," *Nat. Nanotechnol.*, vol. 14, no. 11, pp. 1042–1047, 2019.

[41] K.-N. Tu, C. Chen, and A. T. Wu, "Stress analysis of spontaneous Sn whisker

growth," in *Lead-Free Electronic Solders*, Springer, 2006, pp. 269–281.

[42] E. Chason, N. Jadhav, W. L. Chan, L. Reinbold, and K. S. Kumar, "Whisker formation in Sn and Pb–Sn coatings: Role of intermetallic growth, stress evolution, and plastic deformation processes," *Appl. Phys. Lett.*, vol. 92, no. 17, p. 171901, 2008.

[43] Y. Fukuda, M. Osterman, and M. Pecht, "The impact of electrical current, mechanical bending, and thermal annealing on tin whisker growth," *Microelectron. Reliab.*, vol. 47, no. 1, pp. 88–92, 2007.

[44] X. Hou, R. Zhang, and D. Fang, "Novel whisker-reinforced Al2O3–SiO2 aerogel composites with ultra-low thermal conductivity," *Ceram. Int.*, vol. 43, no. 12, pp. 9547–9551, 2017.

[45] A. Baated, K.-S. Kim, and K. Suganuma, "Effect of intermetallic growth rate on spontaneous whisker growth from a tin coating on copper," *J. Mater. Sci. Mater. Electron.*, vol. 22, no. 11, pp. 1685–1693, 2011.

[46] J. W. Shin and E. Chason, "Stress behavior of electroplated Sn films during thermal cycling," *J. Mater. Res.*, vol. 24, no. 4, pp. 1522–1528, 2009.

[47] M. J. Bozack, E. K. Snipes, and G. T. Flowers, "Influence of small weight percentages of Bi and systematic coefficient of thermal expansion variations on Sn whiskering," *IEEE Trans. Compon. Packag. Manuf. Technol.*, vol. 7, no. 3, pp. 338–344, 2016.

[48] E. R. Crandall, *Factors governing tin whisker growth*. Springer Science & Business Media, 2013.

[49] R. J. McCabe and M. E. Fine, "Creep of tin, Sb-solution-strengthened tin, and SbSn-precipitate-strengthened tin," *Metall. Mater. Trans. A*, vol. 33, no. 5, pp. 1531–1539, 2002.

[50] T. Chen and I. Dutta, "Effect of Ag and Cu concentrations on the creep behavior of Sn-based solders," *J. Electron. Mater.*, vol. 37, no. 3, pp. 347–354, 2008.

[51] M. J. Esfandyarpour and R. Mahmudi, "Microstructure and tensile behavior of Sn–5Sb lead-free solder alloy containing Bi and Cu," *Mater. Sci. Eng. A*, vol. 530, pp. 402–410, 2011.

[52] J. Bernardini, P. Gas, E. D. Hondros, and M. P. Seah, "The role of solute segregation in grain boundary diffusion," *Proc. R. Soc. Lond. Math. Phys. Sci.*, vol. 379, no. 1776, pp. 159–178, 1982.

[53] K. Tsuji, "Role of grain boundary free energy & surface free energy for tin whisker growth," in *Proc. of the IPC/JEDEC 4th Intl. Conf. on Lead-Free Electronic Components and Assemblies*, 2003, pp. 21–22.

[54] "Tin, Sn." http://www.matweb.com/search/DataSheet.aspx?MatGUID=64d7cf04332e428dbca9f755f4624a6c&ckck=1 (accessed Aug. 09, 2021).

[55] K. S. Kim, C. H. Yu, S. W. Han, K. C. Yang, and J. H. Kim, "Investigation of relation between intermetallic and tin whisker growths under ambient condition," *Microelectron. Reliab.*, vol. 48, no. 1, pp. 111–118, 2008.

[56] E. R. Crandall, G. T. Flowers, P. Lall, and M. J. Bozack, "Whisker growth under controlled humidity exposure," in *2011 IEEE 57th Holm Conference on Electrical*

Contacts (Holm), 2011, pp. 1–6.

[57] P. Oberndorff, M. Dittes, P. Crema, P. Su, and E. Yu, "Humidity effects on Sn whisker formation," *IEEE Trans. Electron. Packag. Manuf.*, vol. 29, no. 4, pp. 239–245, 2006.

[58] G. C. Wei and P. F. Becher, "Development of SiC-whisker-reinforced ceramics," *Acad R Sci ColonBrussels Bull SeancesBelgium*, vol. 64, no. 2, 1985.

[59] T. Fang, M. Osterman, and M. Pecht, "Statistical analysis of tin whisker growth," *Microelectron. Reliab.*, vol. 46, no. 5–6, pp. 846–849, 2006.

[60] F. Yang, "A note on the effect of surface energy on the growth of a tin whisker," *Philos. Mag. Lett.*, vol. 100, no. 10, pp. 486–493, 2020.

[61] X. J. Wang, X. S. Hu, Y. Q. Wang, K. B. Nie, K. Wu, and M. Y. Zheng, "Microstructure evolutions of SiCp/AZ91 Mg matrix composites during hot compression," *Mater. Sci. Eng. A*, vol. 559, pp. 139–146, 2013.

[62] P. Eckold, M. S. Sellers, R. Niewa, and W. Hügel, "The surface energies of β-Sn—A new concept for corrosion and whisker mitigation," *Microelectron. Reliab.*, vol. 55, no. 12, pp. 2799–2807, 2015.

[63] E. R. Crandall, G. T. Flowers, P. Lall, and M. J. Bozack, "Whisker growth under controlled humidity exposure," in *2011 IEEE 57th Holm Conference on Electrical Contacts (Holm)*, 2011, pp. 1–6.

[64] J. Weertman, "Compressional creep of tin single crystals," *J. Appl. Phys.*, vol. 28, no. 2, pp. 196–197, 1957.

[65] J. Svoboda, F. D. Fischer, P. Fratzl, and E. Kozeschnik, "Modelling of kinetics in

multi-component multi-phase systems with spherical precipitates: I: Theory," *Mater. Sci. Eng. A*, vol. 385, no. 1–2, pp. 166–174, 2004.

[66] J. Svoboda and F. D. Fischer, "Modelling for hydrogen diffusion in metals with traps revisited," *Acta Mater.*, vol. 60, no. 3, pp. 1211–1220, 2012.

[67] M. G. Martin, A. P. Thompson, and T. M. Nenoff, "Effect of pressure, membrane thickness, and placement of control volumes on the flux of methane through thin silicalite membranes: a dual control volume grand canonical molecular dynamics study," *J. Chem. Phys.*, vol. 114, no. 16, pp. 7174–7181, 2001.

Table 1 Numerical constants with input values and definitions

Definition	Symbol	Value	Unit	Ref
Young's modulus	E	41.6	GPa	※*Strength of Materials*
Poisson's ratio	ν	0.33	-	※*Strength of Materials*
Boltzmann's constant	k	$1.38*10^{-23}$	$m^2kgs^{-2}K^{-1}$	※*Strength of Materials*
CTE mismatch between Sn and Si	$\Delta\alpha$	$1.7*10^{-5}$	$^oC^{-1}$	※*Strength of Materials*
Sn atomic volume	Ω	$2.7*10^{-29}$	m^3	※*Strength of Materials*
Nominal yield stress of Sn	σ_0	⸸11	MPa	‡MatWeb
Grain size constant	k_G	1.57	$\mu m^{0.5}$	Tsuji (2003)
Grain boundary width	δ	0.5	nm	Vianco et al. (2015)
Stress exponent for power-law creep	m	2.2	-	Vianco et al. (2015)
Characteristics strain rate for power-law creep	$\dot{\varepsilon}_0^p$	$9.6*10^{-2}$	s^{-1}	Pei et al. (2017)
Activation energy for power-law creep	Q_{cr}	0.415	eV	Pei et al. (2017)
Activation energy for grain boundary diffusion	Q_{gb}	0.399	eV	Pei et al. (2017)
Pre-exponential coefficient for grain boundary diffusion	D_0	$1.7*10^{-5}$	m^2s^{-1}	Bernardini et al. (1982)
Step height of whisker site	Δh	0.3	nm	Tu (1994)

※ James M.Gere, Barry J.Goodno. *Strength of Materials,* ISBN-10: 8131509273.

⸸ @ 300 K

‡ MatWeb: http://www.matweb.com/search/DataSheet.aspx?MatGUID=64d7cf04332e428dbca9f755f4624a6c

Table 2 Symbols with definitions in this model

Definition	Symbol	Unit
Average whisker radius	a	μm
Half of average whisker spacing	b	μm
Whisker density	N	cm^{-2}
Average whisker length	L	μm
Incubation duration	t	s
Temperature	T	K
Elastic Strain	ε_e	-
Creep Strain	ε_c	-
Diffusion Strain	ε_d	-
Strain caused by DRX grain expansion	ε_{rec}	-
Strain caused by CTE mismatch between deposition and substrate	$\varepsilon_{thermal\ expansion}$	-
Rate of Creep Strain	$\dot{\varepsilon}_c$	s^{-1}
Strain bias	ε_{bias}	-
Effective diffusivity	D_{eff}	m^2s^{-1}
Grain boundary self-diffusivity	D_{gb}	m^2s^{-1}
Deposition film thickness	h	μm
Grain size	G	μm

Table 3. Experimental data of Sn/Si samples from previous studies and related simulation results

Ref.	Thickness	Incubation Method	Incubation Duration	Whisker Density	Average Length	Avg. Len. STDV
	μm	-	days	cm^{-2}	μm	μm
Fang et al. 2006	5.0	150 °C for 2h, 50 °C for 2w, RT afterwards	240	14240	24.0	12.7
			390	14360	25.7	11.5
			540	14520	26.0	11.4
Crandall et al. 2010	0.16	RT, RH	50	15195	6.6	9.1
			116	38152	6.5	7.9
Crandall et al. 2011	0.2	RT, RH	32	4585	4.3	
				7991	16.5	
			96	15850	5.3	
				12051	26.8	
Crandall et al. 2011	0.15	RT, multiple humidity	30	14409	3.3	
				11134	3.7	
			137	110296	7.1	
				164527	3.7	
Snipes et al. 2014	0.1	Thermal cycling: -40~125°C	24	9120	43.7	
			54	25760	30.5	
		RT, N^2	140	8320	13.3	8.4
		RT	150	1729	14.2	
Bozack et al. 2016	0.12	RT, RH	426	116000	11.7	
	0.2			12000	56.0	
Bozack et al. 2017	0.5	Thermal cycling: -40~125°C	37	165100	34.0	

Table 4 Simulation errors from output_0 and output_1.86 to reference results

	Slope	**R^2**	**RMSD (m/m)**
Output_0	0.728	0.495	8.631
Output_1.86	1.000	0.796	6.229

Table 5 Test values for incubation environment parameters

Environmental Inputs	Value
Incubation Duration	30 days
Minimum Temperature	298 K
Maximum Temperature	298 K
External Stress (downward to Sn surface)	0 Pa
Gas Pressure	$1.01*10^5$ Pa
Key Inputs	**Value**
Film Thickness	0.2 μm
Whisker Density	15000 cm^{-2}

Table 6 Constants involved for uncertainty and test results

Symbol	**Suggested Value**	**Units**	**Value Variation**
⸸k_G	1.57	-	1.49 1.65
⸸δ	0.5	nm	0.48 0.53
⸸m	2.2	-	1.2 6
⸸$\dot{\varepsilon}_0^p$	0.096	s^{-1}	0.0957 0.0963
‡σ_0	11	MPa	4.5 20.1
⸸Δh	0.3	nm	0.25 0.35

⸸Extracted from Table I, with ±5% as variation

‡11Mpa is measured @ room temperature (27ºC), and the variation values refers to yield stress @-40ºC and 200ºC, respectively.

Table 7 Statistics data of fitting lines for Figure 6e and 6f

	Equation	Constants	Values	R^2	Uncertainty Range
Figure 5b	$y = c + dx$	c	1.277	1	-13.97%
		d	7.854		+16.52%
Figure 5d	$y = c_0 + c_1x + c_2x^2 + c_3x^3 + c_4x^4 + c_5x^5 + c_6x^6 + c_7x^7 + c_8x^8 + c_9x^9$	c_0	10.246	0.999	-11.71%-
		c_1	-0.938		
		c_2	0.044		
		c_3	-0.001		
		c_4	$1.974*10^{-5}$		
		c_5	$-2.082*10^{-7}$		
		c_6	$1.394*10^{-9}$		
		c_7	$-5.738*10^{-12}$		+12.53%
		c_8	$1.321*10^{-14}$		
		c_9	$-1.304*10^{-17}$		

Table 8 Methods to calculate ε_{cr}

Ref.	Equations
Barnett et al. (2000)	$\varepsilon_c = \left[A(1-a)\dot{\varepsilon}(0.0145)^{\frac{1}{n}}\right]^{\frac{1}{1-a}}$
Barnett et al. (2002)	$\varepsilon_c = Ad_0^{0.3}(\dot{\varepsilon}\ e^{\frac{312000}{RT}})^{0.17}$ $\varepsilon_c = 0.0026\dot{\varepsilon}^{0.24}e^{\frac{56500}{RT}}$
Pettersen et al. (2003)	$\varepsilon_c = \frac{D_o}{2\sqrt{3}\cdot\delta}$
Vianco et al. (2015)	$\varepsilon_c = AD_o^m Z^n$
Huang and Loge (2016)	$\varepsilon_c = \ln\left(\frac{K_1 D_o}{\delta}\right)$
†Yang (2020)	$\varepsilon_c = \sqrt{18h\gamma^2 / M^2 a^2}$

†Yang proposed calculation of critical strain energy U_{cr}. Here we derive ε_c from this equation.

Table 9 Performance of model simulation on different humidity

Humidity (%)	†Average Whisker Length (um)	Simulation Results (um)
33.1±0.2	3.6	3.98
43.2±0.4	2.9	5.84
69.9±0.3	3.3	8.54
75.5±0.2	3.7	9.36
85.1±0.3	2.3	11.95
96.6±0.6	2.3	12.83
33.1±0.2	5.7	4.28
43.2±0.4	9.3	6.31
69.9±0.3	7.1	8.67
75.5±0.2	3.7	9.42
85.1±0.3	4.7	12.21
96.6±0.6	5.7	13.41

† Data is extracted from Crandall et al. (2011)

Table 10 Multiple methods for critical strain calculation

Ref.	Equations
Barnett et al. (2000)	$\varepsilon_c = \left[A(1-a)\dot{\varepsilon}(0.0145)^{\frac{1}{n}}\right]^{\frac{1}{1-a}}$
Barnett et al. (2002)	$\varepsilon_c = Ad_0^{0.3}(\dot{\varepsilon}\ e^{\frac{312000}{RT}})^{0.17}$ $\varepsilon_c = 0.0026\dot{\varepsilon}^{0.24}e^{\frac{56500}{RT}}$
Pettersen et al. (2003)	$\varepsilon_c = \frac{D_o}{2\sqrt{3}\cdot\delta}$
Vianco et al. (2015)	$\varepsilon_c = AD_o^m Z^n$
Huang and Loge (2016)	$\varepsilon_c = \ln\left(\frac{K_1 D_o}{\delta}\right)$
†Yang (2020)	$\varepsilon_c = \sqrt{18h\gamma^2 / M^2 a^2}$

†Yang proposed calculation of critical strain energy U_{cr}. Here we derive ε_c from this equation.

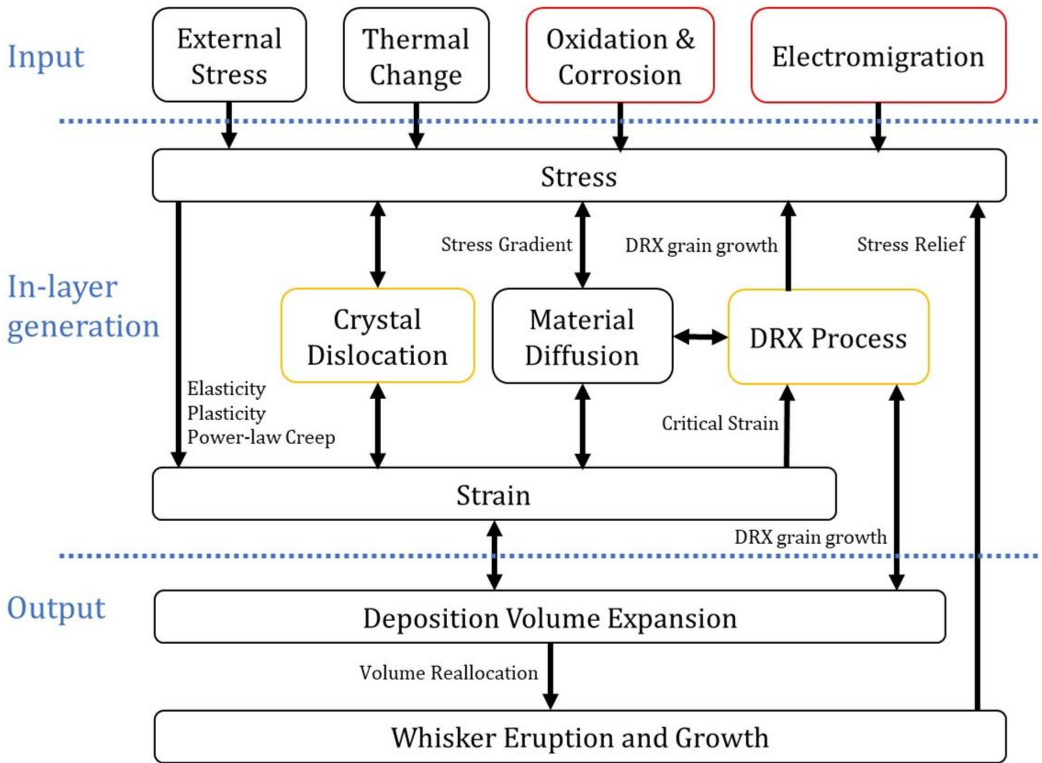

Figure 1. Analytical concept diagram for whisker formation mechanism on Sn/Si specimens. Red marks concepts not taken into consideration, and yellow marks concepts estimated without quantitative analysis in this model. Specially, the "IMC expansion" is ignored in the in-layer generation section, due to no existence of IMC between the material combination of Sn and Si.

Top View

$2b$

$r = b$

Side View

l_w

h

$d = 2a$

Whisker and Whisker Grain

Sn layer

Whisker Zone

Figure 2 Geometrical sketches for the whisker sites studied in this model. The whisker is modeled as a cylinder associated with the whisker grain, and the whisker site is the area surrounding the grain, extending to the midpoint of neighboring spacing.

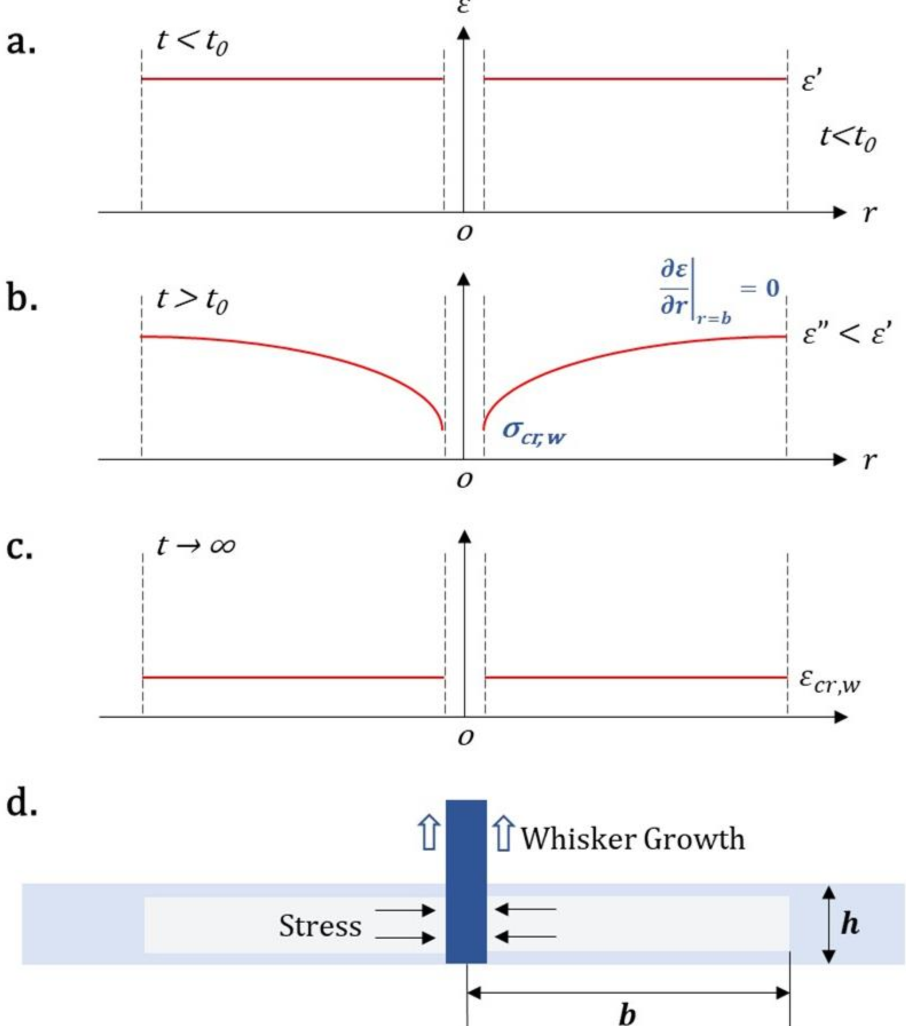

Figure 3 Sketches illustrating the stress patterns at different stages of whisker growth: (a) before; (b) after; and (c) cease of whisker growth. The spatially uniformity leads to the even stress across the site in (a) and (c), and with the stress release effect of whisker ever since its growth at t_0, the peak stress in (b) is smaller than that before t_0.

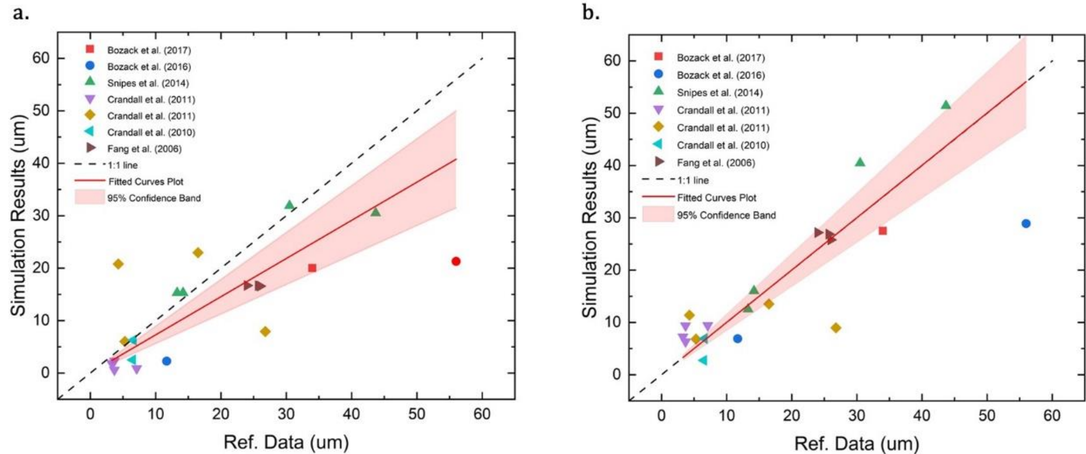

Figure 4 The comparison plots between model output and historical experimental data with value of $\boldsymbol{\varepsilon}'_{\boldsymbol{bias}}$ equals to (a) 0; and (b) 1.86*10-3. Linear fitting lines present as solid red lines associated 95% confidence bands with y-intervals fixed at 0. 1:1 reference line is illustrated as dashed line in both figures. Statistics data of linear fitting lines are shown in Table IV. With calibration on ε'_{bias} to a satisfying value, model output is in good agreement with experimental data.

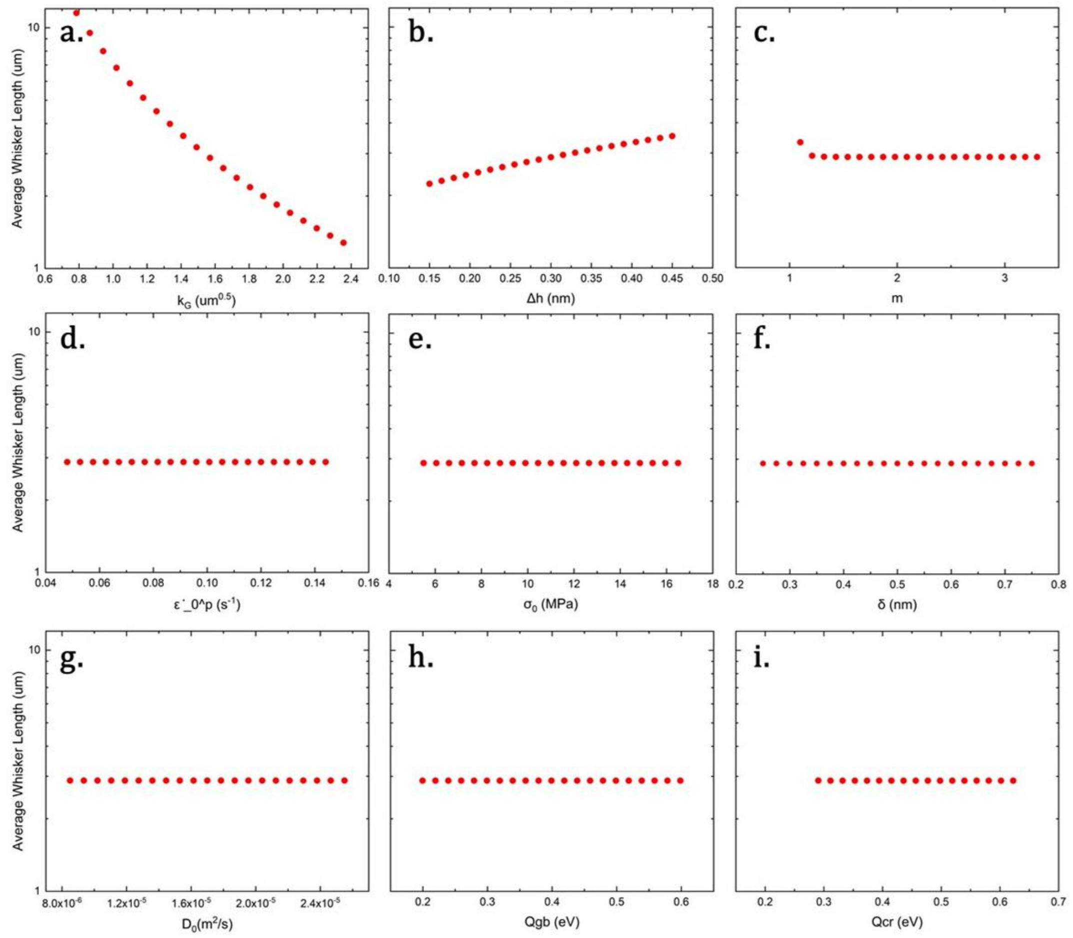

Figure 5 Sensitivity test results on parameters $\boldsymbol{k_G}$, $\Delta\boldsymbol{h}$, $\boldsymbol{m}$, $\dot{\boldsymbol{\varepsilon}}_{\mathbf{0}}^{\boldsymbol{p}}$, $\boldsymbol{\sigma_0}$, $\boldsymbol{\delta}$, $\boldsymbol{D_0}$, $\boldsymbol{Q_{gb}}$ and $\boldsymbol{Q_{cr}}$, are plotted from (a) to (i), respectively. Ranges of y-axis are set same in all figures for illustration convenience. Test statistics is presented in Table V. The tests claim that the model is more sensitive to k_G and Δh than the other parameters tested where slight linearities are present, directing to higher governing effect of grain size and depleted step height of site in film thickness on whisker length.

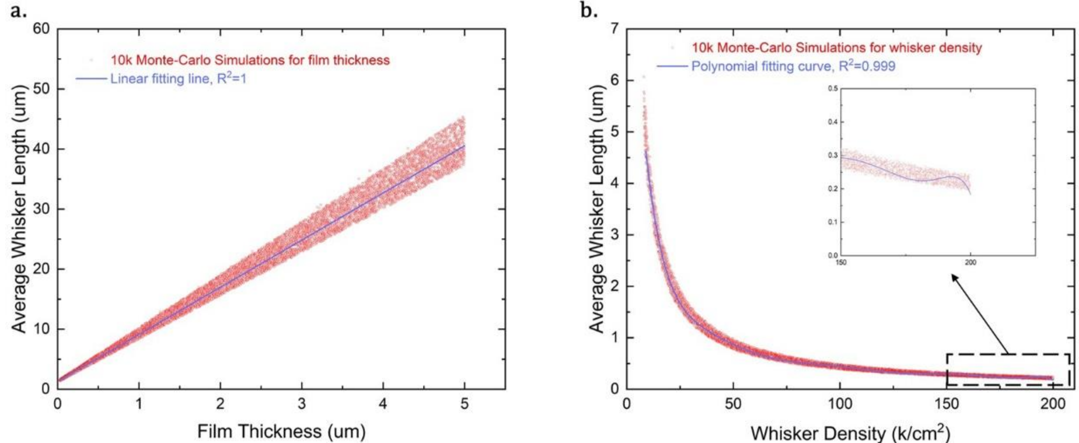

Figure 6 Monte-Carlo simulations on the two key input parameters: film thickness $\boldsymbol{h}$ and whisker density $\boldsymbol{N}$. a. plots the output of 10,000 points simulation vs h, and **b.** for and N as red circles, with 9 constants varying in certain range as Table VI listed. Linear and polynomial fitting lines are plotted in solid blue lines. Statistical data of fitting lines are listed in Table VII. The sub figure in **b.** illustrates the amplified plots in the range of 150k/cm^2 to 225k/cm^2, where the polynomial fitting line begins to present obvious fluctuation

Chapter 3.

Effects of Interrupting the Contiguous Sn Thin Film Network in Whiskering

3.1 Abstract

Tin (Sn) whiskers have threatened electronic devices for decades due to their high conductive properties and bridging failures, affecting the overall reliability of electronic devices based on Pb-free materials. In this paper, we have studied the effect on whiskering of altering the long-range contiguous film network in a thin (sub-micron) sputter-deposited 500 Å Sn film, produced by depositing tiny squares of Sn on a Si wafer through a shadow mask with successively large hole sizes ranging from 1 to 153 m in size. The deposited specimens were then divided into three groups and incubated for 34 days at room temperature, 100oC, and successive 12-hour-loop thermal cycling (-40oC < T < 125oC). We find that interrupting the contiguous Sn film network resulted in a 44% loss in whisker density when compared to comparable, but large-area continuous Sn film (1 cm x 1 cm) on silicon. A discontinuous transition in whisker growth was observed at the size of 19 m, with whisker growth absent on areas < 11.5 μm in size, observed under all three conditions. The lack of whiskering from the smallest areas of deposited Sn may be indicative of the role played by long-range diffusion and/or limited feedstock from angstrom-scale thin Sn films.

3.2 Introduction

Sn whiskers were first recognized as spontaneous crystal eruptions growing from deposited films by Hunsicker and Kenpf in 1947 [1]. Whiskers have been identified as the cause of catastrophic failures in many defense-related and high-dollar electronic devices and systems. Their formation has been attributed to a stress-relief phenomenon within the Sn film, motivated by long-range Sn diffusion and dynamic recrystallization [2], [3]. The sources of the stress can be cataloged into five major groups: (1) intermetallic compound growth at the film/substrate interface ("IMC-induced whiskers") [4]–[7]; (2) externally applied stress ("contact whiskers") [8]–[10]; (3) oxidation and corrosion of Sn and alloying elements ("corrosion whiskers") [11]–[14]; (4) electromigration ("electromigration whiskers") [15]–[18]; and (5) thermal expansion mismatch between film and substrate, particularly during thermal cycling ("thermal cycling whiskers") [19]–[22].

Many of the early studies concentrated on the deliberate introduction of external sources of stresses, which failed to adequately explain the effect of whisker incubation periods and other important drivers of Sn whiskers [23]. For instance, compressive stress was often identified as the primary condition to stimulate whisker growth, but studies eventually reported that tensile stress environments could also trigger the occurrence of whiskers [23], [24]. Furthermore, the volumetric change at the film level during metal oxidation was once considered as a major source of in-layer compressive stress; nevertheless, whiskers were observed to grow in vacuum environments with extremely low exposure to oxygen and under clean surface conditions [25]. Most

fundamental drivers of whisker formation are still being identified.

Woodrow and Works (2006) conducted an elegant work designed to understand the role of long-range Sn diffusion in whiskering by using secondary ion mass spectroscopy (SIMS) and Sn isotope tracer techniques to measure the lateral long-range atomic Sn diffusion over several thousands of microns of a Sn film [2]. Later, Vianco and Rejent proposed the dynamic recrystallization (DRX) mechanism which identified stress-induced recrystallization as the foundational mechanism stimulating whisker growth [26]. According to their theory, whisker growth initiates by local film stress, which exceeds a critical value on “DRX grains” in the film, which then recrystallize, undergo grain boundary pinning, and the grain relieves stress through the growth of a Sn whisker [27].

Inspired by the direct observation of long-range diffusion and DRX theories, this work has investigated the effect on Sn whiskering of very thin (submicron) Sn films and deliberate interruption of the continuous network of Sn in the film. The sputtered Sn coated silicon substrates were partitioned into periodic areas of Sn by depositing through a series of TEM grid apertures having varied (mostly) square size. We then incubated the specimens under three different isothermal and thermal cycling conditions and collected whisker density and “type of whisker” data through SEM evaluations.

3.3 Experimental

A series of commercial transmission electron microscope (TEM) grids with square open apertures ranging in sizes from 1μm to 153μm, were affixed atop a 1 cm x 1 cm Si (111) oriented silicon wafer [28]. The grid partitioned (masked) the wafer into tiny, small and open areas through which Sn was deposited in a magnetron sputter system. The masked areas also introduce Sn-free increments which interrupted the Sn deposits. The TEM grids are fixed onto the Si substrates before sputtering and removed immediately after sputtering, as shown in Figure 7, and detailed information citing the grid opening and gap sizes are listed in Table 11. The "Margin Density" column is calculated as follows:

$$Margin\ Density = \frac{4 \times Dimension}{(Dimension + Spacing)^2}$$

, which represents the density of total margin length on one specimen with a certain limited area size. The TEM grid named "SVQG" consisted of meshed areas with four different sizes, and whisker statistics collected from SVQG grids were sorted to these four sizes respectively.

The substrates applied for the whisker growth specimens were 1-cm square n-doped silicon wafers, and all TEM grids had the same diameter of 3.05 mm. The TEM grids were mounted on the substrates firmly by vacuum-compatible C tape to avoid Sn scattering on the tape edges; subsequent SEM and Auger electron spectroscopy (AES) examination showed that the aperture windows and tape-down procedure allowed for creation of sharply defined Sn deposits with no Sn scattering beyond the straight borders of the grid openings. Usually, two or three TEM grids were mounted

simultaneously on a single substrate to save pump down time in the sputtering chamber, which had a base pressure of 10^{-7} torr, achieved by turbomolecular pumping. The Sn films were then sputtered deposited to a thickness of 500 Ǻ, using a 99.99% pure Sn target, with an Ar plasma (currents of 0.18A±0.02A and potentials of 380V±10V) for all substrates. The 500 Ǻ film thickness was verified using AES depth profiling through the film. A magnetron sputtering system is capable of "dialing-in" various amounts of intrinsic compressive/tensile film stress without the need to stress the wafers through forced external clamping [17, 18]. The plot in Figure 8 illustrates the Ar "compressive/tensile/no stress" gas pressure conditions when sputtering Sn. The sputtered Sn films were put under intrinsic compressive stress in this study by adjusting the background Ar gas pressure in the system to 2 mTorr.

After sputtering, the deposited specimens were divided into three groups with three different incubation-temperature conditions to explore the whisker initiation and growth. One group was isothermally held at 23ºC (room temperature), one group at 100ºC (isothermal), and the final group was subjected to thermal cycling between -40ºC < T < 125ºC. The duty cycle for the thermal cycling is shown in Figure 9, which is a common cycling protocol for reliability testing [19, 20]. Each group was tested to for 34 days of incubation.

The whisker observation protocol consisted of a low magnification (1000X) scanning electron microscopy (SEM) coarse evaluation of whisker growth across each specimen, followed by a high-resolution examination (20-30kX). Regarding the average grain size of 0.5 mm, any crystal eruption larger than 2 mm in one dimension

will be taken as a whisker, regardless of different morphological characteristics such as needle-like and hillock. The areal densities were obtained by manually counting whiskers observed in five, randomly chosen 100 mm x100 mm areas of the deposited Sn film, determining the total whisker number, and then averaging this value over the total area. Only areas of limited Sn layers involved in the observation areas were obtained as “effective areas” when determining the whisker value, due to the zero possibility of whiskers incubated from void areas.

3.4 Results

The Sn whisker densities (cm^{-2}) observed for the various deposited sizes and incubation conditions are detailed in Table 12. The whisker densities vs. deposited Sn volumes and vs. deposited areal dimensions from different specimens are plotted in Figure 10(a), with 0 whisker density plots masked. And the whisker densities vs. deposited areal dimensions are plotted in Figure 10(b), and three linear fitting lines over data from 23 μm to 153 μm are also shown, with the data of control specimen masked. The deposited Sn volume is estimated by the grid dimensions and Sn layer thickness, while the deposited areal dimensions represent the typical dimensions of the limited area (edge lengths of squares, width of rectangular, and diameters of circles) (Table 11).

As the results, whisker densities were found decreasing monotonically as the deposited Sn volumes and areal sizes decrease, for each of the incubation conditions. The highest whisker density occurred with the control specimen, deposited with no

area-limiting aperture. For the largest apertured area (153μm x 153μm) the whisker density decreased by 44.2%, 77.5% and 86.0% respectively, for the 23°C, 100°C, and (-40°C < T < 125°C) cases compared to the control specimen, deposited under the same sputtering and incubation conditions. The % loss in whisker density from the control specimen is greater as the incubation temperature increases, with a trend observed for the entire range of specimens due to the linear behavior of the whisker density vs. area size characteristic over the size range between 23 μm to 153 μm. Thermal cycling, using the standard -40°C < T < 125°C range, employed in reliability studies is well-established [21] to encourage fast whisker generation, as it results in a strong thermal driver for coefficients of thermal expansion ("CTE" hereafter) mismatched materials. The other two incubation methods using steady temperature conditions typically result in weaker drivers to stimulate whisker growth [30].

The whisker densities monotonically decrease as the deposition areas get smaller. Over the areal range from 153 μm to 23 μm, the whisker densities decrease linearly under all the three incubation conditions, with R^2 values higher than 0.9 (Figure 10b). The thermal cycling slope is the largest followed by the 100°C annealing and room temperature cases. We can extend these linear fitting lines to 10000 μm to speculate the whisker densities at the scale the control specimen (10000 μm x 10000 μm): The speculated densities are 19139 cm^{-2}, 251089 cm^{-2} and 607022 cm^{-2} for the three incubation conditions, respectively, which are ~5-10 times larger than the experimental results (Table 12). This may indicate more than one whisker attenuation mechanism is present for areal sizes between 153 μm and 10000 μm, or a monotonical increasing

relationship between whisker density and areal size in a form of $density = A(1 - e^{-Bd})$, where A, B are two constants, and d represents the areal size.

Most significantly, the whisker densities display a discontinuous downward transition when the deposition areal size decrease to 11.5 μm and below. Very few whiskers were observed on the 11.5 μm x 11.5 μm area after 100°C annealing and the 7.5 μm x 7.5 μm area under thermal cycling. No whiskers were found on 7.5 μm x 7.5 μm and 11.5 μm x 11.5 μm areas under room temperature, nor on the 7.5 μm x 7.5 μm area under 100°C annealing. Under all three incubation methods, *no whiskers* were observed on the 4 μm x 4 μm and 1 μm x 1 μm Sn deposition areas.

Moving now to describe the whisker volume, shape, and appearance, those physical characteristics of the whiskers were also highly affected by areal sizes of the Sn deposition. We observed whiskers which were "needle-like", "grass-root-like," and "hillock-like" structures, shown in Figure 11. It is notable that most whiskers from deposition areas < 54 μm x 54 μm were "hillock-like" in shape, with a smaller fraction of "needle-like" whiskers (see Figure 12).

3.5 Discussion

3.5.1 Different whisker density behaviors between deposited Sn volume and areal dimension

Although it has been noted that whisker formation is strongly related to feedstocks on multiple deposition and substrate materials [31], few researches have focused on confining whisker feedstock primarily, due to the high commercial cost

and small amount of feedstock for a whisker formation [32], [33]. In our study, we applied TEM grids during sputtering to limit the available Sn feedstock on each separated Sn layer, and we found a significant decrease in final whisker production (Table 12).

The whisker density plots clearly illustrate the monotonic retarding trend with the limited deposited areas getting smaller (Figure 10), where deposition layer limitation was proven an effective method in whisker reduction. In Figure 10a, the monotonic relationship between density and Sn volume was disturbed at 6900 mm^3 in all three incubation methods, where the data is extracted from 46 mm x 3000 mm rectangular-shaped limitation layers. After inspection, we found that these whisker density data lies between the densities of 54 mm x 54 mm and 23 mm x 23 mm layers, and the whole plot possesses an enhanced monotonic decreasing effect when we moved the 46 mm x 3000 mm data between those two, where the Figure 10b comes from.

Figure 10b concentrated on illustrating the relationship between whisker density and typical deposited areal dimension. For the 46 mm x 3000 mm case, the typical dimension is 46 mm, the shorter edge of rectangular. The smooth relationship between these two factors implies that the whisker production ability of one Sn layer relies more on the typical areal dimension rather than the total feedstock. We surmise that the characteristic of stress releasement may play a major role in governing this phenomenon. For a squared-limited deposition layer with width m and length n $(m < n)$, we can analyze two thin cut sections horizontally and vertically with same width p, as shown in Fig 8. Due to the different substantial structures, some grains are deposited with high

concentration of stress from neighboring grains and results in a higher whisker production [34], [35], which were represents as blue dots in Fig 8. Due to lack of related distribution theory, we assume those high-whisker-likelihood grains were evenly distributed on Sn surfaces, with density $\rho_g = \frac{N_g}{mn}$, where N_g represents the number of high-whisker-likelihood grains on this layer. The effect of stress releasing is linearly related to the length of limitation edges, resulting in the same stress release amount F in Figure 14b and 8c on their same width p. Such stress releasing effect was mainly concentrating on to the high-whisker-likelihood grains for their higher stress concentration, and help to decrease the whisker production. However, with the same F in Figure 14b and 8c, the section in Figure 14c possesses less high-whisker-likelihood grains than the section in Figure 14b: $N_{g,c} = \rho_g pm < \rho_g pm = N_{g,b}$, and the stress release amount on each grain is more significant than the other ones $\frac{F}{N_{g,c}} = \frac{F}{\rho_g pm} > \frac{F}{\rho_g pn} = \frac{F}{N_{g,b}}$, reducing the whisker production likelihood of grains. As a result, sections with less high-whisker-likelihood grains usually produce less whisker, which result in a higher coherence of whisker decreasing effect on the shorter edge of a squared-limited deposition layer.

3.5.2 Effects of Sn layer thickness on whisker shapes and volumes

In our previous work, Snipes et al. (2014) conducted a similar experiment on a Sn/Si specimen [36]. The Sn deposit thickness using in this study (0.05 μm) is 10X thicker than the ones used in Snipes et al. (2014) (0.5 μm), keeping the remainders

(systems, methods, and air repressure during sputtering, material, incubation duration, and incubation methods) consistent.

There are some differences existing between these two studies, where lies the whisker density. The whisker densities in Snipes et al. (2014) were reported $5\times10^{3}cm^{-2}$ through room temperature incubation and 1.4×10^{5} cm^{-2} after thermal cycling, which are 29% and 33% larger than the results in this study (Table 12). Such differences emphasize the whisker density variations can be caused by the thickness of deposited layer.

A second difference between the two studies lies in the predominance of characteristic whisker morphologies. In this study, we observed a large fraction of "hillock" whiskers using very thin Sn films (Figure 13), which implies most needle-like whiskers erupt from a hillock at its base, while most of the whiskers in Snipes et al. (2014) are needle likes shaped. A theoretical explanation to the growth of hillock whisker can be adopted from Vianco and Rejent (2009) [27]. Conventionally, a whisker begins to grow by momentary pinning of boundaries (Figure 15a) [37]. The loss of pinning allows the in-layer growth of DRX grain (Figure 15b). With cyclic occurrences, the intermittent pinning of grain boundary creates steps, with steps getting smaller as the strain energy decreases, until the growth ceases completely (Figure 15c) [21, 22]. Due to the unexpected grain allocations beneath the upper surface of the Sn layer, such growth is confined by neighboring grains, resulting in a hillock whisker morphology (Figure 10, 9c). However, the shapes of observed whiskers show large variations in the diffusion mechanism. The unpredictable microstructure does not

interrupt the normal diffusion of Sn atoms, but might disturb the expansion of Sn oxide or intermetallic compound atoms, which make the whisker shape irregular.

Besides, we found the volume of whiskers observed in this study is smaller in volume than the needle like ones observed in Snipes et al, (2014) [36], primarily due to the significantly short length of hillock shaped whiskers. Needle whiskers, with an average diameter of 1.4 mm and observed length varying from 22 mm to 185 mm in our experiment, possess a volume of 33.8 mm^3 to 284.6 mm^3. Hillock whiskers, as comparison, grow no larger than 8 mm^3. Although diameters of hillock are 2x to needle whiskers, their averaged short length made the volume smaller than needle whiskers. Grain boundary pinning determines needle whisker or hillock form [38], which also result in their different volumes. The diameters of whiskers reflect the size of grain from which they originated. Most hillock whiskers possess a >2X diameter compared to needle whiskers (Figure 11, 7), implying a larger size of hillock grain to needle grain. Grains are stressed from multiple grain boundary pinning, with the strain energy being lost with expansion [40]. With a larger size, hillock grains expand with a larger loss of energy than needle grain, and cease to grow in a shorter expansion duration, resulting in most hillock whiskers possessing a small size, or even ceasing growing at the early stage. On the other hand, the growing process of needle-like whiskers usually lasts longer under a suitable environment, such as thermal cycling.

3.5.3 Factors governing the whisker density from small deposition areas

3.5.3.1 Influence of Sn atoms diffusion to whisker production

The areal dependence we observe on whisker formation can be explained by the extent of long-range Sn diffusion in whisker growth (Figure 10, Table 12). Although it has been widely accepted that diffusion plays an important role in the growth of Sn whiskers [22, 23], the associated quantity investigation is still scant. To fill this knowledge gap, concerning Sn layer sizes, this study may add clues to the necessity of diffusion range scales to whisker growth. The sudden and discontinuous downward transition in whisker densities observed at the ~10-20 mm areal sizes of deposited Sn, with whisker growth *absent* on areas < 11.5 µm under all three incubation conditions may suggest a limit on the "long-range" Sn diffusion necessary to create whiskers, particularly for the submicron film thicknesses, which is typically studied in our laboratory (Figure 10). To clear illustrate the influence of long-range diffusion lack to whisker production, a comparison can be made between some previous works and ours. Both Vianco et al (2015) [38] and Lin et al (2021) [43] have remarked on the unusual features of Sn films approaching surface physics (angstrom) thicknesses, in contrast with thin film (micron) thicknesses applied in our experiment. Their largest concern was whether the Sn grain networks for their submicron films were comprised of a noncontiguous network of Sn grains, characteristic of the early stages of thin film deposition. More extensive analysis using FIB (focused ion beam) and top-down high-resolution SEM confirmed that the Sn grain networks for the thinnest Sn film in his study (0.25 mm) were interconnected over significant distances. In the case here,

while we were not able to do FIB analysis on our angstrom-scale films, we did not observe obvious breaks in the film in top-down views using high-resolution SEM, and regularly have produced abundant long whisker using such angstrom-scale films of Sn on 1cm^2 silicon specimens, which do not indicate preferred Sn diffusion paths on the Sn surface. Further, recall that the thin films deposited for this work were *all* deposited simultaneously (Figure 7a) using the same sputtering conditions, the same vacuum system, and having the same thickness ~ 500 Å yet, we observe whiskers growing in all cases except those with areal sizes < 11.5 mm. Such experimental results implied that there exists radically different grain network continuity in only the smallest deposited areal sizes.

However, the occurrence of atoms diffusion inside the deposited structures is still validated through numerical calculation. Woodrow reported rapid Sn diffusion along grain boundaries and into the Sn lattice in micron-scale thin Sn films at room temperature [2]. Diffusion of Sn along grain boundaries is known to be very rapid with a diffusion coefficient of 1.3×10^{-8} cm^2/sec at 25°C [23]. It is straightforward to determine that the time required for tin to diffuse a distance x into Sn grain boundaries at 25°C can be *estimated* from equation:

$$L = \sqrt{2Dt}$$

, where L is the mean diffusion length in one dimension, *t* is the time in seconds and D is the grain boundary diffusion coefficient. Using D = 1.3×10^{-8} cm^2/sec and x = 3.1 mm (the approximate thickness of the bright tin plating in Woodrow's experiment), t equals 3.7 seconds. There certainly appears be enough fast diffusion occurring at the

times/temperatures/length scales of the various deposited areas in our experiment, and indeed, we see whisker growth on all specimens expect the smallest area films. Further, surface diffusion is known to be even more rapid than lattice and grain boundary diffusion and the fraction of "surface" over "lattice" available for diffusion grows as feature sizes become smaller in scale. Thus, diffusion blockages or sluggish Sn diffusion kinetics inside the deposited film structures do not appear to be the major reason for the loss of whisker production with areal size scaling.

3.5.3.2 High Sn Diffusion Resistance Between the Deposited Areas

Unlike the diffusion inside deposited areas, the diffusion within the deposited structures was strictly prohibited. By creating patterned deposition areas, the sputtered Sn layers were physically distributed into micro areas surrounded by Sn free gaps (noted "void areas" hereafter). The minimum gap width (Table 11) between neighboring Sn deposits used was 1 mm, which effectively isolates the Sn deposits to diffusion only within the deposit area. This is because the diffusivity of neutral Sn atoms (measured by neutron-activation analysis) in near-intrinsic Si has been measured to be

$$D(T) = 32e^{-98000/_{RT}} \quad (1)$$

in cm^2/sec [44]. The experimental points in the D(T) function were determined at high semiconductor activation/annealing temperatures near 1300-1600 K where the D was ~ 2×10^{-15} and 2×10^{-12} cm^2/sec, respectively. When the temperature is room temperature, the D value is ~ 10^{-70} cm^2/sec, meaning there is effectively zero lattice Sn diffusion through the Si void areas between the deposited Sn areas. Lastly, no Sn was observed by AES in the Si void areas between the deposited Sn which could provide a

Sn bridge between the patterned deposits.

3.5.3.3 Mass conservation and sufficient Sn feedstock

In the whisker mechanism described by Woodrow [2], the growth of long needle-like whiskers requires a continuous supply of Sn feedstock around the region of a root whisker by means of diffusion. The Si void areas around the Sn depositions effectively decrease the available feedstock by limiting the available areas. Thus, it is also reasonable that whisker densities are observed decreasing with the areal size getting smaller. The smaller limited areas possess less long-range feedstock compared to larger ones, resulting in fewer whisker densities and/or shorter whisker lengths. The available feedstock of the specimen areas varies from 0.05 mm^3 in the smallest areas to 551.25 mm^3 in the largest ones. The observed results suggest a minimum feedstock to grow whiskers of ~2.8 mm^3 from the sizes of 7.5 mm x 7.5 mm. For example, a 153 mm x 153 mm Sn area can incubate at most 12 long needle whiskers assuming all available Sn feedstock is exhausted, with average diameter of 1.4 mm and average length of 30 mm, while this number is reduced to be 2 whiskers on a 46 mm x 46 mm limited area, and all areas with sizes below 23 mm x 23 mm are not able to incubate even one of such needle whisker. However, for hillock whiskers, this number is different: with the most common sizes of 2 mm x 1 mm x 1 mm on the observed hillock whiskers, the minimum size to incubate one hillock whisker is reduced to be 7.5 mm x 7.5 mm with the applied thickness of 500 Ǻ. The minimum limited areal size is invalidated to be 7.5 mm with whiskers start to grow from.

3.5.4 Occurrence of DRX grains within smaller deposition areas

DRX mechanism provides a solid explanation for the observed results in our study (Figure 14). Recrystallization, as a relevant phenomenon, will occur at boundaries of pre-existing grains under certain incubations (found most active under thermal cycling) [45]. The continuous occurrence of recrystallization results in DRX grains growing at the boundaries of existing grains. These growing DRX grains possess a very high degree of deformation and introduce strain energy into the sputtered layer. Finally, along with the building up strain energy and the limited horizontal growing spaces, the DRX grain will grow in the z-direction, forming a crystal eruption on the Sn surface, which also noted as a "DRX whisker" hereafter. Such DRX whiskers continuously grow with enhanced recrystallization. In conclusion, the growing of a DRX whisker is the result of the strain energy release which is introduced with the recrystallization.

It has been suggested that, with the decrease in sizes of limited areas, the densities of margins introduced by void areas are elevating, resulting in more spaces for strain energy release in one united area, and fewer whisker densities during the same incubation period (Table 12). The experimental influence of applied TEM grids onto Sn layers helps to explain the large reduction in whisker densities by observed results. In our experiment, the applied TEM grids introduced void areas which are distributed evenly on the sputtered layer (Figure 7). In DRX mechanism, these void areas act as an effective method for alleviating and dredging strain energy. The void areas provide more spaces for dislocated grains that elevate the storage limit of strain energy level in the sputtered layer (Figure 70). On the other hand, in diffusion theory, these void areas

have physically achieved the “diffusion isolation” to each Sn deposited area, which can substantially decrease the likelihood of long-range diffusion. As a result, the time interval before the appearance of vertical deformation of DRX grains is prolonged, resulting in the observed reduction in whisker densities.

The two widely acknowledged mechanisms, diffusion and DRX, direct towards different whisker volume production. In both mechanisms, the whisker formation contributes to the rearrangement of the expanded volume. Though the available feedstock is limited on any Sn layers or limited areas, the usage ratios to the feedstock of the two mechanisms are different. For the diffusion mechanism, the change in volume is induced by the forming of Sn oxidation, or intermetallic compounds [46], while diffusing is a method transporting atoms to react with oxygen or other metal atoms. The ratio, representing expanded volume vs. original deposited volume, varies according to the combination of materials. For example, this ratio is 1.509 for an Sn/Si specimen (Sn deposited onto Si substrate), which mostly depends on the forming of Sn oxidations; as a comparison, the ratio is 1.453 for an Sn/Cu specimen, contributed mostly by the formation of the Sn-Cu compound [47]. These different ratios are related to different maximum expansion volumes, and the resultant final whisker production volumes [48]. Similarly, in the DRX mechanism, the grown volume is originated from the DRX grains expansion. Thus, a similar value can be measured to represent the available feedstock for recrystallization, which is comparable to the volume change ratio in the diffusion mechanism. Note that the reference DRX ratio has not been well measured in the previous studies to the best of our knowledge. However, we expect a

significant difference in the values of DRX ratio and diffusion ratio, primarily due to the chemical reactions of the two mechanisms to a different final whisker volume production.

Our results explicitly imply a threshold of deposited size which triggers the starting point of whisker growth (Table 12). Theoretically, it is reasonable to presume that a minimum amount of accumulated stress is required to induce the formation of whiskers [49]. At any possible whisker-growing spots on the Sn layer, the accumulated stress is influenced by but not limited to the incubation temperature, the volume expansion coefficient of materials, and the available feedstock contribute to these spots:

- A proper environmental temperature supports an efficient volume expansion without melting, which may lead to a large loss of rigidity of the layer; thermal cycling, the specially designed incubation method, is the source of periodic stress accumulation.
- The volume expansion coefficient of materials (including sputtered materials and substrates) regulates the total stress introduced into the specimen by temperature changes: denser whiskers were observed on specimens with a larger difference in coefficients of sputtered material and substrates [21].

The available feedstock is regulated by many parameters, including the thickness of the Sn layer, the sizes of defined areas, some environmental parameters, and relevant parameters of the material itself.

3.5.5 Suppression prediction to whisker occurrence in limited areas

The linear correspondence (Figure 10) between areal size and whisker densities is curious. Further, the Sn-free void areas between each of the deposited areas offer a diffusion-free zone where the Sn diffusion is effectively zero. The discussion below presumes for simplicity a squared deposition area; Table 11 shows that most of the grid apertures used in this experiment were square. Assuming a represents the length of the squared area, and h represents the film thickness of the Sn layer, the available feedstock f (as the total Sn mass, mg/um^{-3}) can be represented as:

$$f = \rho_{Sn} \times a^2 \times h \tag{2}$$

where ρ_{Sn} is the density of Sn material. As discussed in section 4.2, the influence of void areas on whiskering problem in limited areas is stress relief, which is related to the perimeter of the limited areas (the length of edges defining Sn deposited areas and void areas). Here, a parameter s can be assumed to evaluating the suppression to whiskers production from the limited areal size, which can be represented as:

$$s = c_{s,f}\sqrt[3]{\frac{f}{\rho_{Sn}}} - \sqrt{l_{void}h} + n \tag{3}$$

where $c_{s,f}$ is a constant compensating the different increasing rate between $\sqrt[3]{\frac{f}{\rho_{Sn}}}$ and $\sqrt{l_{void}h}$ with the size rises, l_{void} represented the marginal length, which is equal to perimeter of the limited area, and n is an offset constant to the existing threshold mentioned in section 4.2.

To establish a predictive suppression of s regarding to the experimental results, multiple values are required for the parameters in Eq. (3). Here, due to lack of enough

theories and information, $c_{s,f}$ is assumed for one particular incubation method. The value of $c_{s,f}$ is estimated from data of Crandall [32], as shown in TABLE 14

$$c_{s,f} \cong 0.47 \quad (4)$$

Besides, it is obvious that the $c_{s,f}$ is influenced by environmental conditions, which makes them functions of the different incubation methods. Given that in all three incubation methods, the whisker densities appear to be plateauing, and the ratios of observed whisker densities are fluctuating little on sufficient large areas. The relationship among the values of $c_{s,f}$ in three incubation methods can be extracted from the work of Bozack et al. [19, 26], as

$$c_{s,f,room\ temperature} : c_{s,f,annealing} : c_{s,f,thermal\ cycling} = 1 : 3 : 6 \quad (5)$$

Then, according to the existence of whiskers incubated on different specimens, the available range of n can be derived from Table 13. With such preconditions, the available value of n can be picked in [61.83, 72.10]. Subsequently, the suppression s value can be calculated on any limited Sn-sputtered area to predict the occurrence of whiskers in this area. A negative s value represents a possibility that whiskers grow in this area, while a positive s value represents no possibility that whiskers grow.

3.5.6 Perspectives from the DRX Model of Whisker Production

The start point of the whisker growth in the cyclic DRX mechanism involves three hierarchal requirements [38], especially when needle or hillock whiskers are formed.

1. The occurrence of DRX: the strain must exceed the critical strain.

The critical strain is an evaluation parameter to assemble the five variables governing the DRX process, including stress (σ), strain (ϵ), strain rate ($^{d\epsilon}/_{dt}$), temperature (T) and initial grain size (D_o). The critical strain can be calculated as:

$$\epsilon_c = A{D_o}^m Z^n \tag{5}$$

where A, m and n are material constants. Z is the Zener-Hollomon parameter:

$$Z = \frac{d\epsilon}{dt} e^{\Delta H/_{RT}} \tag{6}$$

where ΔH is the apparent activation energy; R is the universal gas constant; and T is the temperature. In the microstructure, the strain is obtained from physical measurement of the free energy.

Vianco et al. applied external stress in their experiment to introduce strain exceeding the critical strain to grow whiskers [38]. In our experiment, with no external stress applied, the stress is mainly originated from the CTE mismatch ("ΔCTE" hereafter) [21], and the introduced creep strain during sputtering. Some ΔCTEs between deposited Sn and substrates materials are listed in TABLE 15.

Previous researchers have considered ΔCTE as a driving force to whisker formation [16, 21, 25–27]. Thermal cycling, the third incubation method applied in our experiments, is one of the most effective methods for whisker incubation [36]. That is because the cyclic temperature can provide continuous in-layer stress due to the ΔCTE between the deposited material and substrates. In our experiments, strains exceeding the critical strain were largely oriented from it in annealing and thermal cycling (Table 12). For the room temperature method, the stress from ΔCTE is far less than the other two methods, due to the lack of cyclic

and continuous temperature change and the modest temperature difference between sputtering (~18ºC) and incubation (27 ºC) for the room temperature, and 100 ºC for annealing). The stress originating from the creep strain was introduced during the formation of the deposited layer, which usually does not vary with the incubation method.

In these experiments, both the hillock and needle whiskers were observed to grow in all the three incubation methods, which validate the occurrence of DRX mechanism (Table 12). The different stresses resulting from ΔCTE in three incubation methods can support the observed difference in whisker densities, among which, thermal cycling introduces the largest ΔCTE stress to the Sn layer, followed by annealing and room temperature. As a result, whisker densities of room temperature were observed the least comparing to those in the other two methods at all the same sizes of limited areas.

2. DRX to cyclic: $D_o<2D_r$

The cyclic occurrence of DRX mechanism requires $D_o < 2D_r$, where D_o is the initial grain size, and D_r is the final gain size. In our experiment, the initial grain size was averaged to be ~0.6 mm, while the size of most final grain which had incubated whiskers was measured to be 0.4 mm to 0.5 mm. These grain size data validate the cyclic occurrence of the DRX model.

3. Grain boundary pinning (thin films): h versus D_g

Vianco et al. discussed this criteria, basing on the relationship between the grain size D_g and layer thickness h, as an important sign to predict the likelihood

to produce more needle or hillock whiskers [38]. They indicated that when $D_g > h$, grains are constrained from lateral growth, where grain boundaries pinned, and encouraged the growth of more long whiskers as compared to hillock whiskers. When $D_g \approx h$ or $D_g < h$, both long whiskers and hillock whiskers would grow.

However, the observed whisker growth did not behave as predicted by this criterion. In these experiments, the growth of long whiskers was restrained on limited areas with sizes below 46 mm x 46 mm, and began to emerge when sizes went larger than 54 mm, while hillock whiskers were observed incubated from limited areas except areas below 7.5 mm x 7.5 mm, from which no whiskers observed. These differences due to the introduced void areas.

The specimens Vianco et al. used were Si wafers with 25.4mm of diameter and 0.275mm in thickness, and Sn were evaporated onto the wafers, with no void areas introduced [38]. In our experiment, the thickness of Sn layer is 500 Å (0.05 mm), where the ratio of layer size versus layer thickness varying from 20~3,000, while this ratio of Vianco et al. was ~100 x larger (5,000~100,000). Therefore, the criteria "h versus D_g" may not work with small-scaled Sn layers dur the these great decimal differences.

To alleviate the accuracy of this criteria, we introduce a modification. This criterion needs to take the layer size into consideration, which is usually neglected in most past works where large film thicknesses are applied. For the different behavior, the layer thickness h should not be the threshold of the grain size D_g, but the following term

$$D_g / c(d) \tag{7}$$

where $c(d)$ is a functional expression relevant to layer size d. By applying the experimental results of Vianco et al. and this study, the functional expression $c(d)$ can be written as:

$$c(d) = \frac{\ln(d)}{20} \tag{8}$$

for a more accurate prediction of whisker shapes, where d represents the size of the layer, usually diameter.

3.6 Conclusion

This paper examines the whisker growth behavior on deposited Sn layers limited by TEM grids. The whisker production strategy from variations of Sn areal sizes were experimentally incubated, collecting and theoretically analyzed subjected to three independent incubation methods. The following observations and conclusions were obtained:

1) An experimental investigation was performed to examine the influence of limiting Sn layers to whiskering problem. The results confirmed the retarding effect of limited deposition layers on whisker production: as the areal size of Sn layers degrade, whisker production rate monotonically decreases. For the largest limited areas applied in this experiment, whisker densities were reduced by 44.2% at least, and no whiskers were observed on Sn layers smaller than 7.5 μm x 7.5 μm.
2) Theoretical analysis was carried out to evaluate the whisker production performance regarding to various Sn areal sizes, thicknesses and shapes of

whiskers. Regarding to diffusion and DRX mechanisms, the morphological characteristics between needle-like and hillock whiskers were oriented from the different pinning strategies around the grain where whiskers were produced.

3) The void areas, which defined limited Sn layers, was considered as the major reason to the observed whisker production strategies on small-limited areas. The high resistance of Sn atoms diffusing, the extra volume for strain energy release, and the constrains on Sn feedstock provided by void areas prevents whiskers to grow.
4) A parameter was proposed to predict the whisker production possibility on limited Sn layers. The values of involved constants were extracted from related experimental results, and the value of threshold were determined by collected data of these experiments.
5) The DRX mechanism were examined in this deposited-layer-limited case. Among the three hierarchal requirements, two were validated, and the other one was modified to involve this special case into the DRX model.

The retarding effect of limitations to Sn layers has been revealed and theoretically validated. Such limitation is a useful method to deal with whiskering threaten for most electrical devices and systems.

3.7 Reference

[1] H. Y. Hunsicker and L. W. Kempf, “Aluminum alloys for bearings,” SAE Technical

Paper, 1947.

[2] T. A. Woodrow and B. P. Works, “Tracer diffusion in whisker-prone tin platings,” in *Proc. SMTA Int. Conf*, 2006, vol. 1, pp. 24–28.

[3] F. Yang and Y. Shi, “Analysis of whisker growth on a surface of revolution,” *Phys. Lett. A*, vol. 381, no. 34, pp. 2767–2771, 2017.

[4] J. W. Osenbach *et al.*, “Sn whiskers: material, design, processing, and post-plate reflow effects and development of an overall phenomenological theory,” *IEEE Trans. Electron. Packag. Manuf.*, vol. 28, no. 1, pp. 36–62, 2005.

[5] T. Kato *et al.*, “Correlation between whisker initiation and compressive stress in electrodeposited tin–copper coating on copper leadframes,” *IEEE Trans. Electron. Packag. Manuf.*, vol. 33, no. 3, pp. 165–176, 2010.

[6] J. Hektor *et al.*, “Evidence of 3D strain gradients associated with tin whisker growth,” *Scr. Mater.*, vol. 144, pp. 1–4, 2018.

[7] B. Illés *et al.*, “Whisker growth from vacuum evaporated submicron Sn thin films,” *Surf. Coat. Technol.*, vol. 311, pp. 216–222, 2017.

[8] T. Shibutani, Q. Yu, T. Yamashita, and M. Shiratori, “Stress-induced tin whisker initiation under contact loading,” *IEEE Trans. Electron. Packag. Manuf.*, vol. 29, no. 4, pp. 259–264, 2006.

[9] R. M. Fisher, L. S. Darken, and K. G. Carroll, “Accelerated growth of tin whiskers,” *Acta Metall.*, vol. 2, no. 3, pp. 368–373, 1954.

[10] G. E. Carvell and D. J. Simons, “Effect of whisker geometry on contact force produced by vibrissae moving at different velocities,” *J. Neurophysiol.*, vol. 118,

no. 3, pp. 1637–1649, 2017.

[11] J. Jiang, J.-E. Lee, K.-S. Kim, and K. Suganuma, "Oxidation behavior of Sn–Zn solders under high-temperature and high-humidity conditions," *J. Alloys Compd.*, vol. 462, no. 1–2, pp. 244–251, 2008.

[12] A. Baated *et al.*, "Effects of reflow atmosphere and flux on Sn whisker growth of Sn–Ag–Cu solders," *J. Mater. Sci. Mater. Electron.*, vol. 21, no. 10, pp. 1066–1075, 2010.

[13] Y. Li, X. Zhang, Y. Cui, H. Wang, and J. Wang, "Anti-corrosion enhancement of superhydrophobic coating utilizing oxygen vacancy modified potassium titanate whisker," *Chem. Eng. J.*, vol. 374, pp. 1326–1336, 2019.

[14] B. Illes, B. Horváth, A. Géczy, O. Krammer, and K. Dušek, "Corrosion-induced tin whisker growth in electronic devices: a review," *Solder. Surf. Mt. Technol.*, 2017.

[15] S.-H. Liu, C. Chen, P. C. Liu, and T. Chou, "Tin whisker growth driven by electrical currents," *J. Appl. Phys.*, vol. 95, no. 12, pp. 7742–7747, 2004.

[16] C. C. Wei, P. C. Liu, C. Chen, and K.-N. Tu, "Electromigration-induced Pb and Sn whisker growth in SnPb solder stripes," *J. Mater. Res.*, vol. 23, no. 7, pp. 2017–2022, 2008.

[17] A. A. Rulev, A. V. Sergeev, L. V. Yashina, T. Jacob, and D. M. Itkis, "Electromigration in lithium whisker formation plays insignificant role during electroplating," *ChemElectroChem*, vol. 6, no. 5, pp. 1324–1328, 2019.

[18] Z. Zhang, H. Cao, Y. Xiao, Y. Cao, M. Li, and Y. Yu, "Electromigration-induced growth mode transition of anodic Cu6Sn5 grains in Cu| SnAg3. 0Cu0. 5| Cu lap-

type interconnects," *J. Alloys Compd.*, vol. 703, pp. 1–9, 2017.

[19] M. Dittes, P. Oberndorff, P. Crema, and V. Schroeder, "Tin whisker formation in thermal cycling conditions," in *Proceedings of the 5th Electronics Packaging Technology Conference (EPTC 2003)*, 2003, pp. 183–188.

[20] J. W. Shin and E. Chason, "Stress behavior of electroplated Sn films during thermal cycling," *J. Mater. Res.*, vol. 24, no. 4, pp. 1522–1528, 2009.

[21] M. J. Bozack, E. K. Snipes, and G. T. Flowers, "Influence of small weight percentages of Bi and systematic coefficient of thermal expansion variations on Sn whiskering," *IEEE Trans. Compon. Packag. Manuf. Technol.*, vol. 7, no. 3, pp. 338–344, 2016.

[22] S. Q. Wu, Z. S. Wei, and S. C. Tjong, "The mechanical and thermal expansion behavior of an Al–Si alloy composite reinforced with potassium titanate whisker," *Compos. Sci. Technol.*, vol. 60, no. 15, pp. 2873–2880, 2000.

[23] P. Jagtap, V. A. Sethuraman, and P. Kumar, "Critical evaluation of relative importance of stress and stress gradient in whisker growth in Sn coatings," *J. Electron. Mater.*, vol. 47, no. 9, pp. 5229–5242, 2018.

[24] R. Vallabhaneni *et al.*, "In situ tensile testing of tin (Sn) whiskers in a focused ion beam (FIB)/scanning electron microscope (SEM)," *Microelectron. Reliab.*, vol. 79, pp. 314–320, 2017.

[25] E. K. Snipes, G. T. Flowers, P. Lall, and M. J. Bozack, "Impact of thermal cycling and background gas environment on tin whiskering," in *2014 IEEE 60th Holm Conference on Electrical Contacts (Holm)*, 2014, pp. 1–7.

[26] P. T. Vianco and J. A. Rejent, "Dynamic recrystallization (DRX) as the mechanism for Sn whisker development. Part I: A model," *J. Electron. Mater.*, vol. 38, no. 9, pp. 1815–1825, 2009.

[27] P. T. Vianco and J. A. Rejent, "Dynamic recrystallization (DRX) as the mechanism for Sn whisker development. Part II: experimental study," *J. Electron. Mater.*, vol. 38, no. 9, pp. 1826–1837, 2009.

[28] "Electron Microscopy, Light Microscopy, Instruments and Supplies, Ted Pella, Inc." https://www.tedpella.com/ (accessed Apr. 13, 2021).

[29] J. A. Thornton and D. W. Hoffman, "Stress-related effects in thin films," *Thin Solid Films*, vol. 171, no. 1, pp. 5–31, 1989.

[30] K. Suganuma *et al.*, "Sn whisker growth during thermal cycling," *Acta Mater.*, vol. 59, no. 19, pp. 7255–7267, 2011.

[31] J.-B. Zeng, Y.-S. He, S.-L. Li, and Y.-Z. Wang, "Chitin whiskers: An overview," *Biomacromolecules*, vol. 13, no. 1, pp. 1–11, 2012.

[32] E. R. Crandall, *Factors governing tin whisker growth*. Springer Science & Business Media, 2013.

[33] T. N. Taylor and D. S. Phillips, "The surface composition and bonding of silicon carbide powders and whiskers," PhD Thesis, American Vacuum Society, 1988.

[34] P. T. Vianco and J. A. Rejent, "Dynamic recrystallization (DRX) as the mechanism for Sn whisker development. Part I: A model," *J. Electron. Mater.*, vol. 38, no. 9, pp. 1815–1825, 2009.

[35] M. J. Bozack, E. R. Crandall, C. L. Rodekohr, R. N. Dean, G. T. Flowers, and J. C.

Suhling, "High lateral resolution auger electron spectroscopic (AES) measurements for Sn whiskers on brass," *IEEE Trans. Electron. Packag. Manuf.*, vol. 33, no. 3, pp. 198–204, 2010.

[36] E. K. Snipes, G. T. Flowers, P. Lall, and M. J. Bozack, "Impact of thermal cycling and background gas environment on tin whiskering," in *2014 IEEE 60th Holm Conference on Electrical Contacts (Holm)*, 2014, pp. 1–7.

[37] J. Hektor, J.-S. Micha, S. A. Hall, S. Iyengar, and M. Ristinmaa, "Long term evolution of microstructure and stress around tin whiskers investigated using scanning Laue microdiffraction," *Acta Mater.*, vol. 168, pp. 210–221, 2019.

[38] P. T. Vianco, M. K. Neilsen, J. A. Rejent, and R. P. Grant, "Validation of the dynamic recrystallization (DRX) mechanism for whisker and hillock growth on Sn thin films," *J. Electron. Mater.*, vol. 44, no. 10, pp. 4012–4034, 2015.

[39] A. Chakraborty and P. Eisenlohr, "A full-field crystal plasticity study on how texture and grain structure influences hydrostatic stress in thermally strained β-Sn films," *J. Appl. Phys.*, vol. 124, no. 2, p. 025302, 2018.

[40] W.-H. Chen, C. Wang, P. Sarobol, J. Blendell, and C. Handwerker, "Local variations in grain formation, grain boundary sliding, and whisker growth along grain boundaries in large-grain Sn films," *Scr. Mater.*, vol. 187, pp. 458–463, 2020.

[41] V. Ruth and J. P. Hirth, "Kinetics of diffusion-controlled whisker growth," *J. Chem. Phys.*, vol. 41, no. 10, pp. 3139–3149, 1964.

[42] Y. Li *et al.*, "The influence of non-uniform copper oxide layer on tin whisker growth and tin whisker growth behavior in SnAg microbumps with small diameter,"

Mater. Lett., vol. 258, p. 126773, 2020.

[43] K. Lin *et al.*, "Growth behavior of tin whisker and hillock on Cu/Ni/SnAg micro-bumps under high temperature and humidity storage," *Mater. Lett. X*, vol. 9, p. 100060, 2021.

[44] T. H. Yeh, S. M. Hu, and R. H. Kastl, "Diffusion of tin into silicon," *J. Appl. Phys.*, vol. 39, no. 9, pp. 4266–4271, 1968.

[45] P. Sarobol, J. P. Koppes, W. H. Chen, P. Su, J. E. Blendell, and C. A. Handwerker, "Recrystallization as a nucleation mechanism for whiskers and hillocks on thermally cycled Sn-alloy solder films," *Mater. Lett.*, vol. 99, pp. 76–80, 2013.

[46] A. Baated *et al.*, "Effects of reflow atmosphere and flux on Sn whisker growth of Sn–Ag–Cu solders," *J. Mater. Sci. Mater. Electron.*, vol. 21, no. 10, pp. 1066–1075, 2010.

[47] J. Hektor *et al.*, "Scanning 3DXRD measurement of grain growth, stress, and formation of Cu6Sn5 around a tin whisker during heat treatment," *Materials*, vol. 12, no. 3, p. 446, 2019.

[48] M. Sobiech, U. Welzel, E. J. Mittemeijer, W. Hügel, and A. Seekamp, "Driving force for Sn whisker growth in the system Cu–Sn," *Appl. Phys. Lett.*, vol. 93, no. 1, p. 011906, 2008.

[49] M. Dollé, L. Sannier, B. Beaudoin, M. Trentin, and J.-M. Tarascon, "Live scanning electron microscope observations of dendritic growth in lithium/polymer cells," *Electrochem. Solid State Lett.*, vol. 5, no. 12, p. A286, 2002.

[50] J. W. Osenbach, J. M. DeLucca, B. D. Potteiger, A. Amin, R. L. Shook, and F. A.

Baiocchi, “Sn corrosion and its influence on whisker growth,” *IEEE Trans. Electron. Packag. Manuf.*, vol. 30, no. 1, pp. 23–35, 2007.

[51] J. Jiang, J.-E. Lee, K.-S. Kim, and K. Suganuma, “Oxidation behavior of Sn–Zn solders under high-temperature and high-humidity conditions,” *J. Alloys Compd.*, vol. 462, no. 1–2, pp. 244–251, 2008.

Table 11 Aperture Opening Dimensions

Grid	**Shape**	**Dimension (values in μm)**	**Spacing (μm)**	**Margin Density (μm^{-1})**
G150	Square	125×125	40	$18.37*10^{-3}$
G200	Square	90×90	35	$23.04*10^{-3}$
G600	Square	23×23	4	$131.69*10^{-3}$
G1000	Square	19×19	6	$121.6*10^{-3}$
G1500	Square	11.5×11.5	5	$168.96*10^{-3}$
G2000	Square	7.5×7.5	5	$192*10^{-3}$
CF-4/2-2C	Circles	4 μm in diameter	2	$251.2*10^{-3}$
CF-1/1-2C	Circles	1 μm in diameter	1	$697.78*10^{-3}$
G300P	Strip	46 ×3000	10	--
SVQG	Square	153×153	13	$22.20*10^{-3}$
(“Slim-Bar	Square	113×113	12	$28.92*10^{-3}$
Variable	Square	73×73	10	$42.39*10^{-3}$
Quadrant”)	Square	54×54	8	$64.21*10^{-3}$

Table 12 Sn Whisker Density vs. Deposited Size and Incubation Condition

Deposited Size (μm^2)	**Sn Layer Volume (μm^3)**	**Whisker Density (cm^{-2})**		
		Incubation Condition		
		Isothermal (T=23ºC)	***Isothermal (T=100ºC)***	***Thermal Cycling (-40ºC < T < 125ºC)***
10^4 x 10^4 (control)	5000000	3538	26856	93752
46 × 3000	6900	1548	3526	6616
153 × 153	1170.45	1930	6052	13143
125 × 125	781.25	1454	5611	12416
113 × 113	638.45	1754	5239	11199
90 × 90	405	1899	5449	10247
73 × 73	266.45	1802	4034	9695
54 × 54	145.8	1597	3772	7888
23 × 23	26.45	1578	2986	5671
19 × 19	18.05	325	1184	3625
11.5 × 11.5	6.6125	0	486	2446
7.5 × 7.5	2.8125	0	0	1103
4 μm in diameter	0.628	0	0	0
1 μm in diameter	0.03925	0	0	0

Table 13 $\boldsymbol{c_{s,f}}$ VALUE ESTIMATION

Sample #	$\boldsymbol{a}$[†]	$\boldsymbol{h}$[ǂ]	$\sqrt[3]{\frac{f}{\rho_{Sn}}}$	$\sqrt{l_{void}h}$	$\Delta\sqrt[3]{\frac{f}{\rho_{Sn}}}$	$\Delta\sqrt{l_{void}h}$	$c_{s,f}=\frac{\Delta\sqrt{l_{void}h}}{\Delta\sqrt[3]{\frac{f}{\rho_{Sn}}}}$
1	285	0.2	25.32	15.10	/	/	/
2	205	0.2	20.33	12.81	4.99	2.29	0.45
3	125	0.2	14.62	10.00	5.70	2.80	0.49
4	90	0.2	11.74	8.49	2.87	1.51	0.52
5	285	0.12	21.35	11.70	/	/	/
6	205	0.12	17.14	9.92	4.21	1.78	0.42
7	125	0.12	12.33	7.75	4.81	2.17	0.45
8	90	0.12	9.90	6.57	2.42	1.17	0.48
						Average:	**0.47**

Note:

[†] **Grid Dimension (um)**

[ǂ] **Sn layer thickness (um)**

Table 14 OFFSET VALUE CALCULATIONS

a[†]	l_{void}[ǂ]	Value of $\left(c_{s,f}\sqrt[3]{\frac{f}{\rho_{Sn}}} - \sqrt{l_{void}h}\right)$		
		Room Temperature	*Annealing*	*Thermal Cycling*
153	612	-497.91	-1493.74	-2987.48
125	500	-406.79	-1220.37	-2440.74
113	452	-367.74	-1103.21	-2206.42
90	360	-292.89	-878.66	-1757.32
73	292	-237.56	-712.69	-1425.37
54	216	-175.73	-527.19	-1054.38
46	184	-149.70	-449.09	-898.17
23	92	-74.85	-224.54	-449.08
19	76	-61.83	-185.49	-370.98
11.5	46	-37.42	-112.27	-224.54
7.5	30	-24.41	-73.22	-146.43
4	16	-13.02	-39.05	-78.10
1	4	-3.25	-9.76	-19.52

Note:

[†] **Grid Dimension (um)**

[ǂ] **Margin length (um)**

Table 15 Coefficient of thermal expansion (CTE) differences of Sn on multiple substrates, adapted from [21]

Deposited Material	Substrate Material	CTE ($10^{-6}K^{-1}$)	ΔCTE_{Sn}
	Sn	23.4	0.0
Sn (As the deposit material)	**Si**	5.1	-18.3
	Al	22.2	-1.2
	Ag	19.5	-3.9
	Brass	18.7	-4.7
	Zn	29.7	6.3
	Ni	13.0	-10.4
	Ta	6.5	-16.9
	GaAs	5.7	-17.7
	InP	4.6	-18.8

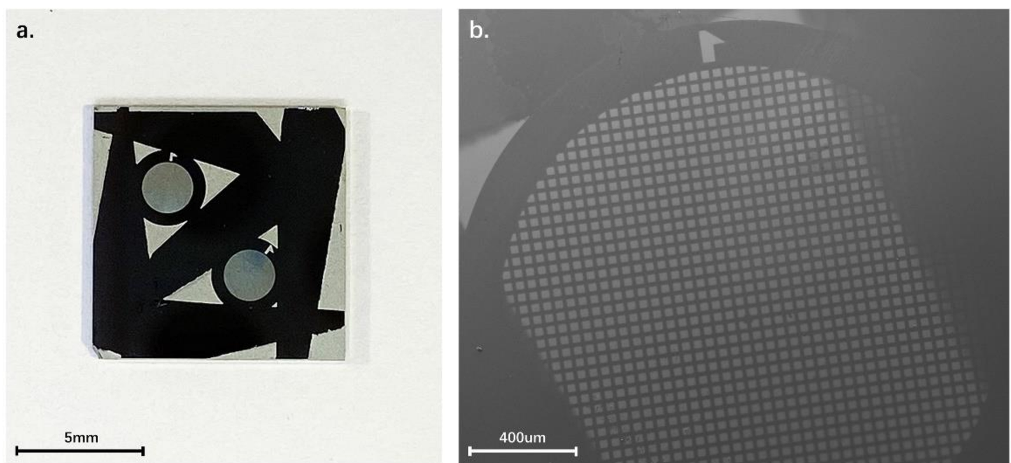

Figure 7 a) Photograph of a specimen, with TEM apertured grids and fixtures just detached. The dark areas are covered with TEM grids and fixtures during sputtering, and the light areas are sputtered with Sn with or without grids. b) A magnified view of the 23 x 23 mm grid pattern.

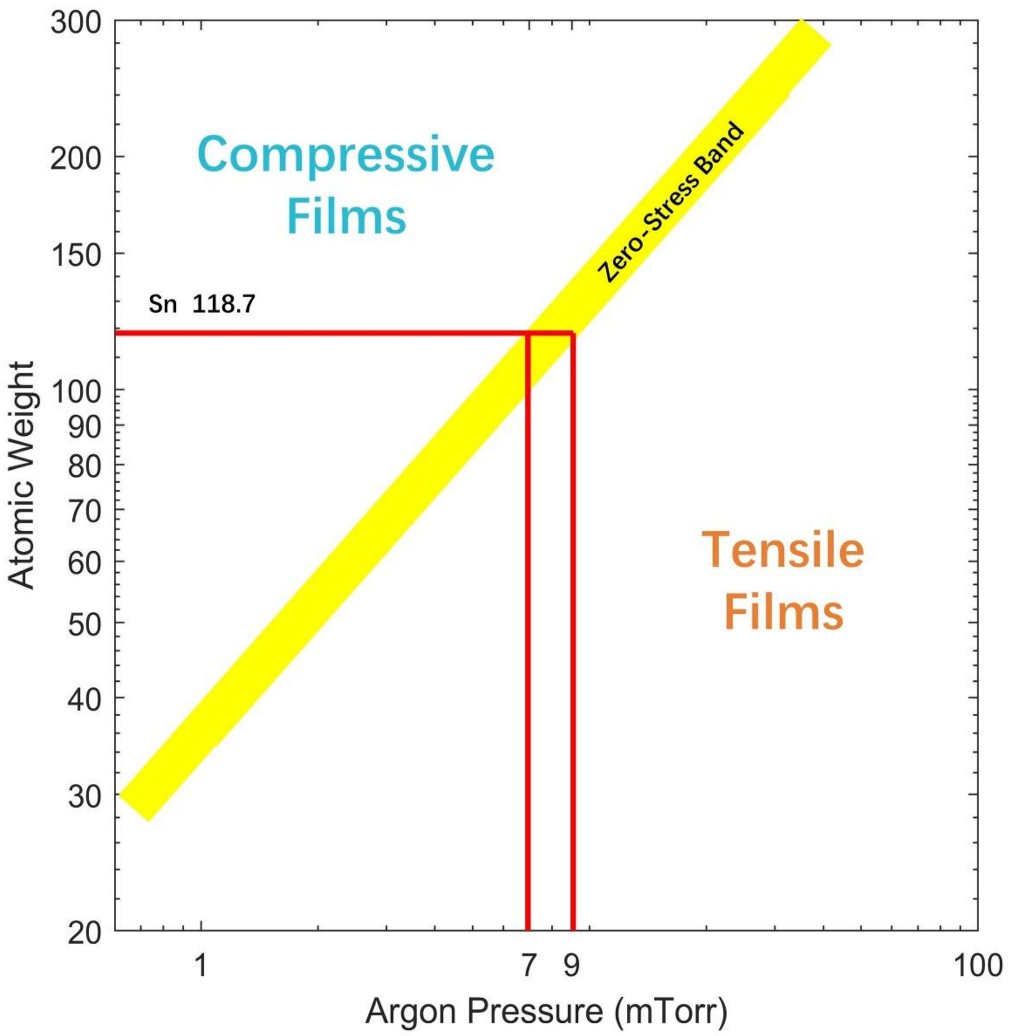

Figure 8 Argon gas pressure in the magnetron sputtering system to produce intrinsic net compressive and tensile stress in deposited films [22]. For Sn (red line, 118.7 atomic weight), an Ar pressure < 7 mTorr produces compressive Sn films and tensile Sn films are produced by Ar pressures > 9 mTorr.

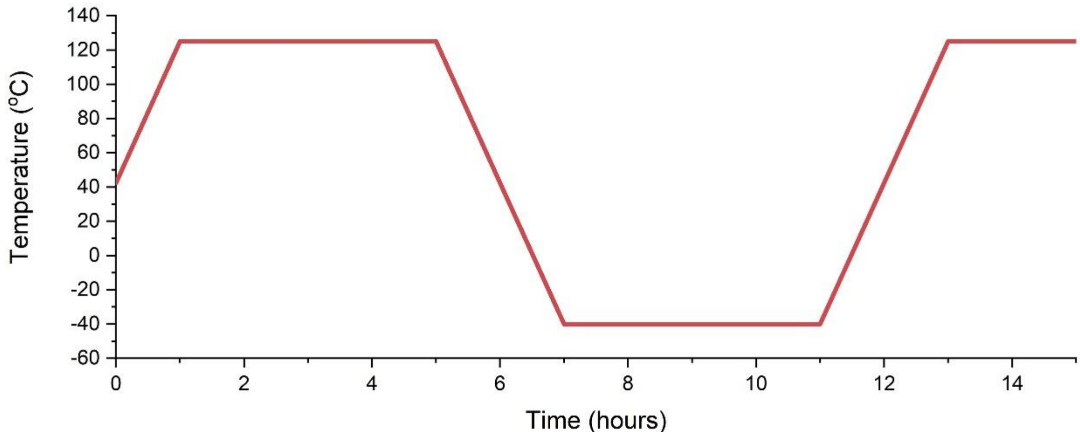

Figure 9 Thermal cycle profile for whisker growth acceleration. The cycle had a 2-hour ramp followed by 4 hours of dwell. The upper dwell is held at 125oC; the lower dwell is held at -40oC. The total time for one cycle is 12 hours.

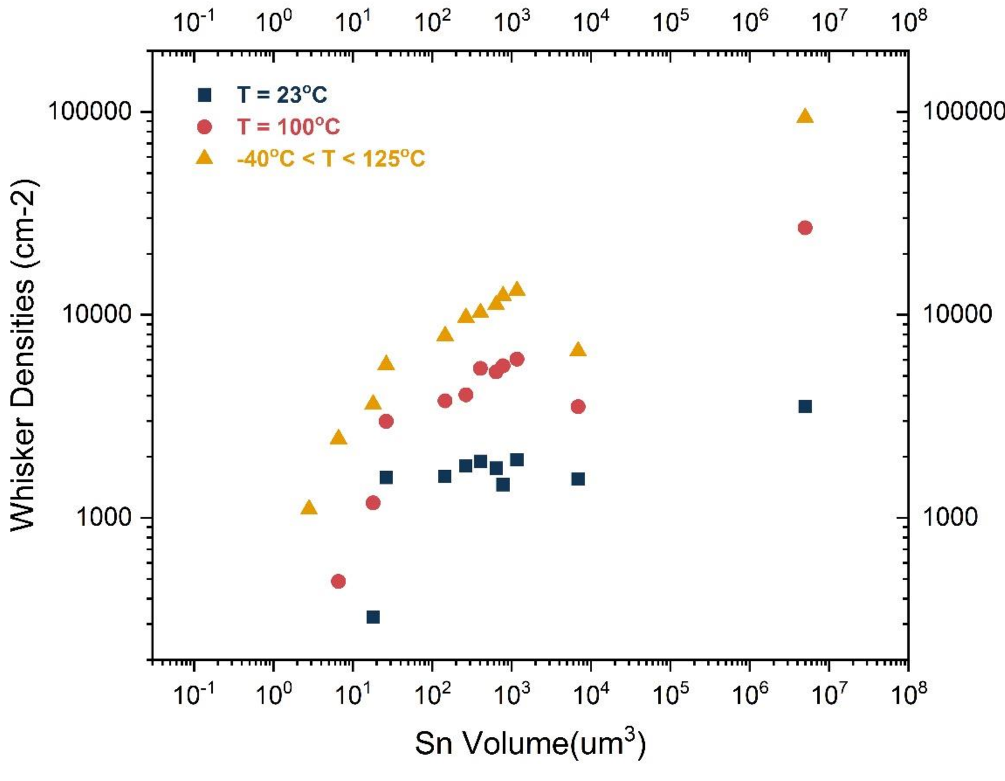

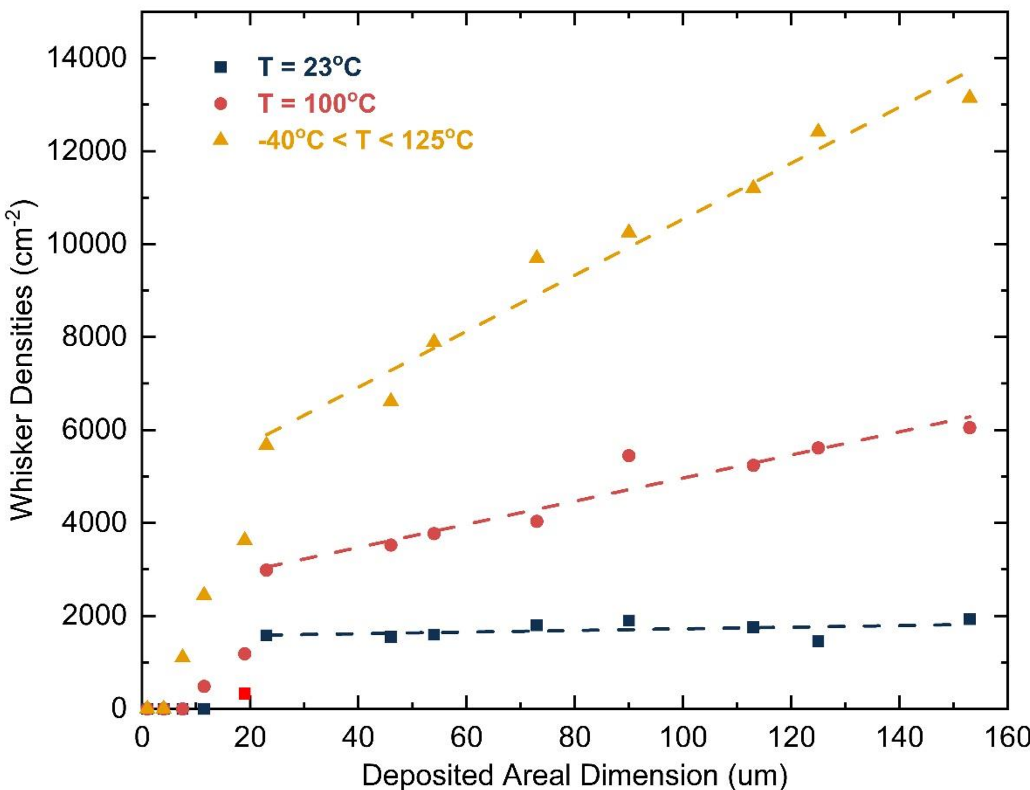

Figure 10 Sn whisker density vs. deposited size per the three incubation conditions. Due

to the rapid transition to zero whisker growth < 23 mm deposition size, the linear least squares fit to data included data only > the 23 mm and not including the point at 10,000 mm (control specimen; no aperture). The R2 fitting value was > 0.9 for the three incubation conditions and the relative slopes of the fitted lines were: 1.8, 24.9, and 60.3.

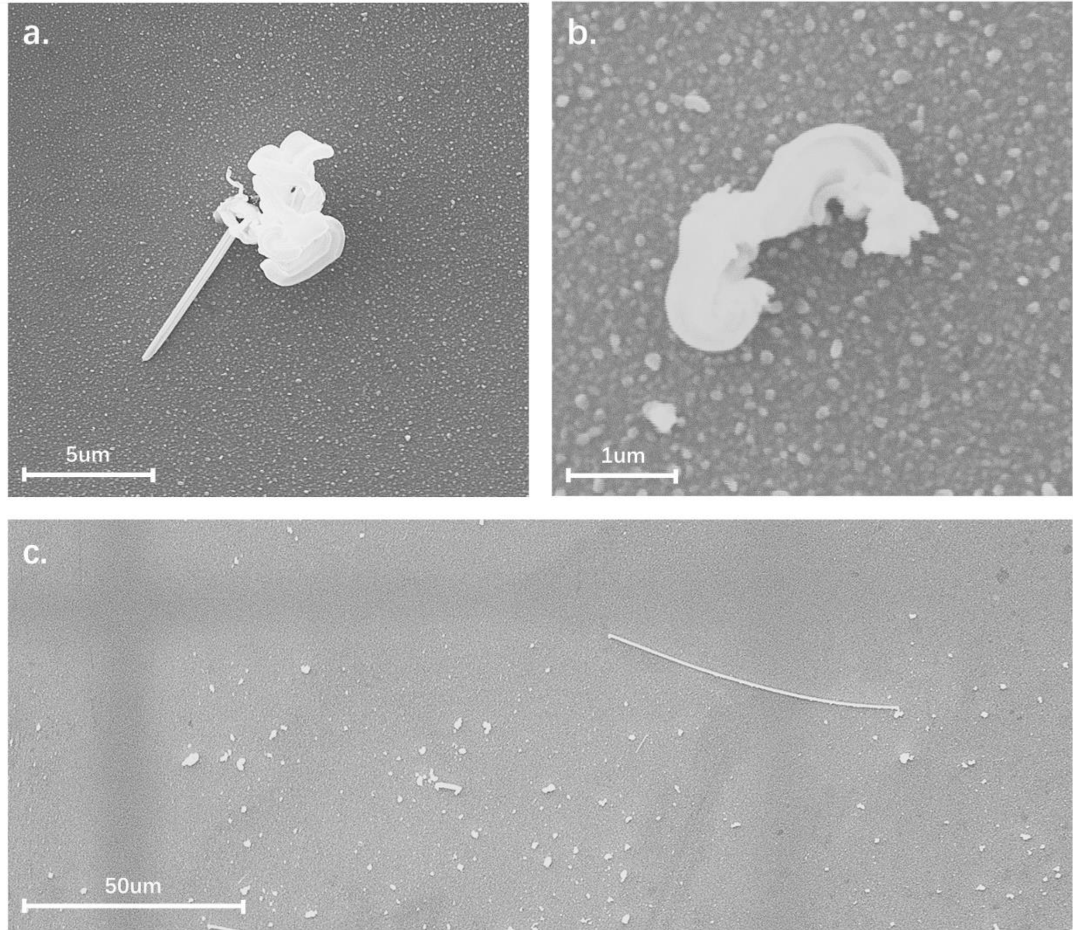

Figure 11 SEM photos of whiskers incubated from various deposition areas. a) A combined hillock and needle whisker from 19 mm2 area; b) A "toothpaste-like" whisker from a 90 mm2 area; c) A traditional "needle-like" whisker from a 153 mm2 area, shown to bridge two neighboring deposition areas.

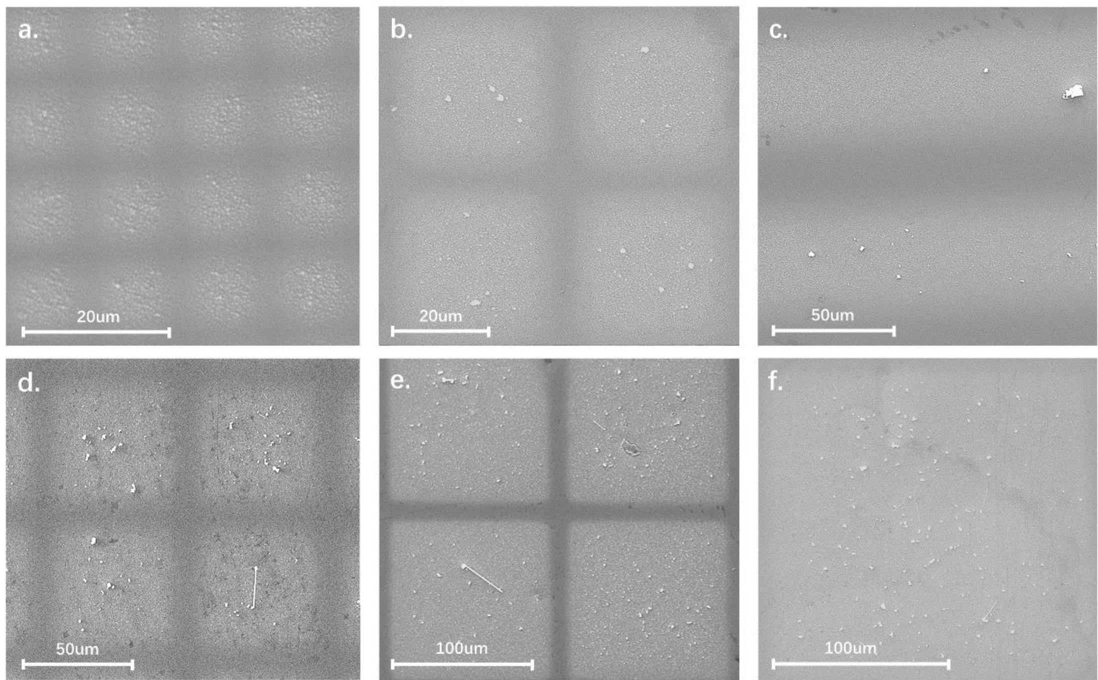

Figure 12 A series of SEM photos showing whiskers over successively larger deposited areas. a) 11 mm x 11 mm; b) 23 mm x 23 mm; c) 46 mm x 3000 mm strip; d) 54 mm x 54 mm; e) 113 mm x 113 mm; f) 153 mm x 153 mm. Figure(a) shows areas with no whiskers. The white dots are grains on the Sn surface, which are too small and not considered as whiskers. The needle whiskers seen in the photos above are 0, 0, 0, 1, 2 and 4, respectively. The needle whiskers in (f) are hard to distinguish, which is due to: (1) they are all thinner than those seen in (d) and (e); and (2) the scale is relatively large. The average density of needle whiskers increases with the dimension of limited areas increases.

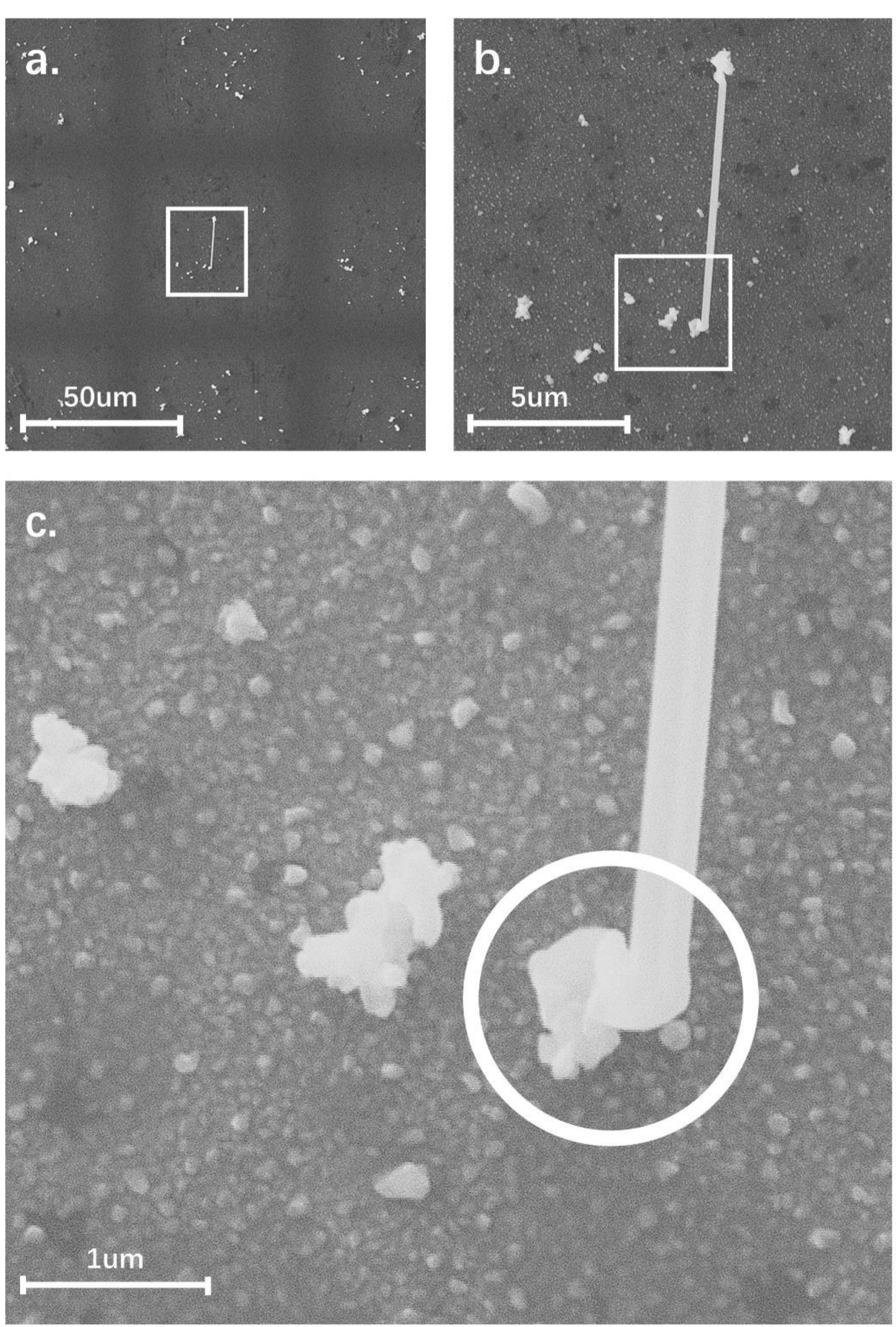

Figure 13 Increasingly higher magnification SEM images of a whisker found on a 54 mm x 54 mm limited area. The needle whisker proceeds from a hillock whisker.

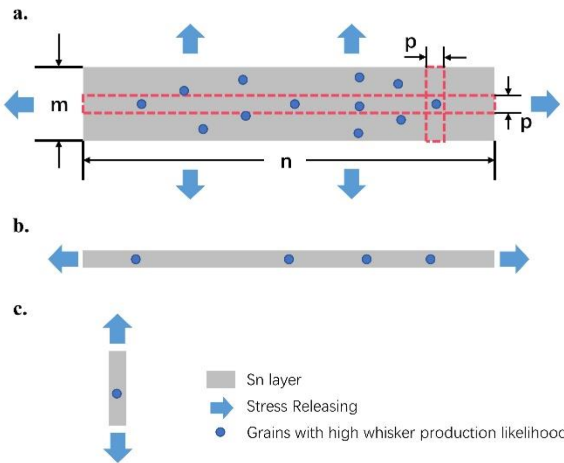

Figure 14 (a) A squared-limited Sn deposition layer, with m and n represents the width and length of this layer. (b) A section seperated from layer in (a) horizontally, with n as the length and p as the width. (b) A section seperated from layer in (a) vertically, with m as the length and have the same width p as the section in (b). With the same amount of stress release in both (b) and (c) at the two edges, their different numbers of high-whisker-likelihood grains result in different final whisker decrease effects.

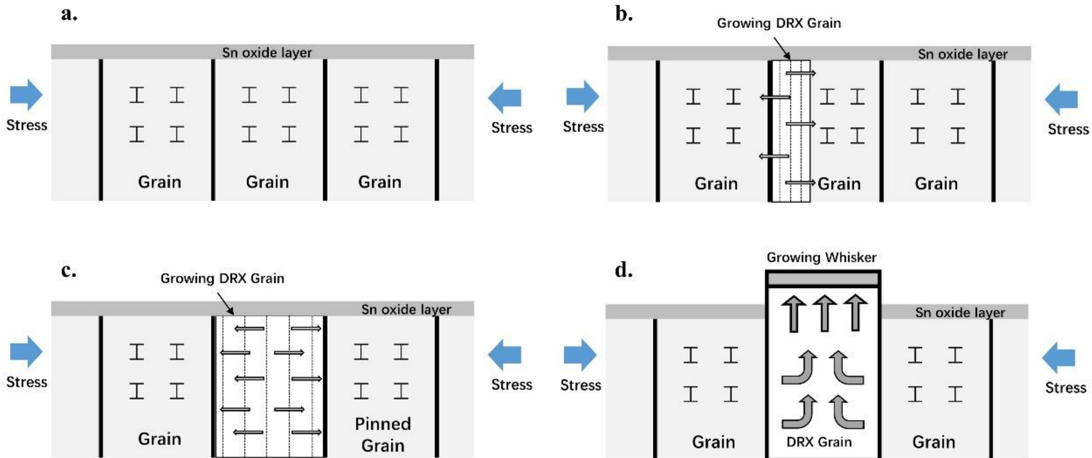

Figure 15 Schematic diagrams illustrating whisker growth process in DRX mechanism: (a) strain energy is built up in dislocation structures; (b) a DRX grain initiates growth; (c) the DRX grain continues growth; (d) with grain boundary pinning, the DRX grain initiates expansion vertically, resulting in whisker growth.

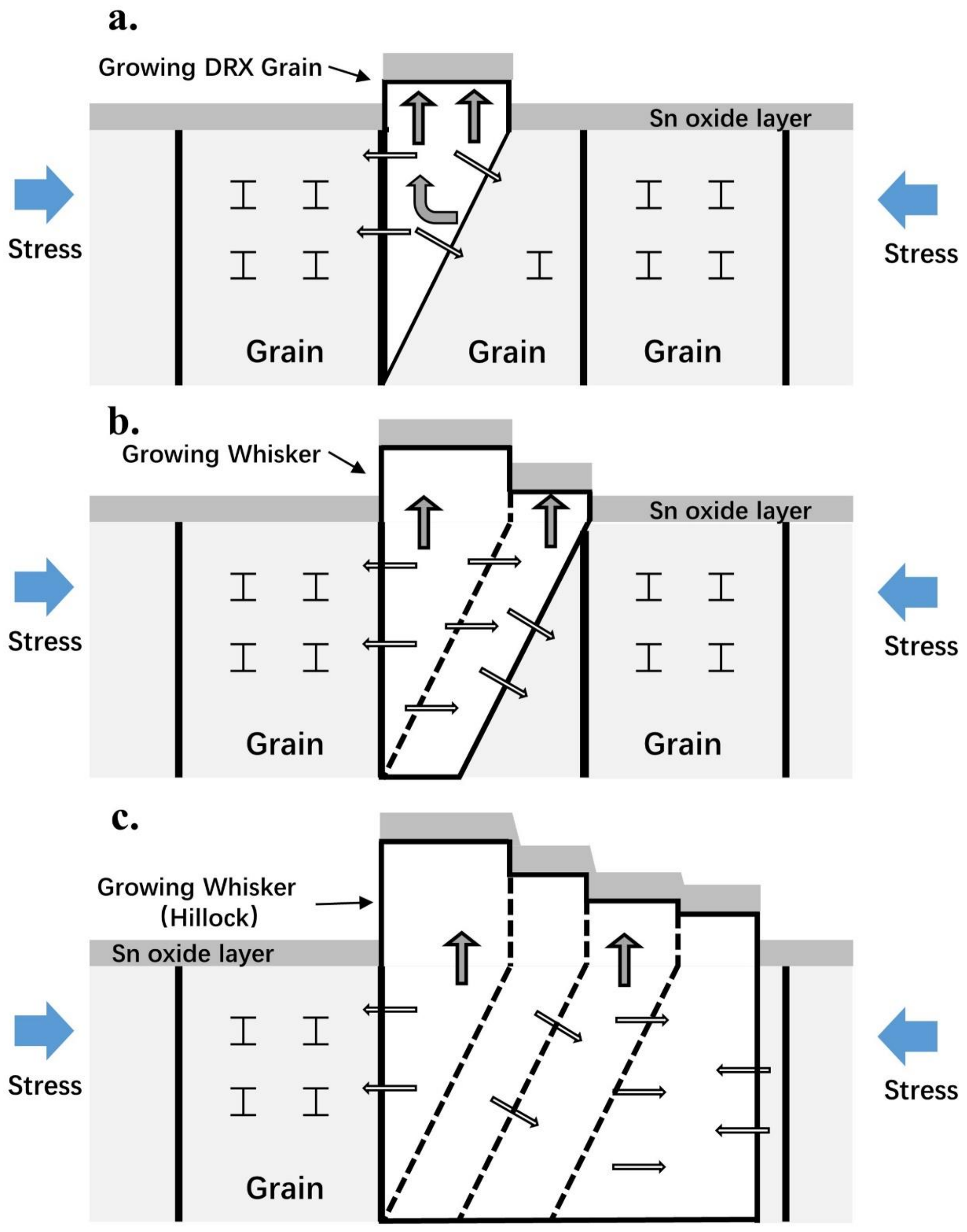

Figure 16 Schematic diagrams illustrating growth process of a hillock whisker in DRX mechanism: (a) a small whisker is growing with the DRX grain expanding; (b) the uneven stress acting on boundaries of DRX grain, allowing lateral growth of the DRX grain; (c) the whisker is a hillock when the process (b) occurs for multiple time until it slows with the loss of strain energy.

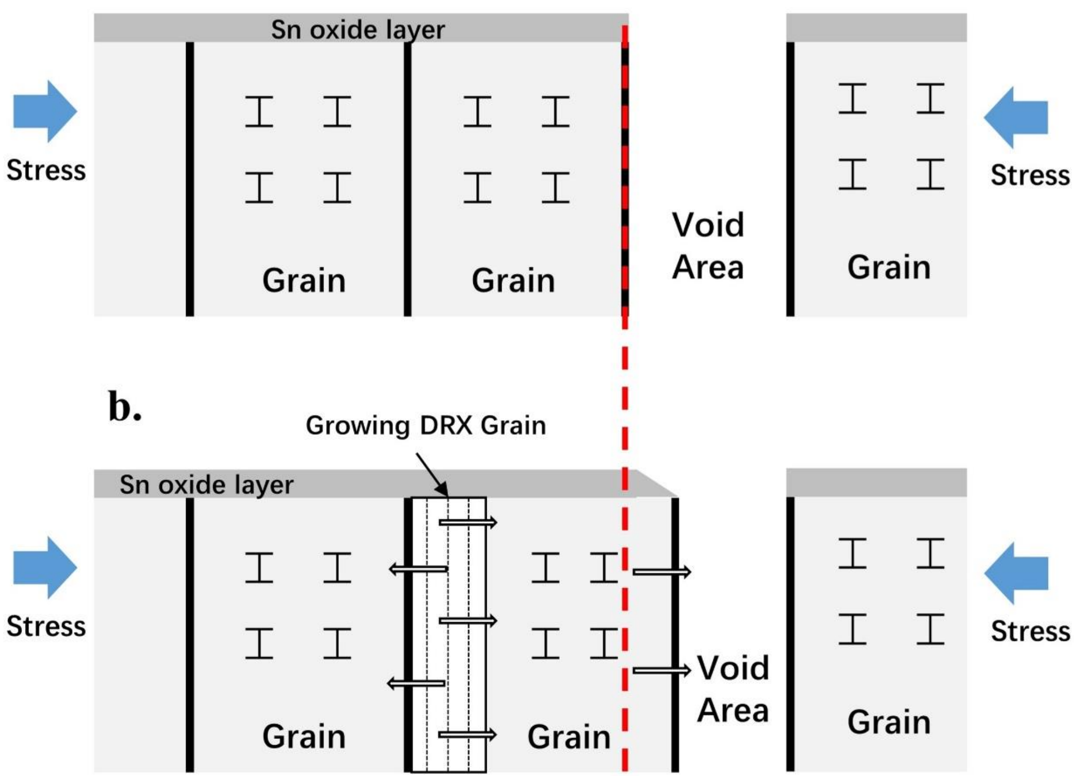

Figure 17 Schematic diagrams illustrate that the existence of void areas provides extra spaces for DRX grains to expand with the loss of strain energy. The expansion of limited areas is shown in an exaggerated manner to illustrate the energy release effect of void areas. Void areas are not observed to become significantly getting narrower than originally sputtered, due to two facts: (1) the volume change caused by limited areas expansion is small comparing to the whole volume of the limited area; (2) due to the small thickness of the Sn layer, the margin line of limited area is blur to define (Figure 6), so the movement of the margin line is hard to observe.

Chapter 4.

Study of Contiguous Sn Deposition Network Interruption in Whiskering

4.1 Introduction

The splendid characteristics in both physical and chemical, such as high conductivity, suitable melting point and high oxidizing, has made tin (Sn) playing an inevitable role in modern manufacture. However, Sn whiskers has also been an almost inevitable threaten to circuits and connectors, ever since the Restriction of Hazardous Substances Directive (RoHS 1) first been adopted in 2003. The unpredictable spontaneous growth from metal surfaces and easy bridging characteristics of whiskers have led to numerous catastrophic failures in many high-cost electronic systems and devices ever since the day that whiskers were fist observed [1]. Researchers has been focusing on studying the formation mechanism of whiskers, eager to find out any method to alleviate or interrupt one step in the growing process of whiskers.

The growth of whiskers is now partly attributed to a stress-relief phenomenon within the Sn film, motivated by long-range Sn diffusion and dynamic recrystallization [2], [3]. Such relief can deal with both external and internal stress. Multiple early studies have focused on deliberating the sources of stress, such as directly applied, electromigrated, self-generated (oxidation, intermetallic compound atoms growth, etc.), thermal expanded, etc. Comparatively, less concentration has been put on those minority drivers stimulating whisker growth [4]. For instance, the resultant volumetric

change of metal oxidation at film surface level was considered as the major stress source [5], [6]; furthermore, clean surface without oxygen is still capable to produce whiskers [7]. Multiple related incidences of whiskers still need to be identified.

Among those works, existing many enlightening fields. The role of lateral long-range atomic Sn diffusion in whiskering was studied and reported by Woodrow and Works [2], which was reported over several thousands of microns beneath the Sn surface. Besides, the dynamic recrystallization (DRX) mechanism, proposed by Vianco and Rejent [8]–[10], was identified as the foundational mechanism producing whiskers.

Inspired by the theories of long-range diffusion and DRX, this work is designed to investigate the influence of confining Sn film area and thickness to deliberate interruption of the continuous whiskering process on Sn films. We partitioned Sn films on silicon (Si) substrates into periodic areas by sputtering Sn materials through a series of TEM grids with different areal sizes during deposition. Then we incubated specimens under thermal cycling, and collected whisker density, type and lengths using SEM evaluations.

4.2 Experimental

The 1 cm x 1 cm Si (111) oriented silicon wafers were chosen as the specimens in this experiment. A series of commercial transmission electron microscope (TEM) grids with open squared apertures, varying in areal sizes from 7.5 mm to 153mm, were

mounted onto the top surfaces of Si wafers as masks. Detailed information citing the TEM grids apertures and spacing dimensions are listed in Table I. The column of "Margin Density" is calculated through the following equation:

$$Margin\ Density = \frac{4 \times Dimension}{(Dimension + Spacing)^2}$$

, which represents the density of margin length on one specimen masked with corresponding TEM grid. The "SVQG" represents a special TEM grid which consisted of four different sized grids.

Then the specimens were deposited using a 99.99% pure Sn target, with an Ar plasma (currents of 0.18A±0.02A and potentials of 380V±10V) in a magnetron sputtering system. Eight thicknesses were sputtered, which were 100Å, 200Å, 500Å, 1,000Å, 2,000Å, 5,000Å, 8,000Å and 10,000Å. A magnetron sputtering system is capable of "dialing-in" intrinsic compressive/tensile film stress of various amounts without the need of external stress applied. The Ar gas pressure condition of "compressive/tensile/no stress" is presented in Figure 18. In this study, specimens were put under intrinsic compressive stress under the background Ar gas pressure of 2mTorr. During sputtering, the TEM grids partitioned the deposition layers into small and confined areas with accurately the same shapes and dimensions as masked apertures. Between all the neighboring Sn areas existed Sn-free areas (noted as "void areas" hereafter), with the width equal to the spacing dimensions of TEM grids (Table I). The TEM grids were removed immediately after sputtering.

To explore the whisker initiation and production, the deposited specimens were subjected to the cycling temperature ranging between -40°C < T < 125°C, of which the

duty cycle is shown in Figure 19. The thermal cycling incubation has been applied as a common cycling protocol for reliability testing [7], [11]–[14]. The incubation duration is 34 days.

Scanning electron microscopy (SEM) evaluation was involved in the observation protocol across each specimen, with a low magnification (~1000x) for whisker counting and a high magnification (20,000-30,000x) for whisker evaluation and measurement. Crystal eruptions measured larger than 2 mm in one dimension were treated as a single whisker during counting, regarding the average grain size is ~0.5mm.

The observation protocol consisted of a low magnification (1000X) coarse evaluation of whisker growth across each specimen, followed by a high-resolution examination (20-30kX) on single whiskers. For each confined area, ten 100mm x100mm areas were randomly picked, and whiskers observed in these areas were manually counted. These numbers were then averaged over the total ten areas ($0.001cm^{-2}$) to obtain the whisker density in this grid-limited area.

4.3 Results

Collected Sn whisker densities (cm^{-2}) from various deposited limitation sizes and thickness, and different incubation methods data are presented in Table II.

Volume of Sn layer is confined by applying TEM grids during sputtering, which leads to monotonically decrease in whisker production as the deposited Sn volumes

decrease. The whisker density vs. deposited Sn volume is first analyzed and plotted in Figure 20. The deposited Sn volume is calculated as

$$V = a^2 h$$

where a and h represent the areal size and layer thickness, respectively. A logarithm "Log3P1" fit curve is presented in the same figure, resulting in the R^2 value higher than 0.9, associated with a related 95% confidence band and a 95% prediction band. The expression of the "Log3P1" fitting is in the form of:

$$y = a + b \times ln(x + c)$$

where a , b and c are parameters to be determined during fitting. Whisker densities presents a monotonical decrease with confined Sn volume getting smaller. All the plots are involved in the 95% prediction band of the fitted Log3P1 curve. The fitting curve also predicts the upper band of the 95% prediction band on whisker density as ~23,000cm^{-2}, with the Sn volume increase.

The monotonic retarding trend of whisker density is clearly illustrated in Figure 20: with the Sn deposition volume lower than 4,000um^3, the whisker density decreases by 45.61% at 100um layer thickness comparing to the control specimen, and by 94.82% at 10,000um thickness; further, whisker formation was found almost ceased when the volume is suppressed to around 5um^3.

Most plots off the 95% confidence band concentrate between the Sn volume from 0um^3 to 5x10^{3}um^3, with the whisker densities higher than the fitting curve predicts. These plots are collected from specimens with low or medium thicknesses such as 1000 Å, 2000 Å and 5000 Å, as well as the areal size a between 54um and 125um.

The relative high whisker densities observed from these specimens imply the small whisker degradation effect on layer thickness between 2,000 Å to 10,000 Å, while being large on thinner Sn layers, as illustrated in Figure 21. Even with different thickness, whisker densities on those specimens with large areal size (90um~153um) show small difference, which are significant on those of 125um and 153um. Specimens with high densities possess similar areal sizes but their thicknesses are varying from 1,000 Å to 10,000 Å, resulting in a large difference in final Sn layer volume, and most of which are plotted above the 95% confidence band (Figure 20). Whisker density data collected from almost all specimens with different areal sizes support the concrete influence to encourage whisker production with the thickness growing larger (Fig. 4.4). For the largest areal sizes, 153um x 153um, whisker density collected from 10,000um thickness is ~2x to that from the thinnest layer of 100 Å, and this ratio become larger with the areal size degrade. Whisker densities are found decreasing at different paces as the areal sizes larger than 23um and smaller than it. Linear degradation relationships on all the layer thicknesses are easy to observe in the areal size range between 23um and 153um. Associated linear fitting lines and associated 95% confidence bands are also illustrated in Fig. 4.4, with all R^2 values larger than 0.94. The slopes of different layer thickness vary: the slopes of data from large thicknesses trend to be as small as ~30($cm^{-2}um^{-1}$) between areal sizes of 23um and 153um, while small thicknesses are fitted with larger slopes for ~ 30($cm^{-2}um^{-1}$) with areal size degradation. Further, when the dimension moving lower than 23um, sudden transitions occur on almost all thicknesses, and whisker production decrease at

lower areal size. Further, zero whisker production are also reported from the thinnest Sn layers on some specimens.

The linear degradation effect of whisker production on areal sizes has been confirmed. However, such degradation cannot speak for the logarithm performance of whisker density vs. the Sn layer volume completely. As a result, a similar retarding effect might exist between Sn layer thickness and whisker density with the areal sizes fixed. A logarithm relationship between whisker density and Sn layer thickness is presented (Figure 22), which is consistent with the relationship shown in Figure 20. Whisker production ability is constrained with the depositions being gridded, and upper limits of whisker density can be experimentally conducted from collected data on different sized depositions, respectively. The upper limit is largely influenced by the areal size, varying from ~5,000cm^{-2} on 7.5um x 7.5um areas to ~15,000 cm^{-2} on 153um x 153um ones. The degradation effect is low at thickness ranging of 2,000 Å to 10,000 Å, and growing larger when the thickness gets lower than 2,000 Å.

The controlling group, consisted of a series of specimens with various thicknesses but no meshed TEM grids during sputtering, produces whisker densities much larger than confined ones but similar growing trend with the layer thickness increase, as shown in Figure 23. At the thickness of 100 Å, the unmeshed specimens produce ~1.8x whisker density comparing to 153um x 153um specimens at the same thickness, and this ratio is growing with the thickness increase, finally reaching ~19x at the 10,000 Å thickness.

Now moving to the whisker appearance on different specimens, these physical characteristics are also found highly influenced by the volume of Sn layer deposition. Both "needle-like" and "hillock-like" structures are observed from our experiments. Besides, hillock whiskers can be found from Sn deposition of all areal sizes and thicknesses, while needle whiskers are found very limited on specimens with areal size smaller than 54um or from thickness smaller than 1000Å. Needle whisker density presents linearity to areal size, which is absent when vs. deposition thickness. Further, the maximum length of needle whisker observed in these experiments shows no obvious correlation to areal size or thickness (Figure 24).

4.4 Discussion

4.4.1 Whisker production governed by confined deposited areas

The experimental data reveals that whisker production ability is largely influenced by the limitation of deposited areas. The great loss in whisker density inspired us to discuss about the mechanism of areas confine, which leads to our experimental results.

The major difference between our experiments from other whisker-incubation ones are the existence of deposition confine. Bozack et al. reported whisker densities of ~150,000cm^{-2} on 5000Å Sn/Si sample after 37days thermal cycling incubation, and 24,265~164,527 cm^{-2} on 1,500Å Sn/Si samples after 137days room temperature and multiple humidity [15]. Whisker densities collected from specimens with same or

closed thickness decreased by 90.39%, and 44.36%~91.78% at the largest confined size 153um, respectively; and these numbers can be larger on smaller limited sizes. Comparing to the controlling groups incubated under exact same conditions, specimens with TEM grids reduced the whisker density by 45.61%~94.82%.

Here, we need to discuss the mechanisms behind the whisker production loss. Ever since the first report of whiskers, the growth of these crystal eruptions has been studied by numerous researchers, and an consensus is now widely accepted that the in-layer stress plays the major role driving the whiskers to form and grow [16], [17]. In this experiment, without any external applied forces, the major source of the in-layer stress comes from incubation temperature. Room temperature provides 23°C, and thermal cycling provides -40°C~125°C to specimens, which differ from the temperature of ~18°C during sputtering. Such differences would introduce dislocation to the surface between Sn deposition and Si substrate through their different coefficient of temperature expansion (noted as "ΔCTE" hereafter) [18]–[21]. Followed by the dislocation, stress is introduced, distributed, and finally concentrated on multiple specific locations due to the in-layer microstructures. The accumulated stress then stimulates the formation of whiskers physically [17], [22], [23] and through the expansion of DRX grains by initiating the dynamic recrystallization to occur [24]. Meanwhile, free Sn atoms diffusion continuously invests in the feedstock consumed by the volume increasing at the locations of growing whiskers [2], [25], [26], and leading to the existence of depleted zones [9], [27]–[29]. Applying area confine on depositions can alleviate the process of both these two mechanisms:

4.4.1.1 Diffusion isolation effect of confining depositions

Lateral diffusion of free Sn atoms has long been convinced to be one of the major reasons to cause whisker formation [2], [25], [26], and long range diffusion was also reported by Woodrow and Works [2]. In this study, however, by applying TEM grids onto specimens during sputtering, we arrange the Sn deposition layers to be small and neat square structures, which are surrounded by Sn-free gaps with width equals to the spacing parameter in TABLE I (noted as "void areas" hereafter). There was no Sn observed by AES among the void areas which might provide a possible Sn bridge between two neighboring confined deposits. The void areas are effectively isolating Sn deposits to diffuse only within the Sn structures themselves. In the void areas, Sn atoms can only diffuse through the Si substrate, while the diffusivity of free neutral Sn atoms in intrinsic Si has been measure as:

$$D_o = 32e^{-98000/RT}$$

in cm^2sec^{-1} (measured by neutron-activation analysis) [25], where R is the moral gas constant and T represents the temperature. It easy to get the D value is ~4.39×10^{-12} cm^2/sec at 125ºC and ~3.42×10^{-21} cm^2/sec at -40ºC as the highest and lowest temperature in these experiments, implying zero lattice diffusion through Sn void areas between neighboring confined layers.

4.4.1.2 Strain release effect of confining depositions

The existence of void areas can not only cut down a large portion of free atoms diffusion but also provide spaces for strain and stress to release. No matter in intermetallic compound atom expansion [5], [30], [31] or the DRX grain expansion

[24], [10], the stress caused by atoms expansion is usually recognized as the major source continuously invests in whisker formation and growth. Applying deposition confine is an applicable method to deal with these stress and strain.

The void areas play the major role in stress-relief. The mechanism of void areas dealing with certain amount of stress is shown in Figure 25. The void areas can accommodate the deformations of neighboring depositions (Figure 25a). Besides, their evenly distributed characteristics results in that very little amount of stress can accumulate to certain spots to form a whisker. Figure 25b presents a closing view of 500Å specimens, where most eruptions are found near the center of the squared areas. Figure 25c and Figure 25d compares specimens of both thickness of 8,000Å and areal size of 11.5um after 34days and 112days incubation. Due to the possible existence of manufacturing error and the blur margins of confined depositions, we should not directly apply the areal size as the length. By assuming the strain occurs in all direction evenly, we use MATLAB to measure lengths of 10 confined areas in each figure, and then taking the average value. The values came out as 13.80um and 14.48um, resulting in a width increase of 0.68um at two observations. This increment confirms strains creeping into void areas, which can be taken as a stress-relief effect of void areas onto confined depositions.

4.4.2 Whisker production behaviors under Sn deposition confined with various thicknesses

Our experimental data reveals that whisker production ability is largely influenced by the limitation of deposited areas. The observed great loss in whisker density inspired us to discuss how the confined areas affect whisker formation and growth.

Whisker formation is strongly governed by the available feedstock of multiple deposition and substrate materials [32]. However, primarily due to the expectable high cost, and the small amount of feedstock for the formation of a whisker [33], [34], few works have concentrated on available feedstock confining effect onto whisker production ability. In our work, we succeeded to limit the Sn feedstock by applying a series of TEM grids during sputtering Sn depositions with different thickness, and the decrease of final whisker production is observed significant.

The monotonic retarding trend of whisker density is clear (Figure 20), and the loss of whisker production by deposition volume is contributed by both the layer thickness and confined areal sizes. Comparing to the control group, whisker densities decreased by no less than 45.61% on all thicknesses (Figure 23), but whisker production ability doesn't affect much by layer thickness at the thickness larger than 2,000 Å (Figure 22).

Backing to soldering in commercial usage, substantial difficulty has been found refers to overcoming the criteria of quality and technique requirements. To ensure the

high conductivity and functional needs of soldering such as anti-erosion, most commercial electronics devices are soldered 20uin-1200uin (~5,080 Å-304,800 Å) in thickness [35], [36], larger than the observed threshold of 2,000 Å. To achieve an equilibrium between the cost and whisker production suppression ability, applying large areal limitation sizes for soldering layer is a more efficient way other than confining deposition areal dimensions to less than 50um or cutting down the soldering layer thickness to be smaller than 2,000 Å.

4.4.3 Characteristics of incubated whiskers in confined deposition areas

The morphology of whiskers incubated from confined areas shows obvious preference. Hillock whiskers were observed from all specimens where whiskers were produced, while for needle whiskers, a threshold exist in the shadowed interval preventing growth of needle whiskers. The shadowed areas in Figure 24a and Figure 24b indicate the thresholds which "turn on" the needle whisker formation mechanism. For example, for all the 11.5um x 11.5um depositions, needle whiskers were only found from Sn layers thicker than 2,000Å; and for all the 500Å-thickness layers, needle whiskers were observed from those with areal sizes larger than 54um. Density of needle whiskers do not increase largely with the layer thickness, while a linearity present when vs. the areal size, as shown in Figure 24. In Figure 24a, the first 4 plots are masked during fitting due to their zero densities which shows no linearity.

The deposition volume can be the parameter connecting the two different

behaviors in these figures. In Figure 24a, the two volumes at 23um and 54um are 26.45um^3 and 145.8 um^3, between which the threshold might exist; while in Figure 24b, the two volumes are 13.225um^3 and 26.45um^3, where the same volume of 26.45um^3 came out to be the exact value standing on the boundary of needle whisker incubated or not.

Besides the density, the maximum length of observed needle whiskers is also notable. The growth rate of needle whiskers from unconfined metal layer was given out as [37]:

$$g_{needle} = \frac{\Delta l}{\Delta t} = \frac{2}{\ln(b/a)} \frac{\sigma_0 \Omega s D}{kTa^2}$$

where $l, t, a, b, \sigma_0, \Omega, s, D, k$ and T represent whisker length, incubation duration, averaged whisker radius, averaged whisker spacing, in-layer stress of Sn film, atomic volume, the height of growth step of needle whisker, the self-grain boundary diffusivity of Sn, Boltzmann's constant and temperature, respectively. In our experiment, all the parameters can be measured to calculated out the growth rate in one duty cycle of thermal cycling. Parameters not varying in one cycle include: $a = 0.3\mu m$, $b = 100\mu m$, $\sigma_0 = 7 \times 10^7 N/m^2$, $\Omega = 2.29 \times 10^{-29} m^3$, $s = 3 \times 10^{-10} m$ [37], and $k = 1.38 \times 10^{-23} Nm/K$. Temperature is changing as designed by cycling file, and diffusivity is governed by temperature. With MATLAB and setting the time interval to be 1min, the growth rate in one cycle is calculated to be $2.2956 \times 10^{-5} m$, and the final expected length in 34days (68 cycles) to be ~1.6mm.

However, the measured maximum length of observed needle whisker is 5x smaller than expected (Figure 24). These maximum lengths fluctuate with areal size

and thickness increasing, and there seems no direct trend or mechanism governing it. The grain size is mainly affected by sputtering circumstances, including temperature, gas pressure, humidity, etc. [38], [39]. In out experiment, all the specimens were sputtered and incubated under the same circumstances, resulting in no obvious differences in grain sizes and whisker diameters, so no preference is shown in volume of whiskers regarding the areal size or thickness of Sn deposition.

Vianco et al. proposed a mechanism based on dynamic recrystallization (noted as "DRX mechanism" hereafter), which attributes the branches of whiskers with multiple morphology to expansion process of a DRX grain [9], [24], [40]. In DRX mechanism, the growth of whiskers is the vertical expansion process of DRX grains, which occur at boundaries of grains, resulting from building up strain energy by anelastic deformation. The growth of a whisker into hillock shape is contributed to the intermittent pinning of the grain boundary, while the pinning is comparatively even and stable to form a needle whisker. Combining the DRX mechanism, we can conclude that the pinning of Sn deposition is dense and distributed even when the deposition is with: (1) high thickness; and (2) large-confined area size. Further, given that most accidents caused by whiskering problem were due to needle whiskers which is conductive and can bridge neighboring circuits, The morphology difference among whiskers from various confined depositions can be utilized to alleviate the whisker threatens in modern manufacturing.

4.5 CONCLUSION

Whisker production on confined Sn depositions were observed decreasing significantly. Whisker were experimentally incubated from various confined areal sizes and thicknesses through thermal cycling, and densities were collected ad theoretically analyzed. From these experiments, following observations and conclusions are obtained:

1. A series of experiments were performed on various areal sizes and thicknesses to examine the effect of confined depositions to whiskering problem. The collected results confirmed the monotonically degradation of whisker production with the decrease of available deposition volume. Whisker density from the largest volume of 23,409um^3 decreased by 94.8% comparing to the data from controlling group of the same thickness.
2. The retarding effect of whiskers on deposition volume was contributed by both the deposition thickness and confined areal sizes (Fig. 4.4 and 4.5). Whisker densities present similar decreasing behavior when the thickness is varying; and present linearity with areal sizes varying between 23um to 153um, and sudden transitions are observed below 23um.
3. The diffusion isolation effect of deposition confined was theoretically confirmed. Without the witness of Sn deposition between neighboring confined Sn depositions, the diffusivity of free Sn atoms was estimated between 1.24×10^{-75} cm^2/sec and 1.84×10^{-66} cm^2/sec. Sn atoms diffusion was limited within the meshed depositions.

4. The strain endurance effect was observed at void areas. Between the two observations at the 34th day and 112th day, width of void areas between 11.5um x 11.5um depositions was measured decreasing of 0.68um. Such phenomenon confirms the stress-relief effect of deposition confine, which provide extra spaces (void areas) for strain to creep.
5. A parameter was proposed to predict the whisker production possibility on limited Sn layers. The values of involved constants were extracted from related experimental results, and the value of threshold were determined by collected data of these experiments.
6. The DRX mechanism were examined in this deposited-layer-limited case. Among the three hierarchal requirements, two were validated, and the other one was modified to involve this special case into the DRX model.

The retarding effect of deposition confine on various thickness has been revealed and theoretically validated. By adjusting areal size and associated thickness, Sn whisker production can be controlled, alleviated, and even eliminated from Sn surface, which is a useful method to deal with whiskering threaten for most electrical devices and systems.

4.6 Reference

[1] H. Y. Hunsicker and L. W. Kempf, "Aluminum alloys for bearings," SAE Technical Paper, 1947.

[2] T. A. Woodrow and B. P. Works, "Tracer diffusion in whisker-prone tin platings,"

in *Proc. SMTA Int. Conf*, 2006, vol. 1, pp. 24–28.

[3] F. Yang and Y. Shi, “Analysis of whisker growth on a surface of revolution,” *Phys. Lett. A*, vol. 381, no. 34, pp. 2767–2771, 2017.

[4] P. Jagtap, V. A. Sethuraman, and P. Kumar, “Critical evaluation of relative importance of stress and stress gradient in whisker growth in Sn coatings,” *J. Electron. Mater.*, vol. 47, no. 9, pp. 5229–5242, 2018.

[5] M. Sobiech, U. Welzel, E. J. Mittemeijer, W. Hügel, and A. Seekamp, “Driving force for Sn whisker growth in the system Cu–Sn,” *Appl. Phys. Lett.*, vol. 93, no. 1, p. 011906, 2008.

[6] C. C. Wei, P. C. Liu, C. Chen, J. C. Lee, and I. P. Wang, “Relieving Sn whisker growth driven by oxidation on Cu leadframe by annealing and reflowing treatments,” *J. Appl. Phys.*, vol. 102, no. 4, p. 043521, 2007.

[7] E. K. Snipes, G. T. Flowers, P. Lall, and M. J. Bozack, “Impact of thermal cycling and background gas environment on tin whiskering,” in *2014 IEEE 60th Holm Conference on Electrical Contacts (Holm)*, 2014, pp. 1–7.

[8] P. T. Vianco and J. A. Rejent, “Dynamic recrystallization (DRX) as the mechanism for Sn whisker development. Part I: A model,” *J. Electron. Mater.*, vol. 38, no. 9, pp. 1815–1825, 2009.

[9] P. T. Vianco and J. A. Rejent, “Dynamic recrystallization (DRX) as the mechanism for Sn whisker development. Part II: experimental study,” *J. Electron. Mater.*, vol. 38, no. 9, pp. 1826–1837, 2009.

[10] P. T. Vianco *et al.*, “Mitigation of Long Whisker Growth Based upon the Dynamic

Recrystallization Mechanism," *J. Electron. Mater.*, vol. 49, no. 1, pp. 888–904, 2020.

[11] J. W. Shin and E. Chason, "Stress behavior of electroplated Sn films during thermal cycling," *J. Mater. Res.*, vol. 24, no. 4, pp. 1522–1528, 2009.

[12] M. J. Bozack, E. K. Snipes, and G. T. Flowers, "Influence of small weight percentages of Bi and systematic coefficient of thermal expansion variations on Sn whiskering," *IEEE Trans. Compon. Packag. Manuf. Technol.*, vol. 7, no. 3, pp. 338–344, 2016.

[13] P. Sarobol, J. P. Koppes, W. H. Chen, P. Su, J. E. Blendell, and C. A. Handwerker, "Recrystallization as a nucleation mechanism for whiskers and hillocks on thermally cycled Sn-alloy solder films," *Mater. Lett.*, vol. 99, pp. 76–80, 2013.

[14] K. Suganuma *et al.*, "Sn whisker growth during thermal cycling," *Acta Mater.*, vol. 59, no. 19, pp. 7255–7267, 2011.

[15] M. J. Bozack, S. K. Snipes, and G. N. Flowers, "Methods for fast, reliable growth of Sn whiskers," *Surf. Sci.*, vol. 652, pp. 355–366, 2016.

[16] T. Shibutani, Q. Yu, T. Yamashita, and M. Shiratori, "Stress-induced tin whisker initiation under contact loading," *IEEE Trans. Electron. Packag. Manuf.*, vol. 29, no. 4, pp. 259–264, 2006.

[17] J. A. Thornton and D. W. Hoffman, "Stress-related effects in thin films," *Thin Solid Films*, vol. 171, no. 1, pp. 5–31, 1989.

[18] M. J. Bozack, E. K. Snipes, and G. T. Flowers, "Influence of small weight percentages of Bi and systematic coefficient of thermal expansion variations on Sn

whiskering," *IEEE Trans. Compon. Packag. Manuf. Technol.*, vol. 7, no. 3, pp. 338–344, 2016.

[19] E. K. Snipes, G. T. Flowers, P. Lall, and M. J. Bozack, "Impact of thermal cycling and background gas environment on tin whiskering," in *2014 IEEE 60th Holm Conference on Electrical Contacts (Holm)*, 2014, pp. 1–7.

[20] M. Dittes, P. Oberndorff, P. Crema, and V. Schroeder, "Tin whisker formation in thermal cycling conditions," in *Proceedings of the 5th Electronics Packaging Technology Conference (EPTC 2003)*, 2003, pp. 183–188.

[21] A. Kosinova, D. Wang, P. Schaaf, A. Sharma, L. Klinger, and E. Rabkin, "Whiskers growth in thin passivated Au films," *Acta Mater.*, vol. 149, pp. 154–163, 2018.

[22] H. Windischmann, "Intrinsic stress in sputter-deposited thin films," *Crit. Rev. Solid State Mater. Sci.*, vol. 17, no. 6, pp. 547–596, 1992.

[23] J. Hektor *et al.*, "Scanning 3DXRD measurement of grain growth, stress, and formation of Cu6Sn5 around a tin whisker during heat treatment," *Materials*, vol. 12, no. 3, p. 446, 2019.

[24] P. T. Vianco, M. K. Neilsen, J. A. Rejent, and R. P. Grant, "Validation of the dynamic recrystallization (DRX) mechanism for whisker and hillock growth on Sn thin films," *J. Electron. Mater.*, vol. 44, no. 10, pp. 4012–4034, 2015.

[25] T. H. Yeh, S. M. Hu, and R. H. Kastl, "Diffusion of tin into silicon," *J. Appl. Phys.*, vol. 39, no. 9, pp. 4266–4271, 1968.

[26] V. Ruth and J. P. Hirth, "Kinetics of diffusion-controlled whisker growth," *J. Chem. Phys.*, vol. 41, no. 10, pp. 3139–3149, 1964.

[27] J. Cheng, P. T. Vianco, J. Subjeck, and J. C. Li, “An assessment of Sn whiskers and depleted area formation in thin Sn films using quantitative image analysis,” *J. Mater. Sci.*, vol. 46, no. 1, pp. 263–274, 2011.

[28] J. Cheng, P. T. Vianco, and J. C. Li, “Hollow tin/chromium whiskers,” *Appl. Phys. Lett.*, vol. 96, no. 18, p. 184102, 2010.

[29] R. Nicolle and A. Rist, “The mechanism of whisker growth in the reduction of wüstite,” *Metall. Trans. B*, vol. 10, no. 3, pp. 429–438, 1979.

[30] Z. Zhang, H. Cao, Y. Xiao, Y. Cao, M. Li, and Y. Yu, “Electromigration-induced growth mode transition of anodic Cu6Sn5 grains in Cu| SnAg3. 0Cu0. 5| Cu lap-type interconnects,” *J. Alloys Compd.*, vol. 703, pp. 1–9, 2017.

[31] J. W. Osenbach *et al.*, “Sn whiskers: material, design, processing, and post-plate reflow effects and development of an overall phenomenological theory,” *IEEE Trans. Electron. Packag. Manuf.*, vol. 28, no. 1, pp. 36–62, 2005.

[32] J.-B. Zeng, Y.-S. He, S.-L. Li, and Y.-Z. Wang, “Chitin whiskers: An overview,” *Biomacromolecules*, vol. 13, no. 1, pp. 1–11, 2012.

[33] T. N. Taylor and D. S. Phillips, “The surface composition and bonding of silicon carbide powders and whiskers,” PhD Thesis, American Vacuum Society, 1988.

[34] E. R. Crandall, *Factors governing tin whisker growth*. Springer Science & Business Media, 2013.

[35] “Tin Plating | Tin Electroplating | Tin Plating Services.” http://www.selectiveplatinginc.com/Tin-Plating.html (accessed Jun. 23, 2021).

[36] “Tin Plating Services (Electroplating) MIL-T-10727, ASTM B545, AMS 2408,”

Advanced Plating Technologies. https://advancedplatingtech.com/electrolytic-plating/tin-plating-services/ (accessed Jun. 23, 2021).

[37] K.-N. Tu, “Irreversible processes of spontaneous whisker growth in bimetallic Cu-Sn thin-film reactions,” *Phys. Rev. B*, vol. 49, no. 3, p. 2030, 1994.

[38] W.-C. Lin *et al.*, “Effect of Sn Film Grain Size and Thickness on Kinetics of Spontaneous Sn Whisker Growth,” *JOM*, vol. 71, no. 9, pp. 3041–3048, 2019.

[39] P. Sarobol, J. E. Blendell, and C. A. Handwerker, “Whisker and hillock growth via coupled localized Coble creep, grain boundary sliding, and shear induced grain boundary migration,” *Acta Mater.*, vol. 61, no. 6, pp. 1991–2003, 2013.

[40] P. T. Vianco and J. A. Rejent, “Dynamic recrystallization (DRX) as the mechanism for Sn whisker development. Part I: A model,” *J. Electron. Mater.*, vol. 38, no. 9, pp. 1815–1825, 2009.

[41] J. W. Osenbach, J. M. DeLucca, B. D. Potteiger, A. Amin, R. L. Shook, and F. A. Baiocchi, “Sn corrosion and its influence on whisker growth,” *IEEE Trans. Electron. Packag. Manuf.*, vol. 30, no. 1, pp. 23–35, 2007.

[42] J. Jiang, J.-E. Lee, K.-S. Kim, and K. Suganuma, “Oxidation behavior of Sn–Zn solders under high-temperature and high-humidity conditions,” *J. Alloys Compd.*, vol. 462, no. 1–2, pp. 244–251, 2008.

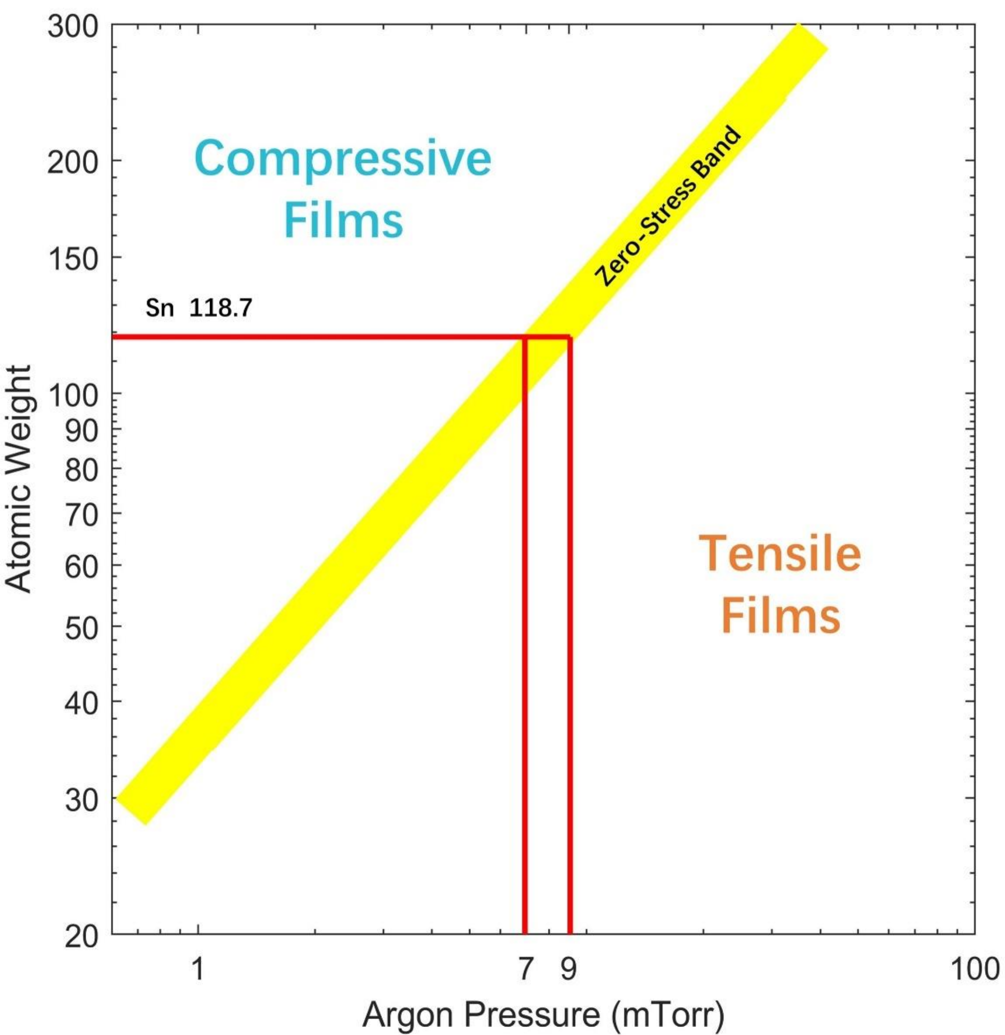

Figure 18 Argon gas pressure in the magnetron sputtering system to produce intrinsic net compressive and tensile stress in deposited films [22]. For Sn (red line, 118.7 atomic weight), an Ar pressure < 7 mTorr produces compressive Sn films and tensile Sn films are produced by Ar pressures > 9 mTorr.

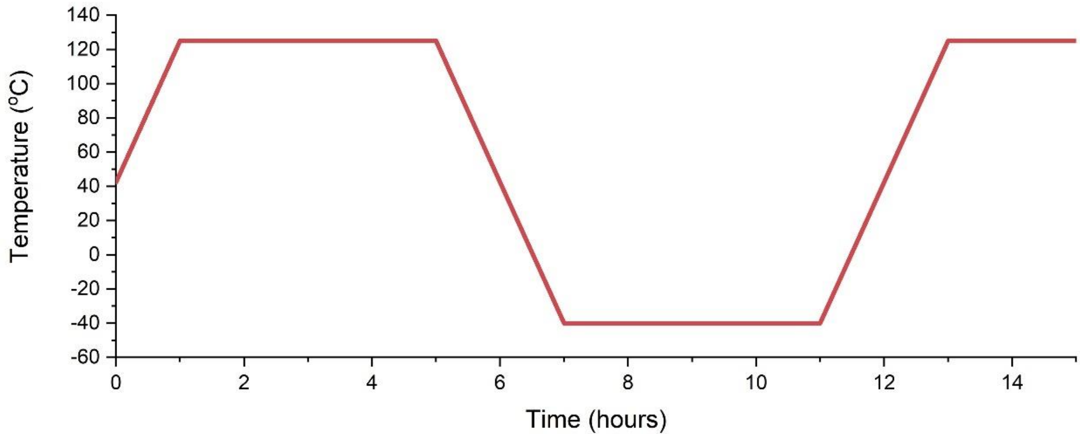

Figure 19 Thermal cycle profile for whisker growth acceleration. The cycle had a 2-hour ramp followed by 4 hours of dwell. The upper dwell is held at 125oC; the lower dwell is held at -40oC. The total time for one cycle is 12 hours.

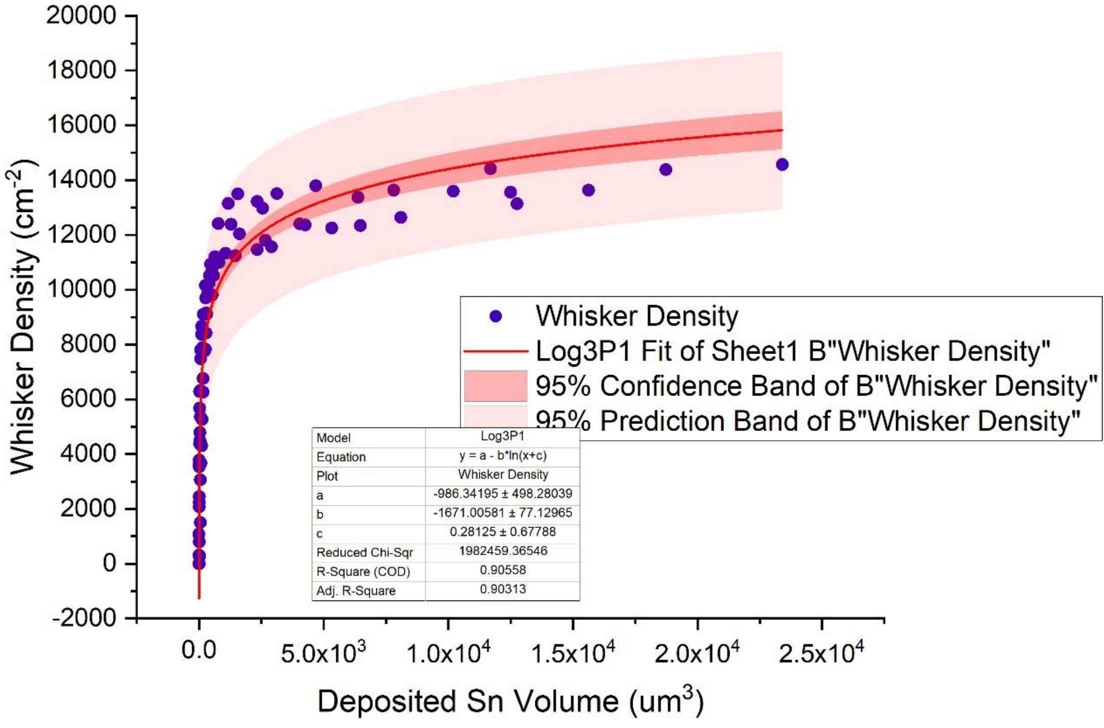

Figure 20 Whisker density v.s. Sn deposition volume

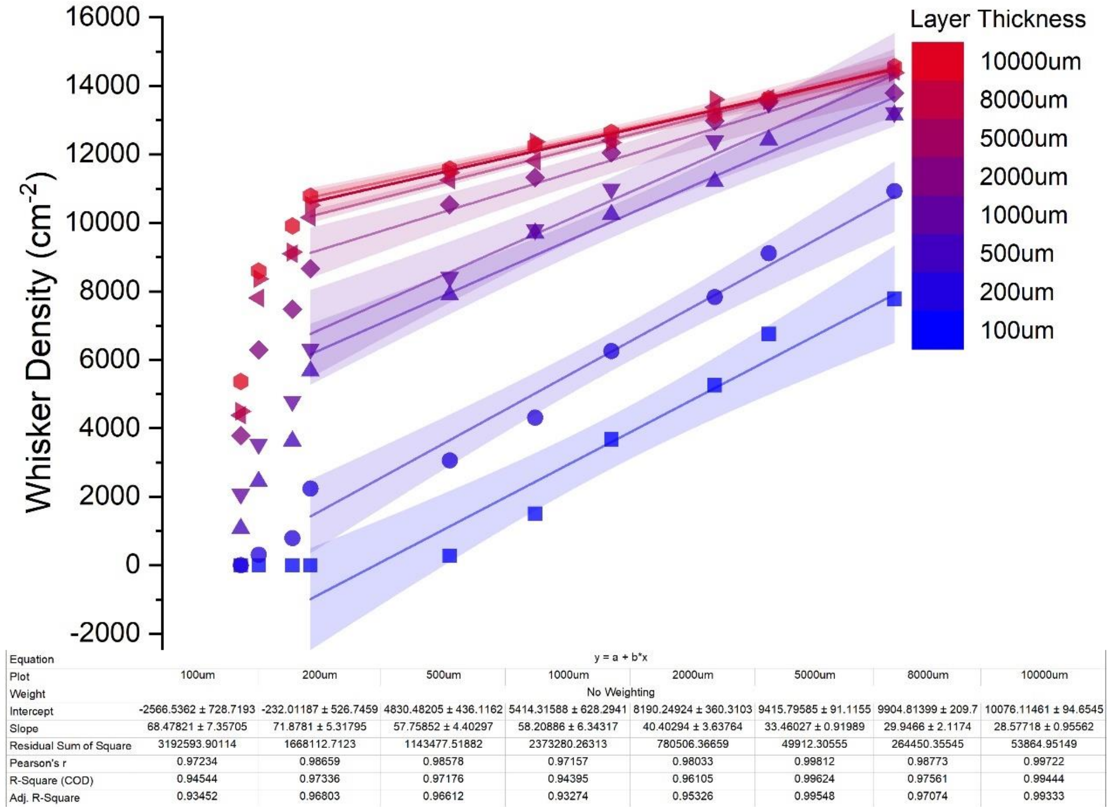

Equation	y = a + b*x							
Plot	100um	200um	500um	1000um	2000um	5000um	8000um	10000um
Weight	No Weighting							
Intercept	-2566.5362 ± 728.7193	-232.01187 ± 526.7459	4830.48205 ± 436.1162	5414.31588 ± 628.2941	8190.24924 ± 360.3103	9415.79585 ± 91.1155	9904.81399 ± 209.7	10076.11461 ± 94.6545
Slope	68.47821 ± 7.35705	71.8781 ± 5.31795	57.75852 ± 4.40297	58.20886 ± 6.34317	40.40294 ± 3.63764	33.46027 ± 0.91989	29.9466 ± 2.1174	28.57718 ± 0.95562
Residual Sum of Square	3192593.90114	1668112.7123	1143477.51882	2373280.26313	780506.36659	49912.30555	264450.35545	53864.95149
Pearson's r	0.97234	0.98659	0.98578	0.97157	0.98033	0.99812	0.98773	0.99722
R-Square (COD)	0.94544	0.97336	0.97176	0.94395	0.96105	0.99624	0.97561	0.99444
Adj. R-Square	0.93452	0.96803	0.96612	0.93274	0.95326	0.99548	0.97074	0.99333

Figure 21 Whisker density v.s. areal dimensions of Sn deposition regarding different thicknesses. Strong linearities have been observed on whisker densities with areal dimension varies.

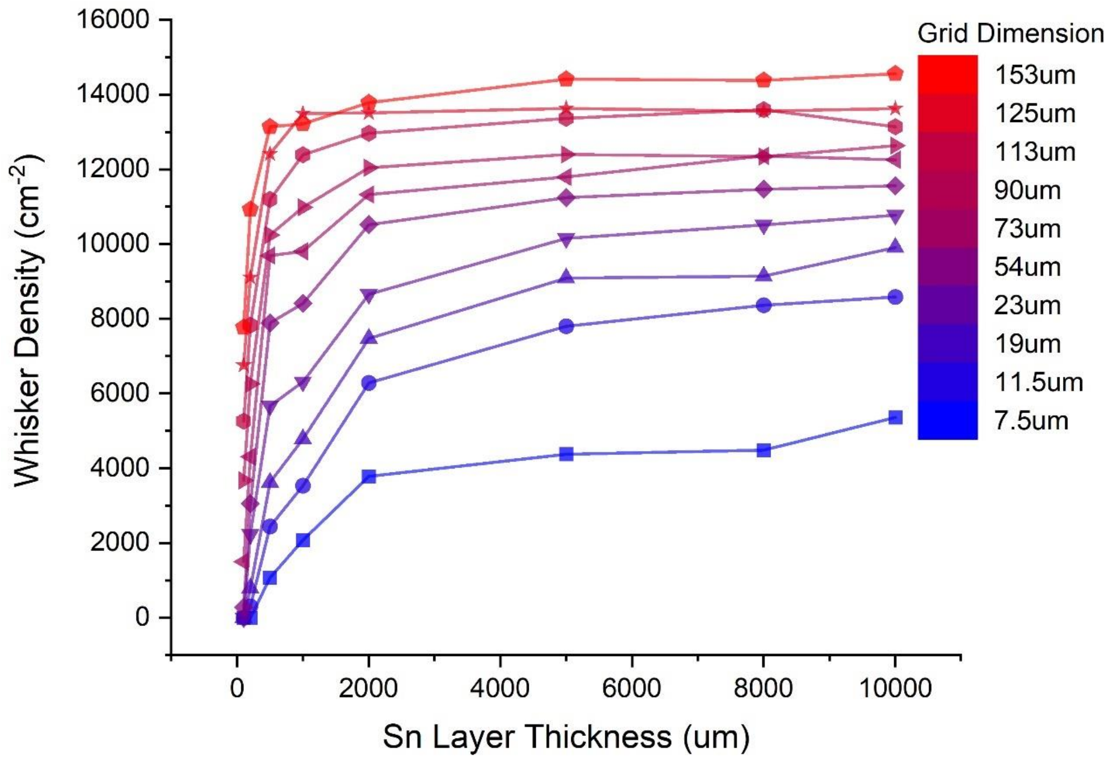

Figure 22 Whisker density v.s. Sn deposition thickness regarding different areal dimensions The whisker densities increase at low thicknesses (<0.2um), and become stable on thicker ones (>0.2um), which applies to all the areal dimensions tested. The governing effect of thickness is weaker than areal dimension, and the maximum thresholds are much easier to reach.

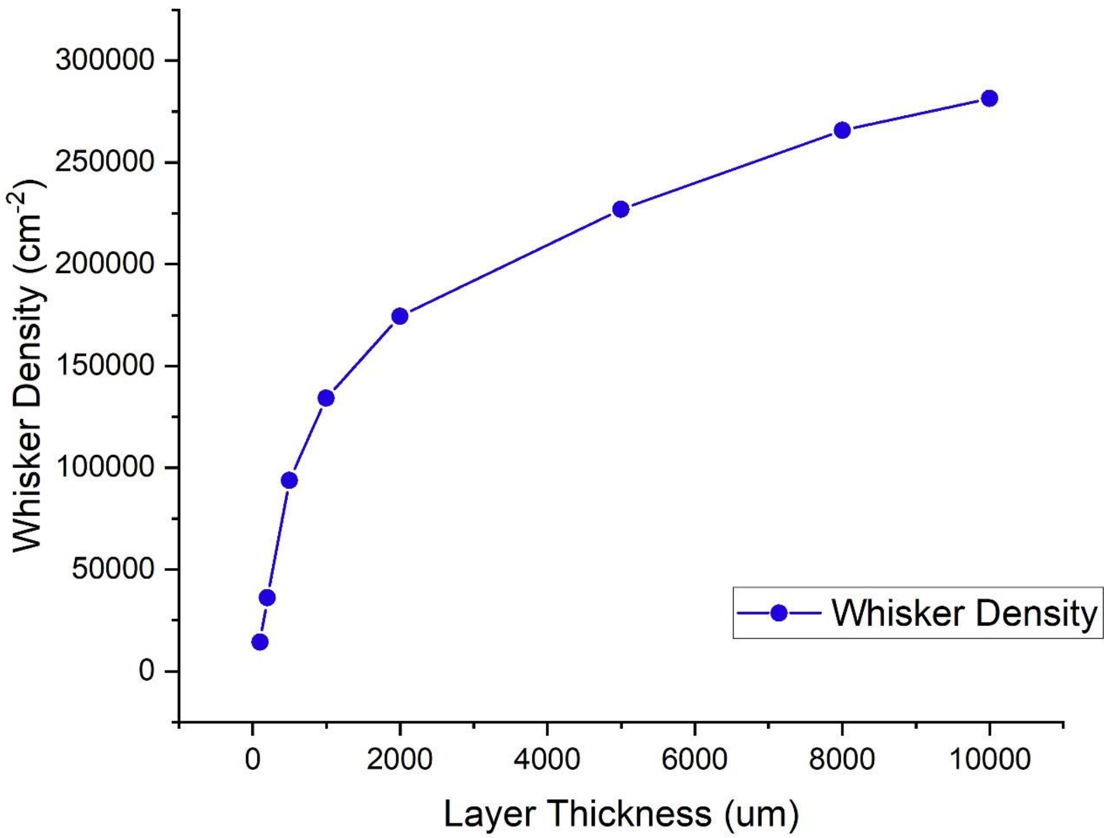

Figure 23 Whisker densities incubated from the control group where depositions are not confined during sputtering (can be treated as 1cm areal dimension). With same incubation methods, the unconfined specimens produce whiskers at least 6x to confined ones.

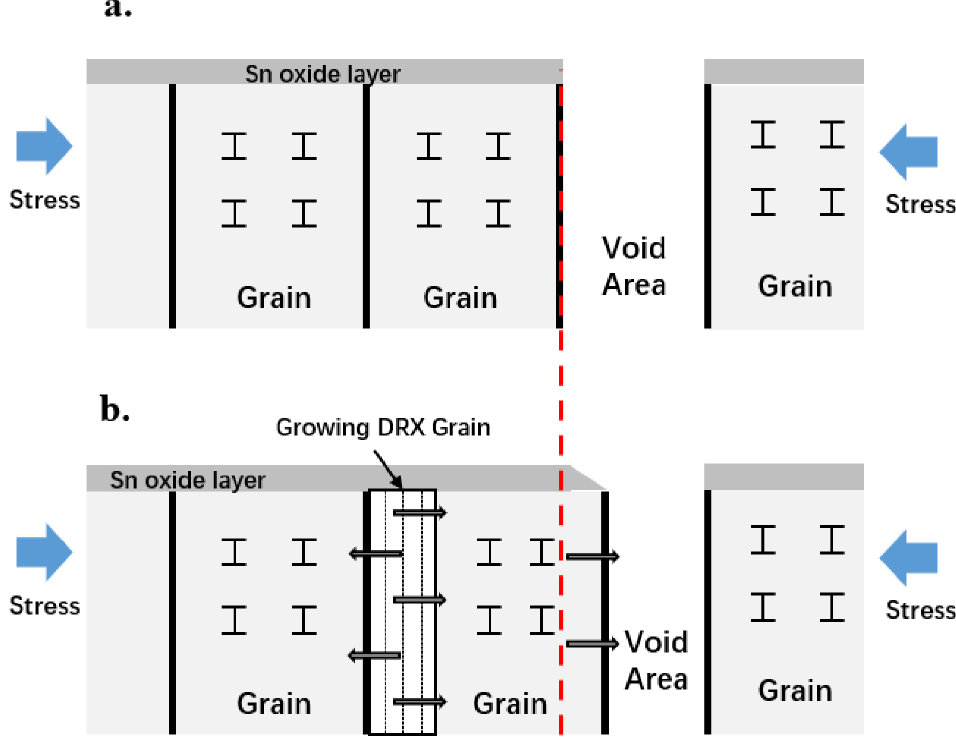

Figure 24 Schematic diagrams illustrating the deposition structure creep towards void areas, during which stress and strain are released.

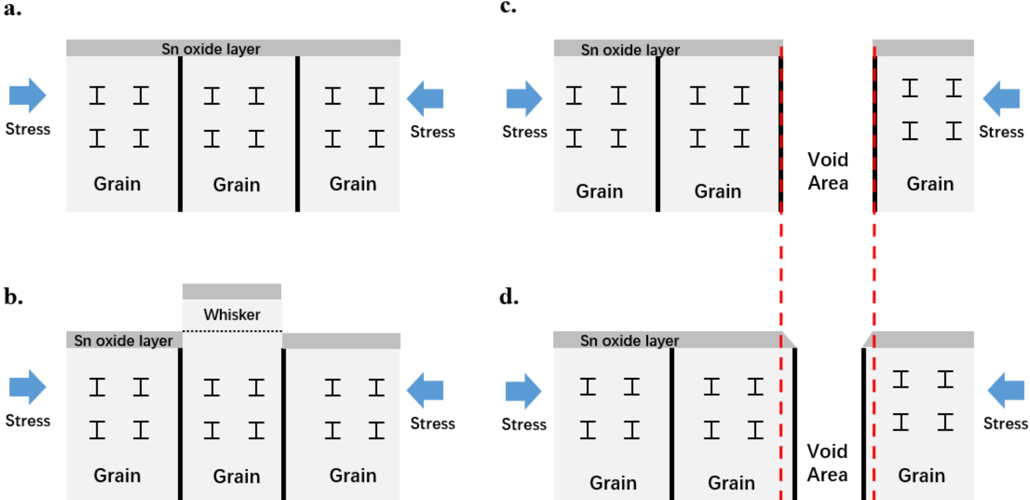

Figure 25 Schematic diagrams illustrating the deposition structure creep towards void areas.

Chapter 5.

Summary of Results

This study is designed to simulate and validate the growth mechanism of Sn whiskers as a result of strain accumulations governed by multiple processes. While it has reached a consensus that stress is the major cause for whisker growth, there are still not an obvious view that which processes are involved in the contribution to whiskering process. During whiskering, multiple variables of material and processes interact to form whiskers, leading to the complexity to develop a clear and comprehensive diagram of whisker growth. With controlled laboratory experiments, a much optimum system is designed in studying whisker production. One of the goals of this study comes from this, which tries to establish a comprehensive strain-driven whisker formation model with controllable inputs to the model. During the establishment of the model, several key factors of whisker growth are involved in, and help to clarify some of the key mechanisms. In the meantime, many previous investigations of whiskers have confirmed the existences of multiple uncontrolled variables during whiskering, which are introduced by thermal expansion, material diffusion, electroplating, etc. Besides, industrial, and/or archival specimens were usually incubated with very unpredictable periods, varying from days to years. In this study, all the experiments are conducted with reliable methods for whisker incubation within reasonable periods (34 days) through magnetron sputtering techniques rather than ordinary evaporation or electrochemical deposition. With the deposition of

magnetron sputtering, we introduce intrinsic compressive film stress into deposition films with certain background Argon pressure. Besides, with deposition conducted in vacuum, the influence of a portion of uncontrolled variables which play roles during electroplating can be eliminated. With such techniques and deposition method, we conduct this study, and the following achievements are reached:

1) Since it has been reported that unpredictable morphology beneath the deposition surface surrounding the whisker root, different locations on films are deposited with different possibility for crystal eruption as whiskers. The range around one location with whisker erupted are named as a "whisker site". As a result, one whisker is observed formed in one whisker site, and the ranges of whisker sites are determined by the distance between neighboring whiskers. Based on multiple previous research and studies on whisker model establishment, we propose an analytic model describing the whisker formation process as a result of accumulation of deposition material within a certain range. With the assumption that the feedstock and material diffusion within the site are contributed to the centered whisker, we can quantitatively express the diffusion rate, the elastic and plastic stress at any locations within the whisker site with determined deposition and environmental parameters initiated from the moment right after the completion of film deposition. Processes within the whisker site can then be transferred into strain, which accumulated with time passing (the incubation period), resulting the formation of the whisker in the center

2) Whiskers are assumed as a strain-relieve mechanism to the deposition film.

With quantitative expression of strain, we can then calculate the material displacement at any location within the whisker site. The whisker, as a result of strain relief, is contributed by such displacement. We then estimate the whisker volume by summing the volume of displacement. Further, with the observed grain size, and the report that radius of needle whisker was same to the grain size in most cases, we can then achieve the length of the whisker. Given the unity of the whisker site in this model, such length is treated as the average length of all the whiskers grown from the deposition surface within the certain incubation period.

3) We collect experimental data from numerous previous reports and studies with certain incubation environmental parameters, including temperature, air pressure, incubation period and methods. We apply these data into the model to calibrate the bias parameter in the model to reach an agreement between them. With the parameters adjusted to $1.86 \times 10^{-3} mm/mm$, a good R^2 is achieved, with value equal to 0.80.

4) Multiple constants about the material and deposition process have been involved in the strain calculation. We conduct sensitivity tests on all the constants related to material (Sn/Si combination) and diffusion process, respectively, and find 3 constants which the model present obvious sensitivity to. The sensitivity tests also reach suggested values to these constants to maintain a stable performance of the model.

5) A number of studies have emphasized the great influence of DRX process to in-layer stress, which also largely governs the whiskering process. Multiple researchers have proven the direct relationship between DRX and whisker formation.

However, due to the lack of enough quantitative theory describing the occurrence as well as the amount of stress DRX can introduce to the film, previous models failed to involve DRX process. In this study, by assuming the bias parameter, the strain of DRX process is successfully involved in the model we proposed. Further, we gather most of the methods from previous studies on the critical strain, which is the threshold strain for DRX initiation. Combining the calculation of critical strain, we finally reach an estimated value of DRX strain in the films, which is estimated as $1.88 \times 10^{-3} mm/mm$ or $2.32 \times 10^{-3} mm/mm$. Such values take large portions in the measured strain beneath the deposition film, implying the important role of DRX process plays in the whiskering process.

6) The material diffusion occurring beneath the deposition surface plays an important role contributing to whisker growth. When long-range diffusion is ceased by confining Sn layers into small dimensional squares and circles by TEM grids during depositing, materials diffusion flux at spacings between neighboring depositions is reduced to less than 10^{-12} cm^2/s. With diffusion suppressed, whisker growth is observed largely alleviated comparing to the controlling group where Sn depositions are not limited.

7) The retarding effect of limitations to Sn layers has been revealed and theoretically validated. The whisker densities presented linearity to limited dimensions during 23um to 153um in all the three incubation methods applied, with slopes varying from approaching 0 (room temperature) to ~$6.1*10^5$ um^{-4} (thermal cycling). For the largest limited areas applied in this experiment, whisker densities

were reduced by 44.2% at least, and no whiskers were observed on Sn layers smaller than 7.5 um x 7.5 um. Among all the three incubation methods, thermal cycling had been proven as the most accelerating methods for whisker growth due to the cyclic thermal expansion stress were induced into deposition layers, resulting in continuous dislocations and pinning.

8) The existence of whisker incubation threshold in limited areal dimensions have been observed, below which the growth of whisker is completed ceased. The thresholds varied with incubation methods, with 11.5um in room temperature, 7.5um in annealing, and 4um in thermal cycling. We speculated it for the induced strain rate which governs the threshold. The application of areal limitation introduced spacings onto Sn layers with different density. Given that the spacings provided a new method for stress releasing, the density of spacings directly affect the stress relief capability of spacings. When the stress amount needed to be released from layers exceeded the capability of spacings, the exceeding part required another method to release, which was whiskering process. In ordinary cases, the relief effect of spacings could be ignored (the deposition was too large for spacing to release stress) or too small to take place of whiskering, the formation of whiskers cannot be prevented; however, when such density was large enough to release most of the stress within the deposition, the formation of whiskers would be restrained.

9) The morphological characteristics between needle-like and hillock whiskers were oriented from the different pinning strategies around the grain where whiskers were produced. Correlation has been observed between whisker morphology and

limited deposition dimensions. For larger dimensions (>54um), a large portion of whiskers were needle-like associated with hillocks; with dimensions getting smaller (<54um), the ratio of needle whisker over hillock was decreasing. However, even few, needle whiskers were still observed from tiny dimensions smaller than 19um*19um through thermal cycling. Given thermal cycling is usually recognized as an accelerating method for whisker incubation, we speculated that needle whiskers could also form through room temperature incubation method from any size of limited depositions.

10) The DRX mechanism were observed occurring on the surface of limited deposition layers. As a major source of in-layer stress, the DRX process was not governed significantly by the limited depositions in both the feedstock and the stress relief effect of spacings. Among all the three hierarchal requirements, two were validated during the deposition-limitation experiment, while the other one was not observed.

11) The retarding effect of whisker incubating ability in deposition limitation is contributed by diffusion isolation effect. Without the existence of Sn deposition in spacings between neighboring Sn depositions, the diffusivity of free Sn atoms was largely reduced to lower than 1.84×10^{-66} cm^2/sec, illustrating that Sn atoms diffusion was confined within the depositing areas.

12) In the other experiment where both deposition horizontal dimension and thickness were varying, deposition volume was varying from 11.45 um^3 to 23,409 um^3. Observed whisker densities were increasing rapidly when deposition volume was

below 2,000 um^3, at then approaching to certain maximum limit of ~16000 whiskers/cm^{-2} at volumes over 2,000 um^3. The whisker density illustrates a logarithm curve to the deposition volume. All the data observed in the experiment fall in the 95% prediction band of the fitting curve, implying enough confidence of this result.

13) Similar linear whisker growing schemes were observed that densities were linear retarding during the limited dimensions from 23um to 153um for different fixed thickness, respectively. All the R^2 values of each linear fitting lines of various thicknesses were over 0.94, indicating concrete linearity when limited dimensions varying. The slopes of whisker density were large on thin depositions, and small on thick ones. Sudden transitions at dimensions below 23um were observed from all the tested thicknesses.

14) Zero whisker densities were only observed on extremely thin and small limited depositions. Such phenomenon implied a threshold of ~2.25um^3 in deposition volume which could cease the whisker growth, which possibly provides enough volume space for the occurrence of nucleation process.

15) Thicknesses of depositions governed the whisker growth differently from grid dimensions. The maximum whisker production ability of depositions increases with the grid dimensions but not directly governed by thickness. Thinner depositions (below 0.2um) effectively decrease the whisker production, while thicker ones (above 0.2um) did not.

16) The density of needle whiskers presented strong linearity to grid dimensions rather than to depositions thickness. With dimensions of deposition limited below

23um, very few needle whiskers were incubated, while the density of them increased clearly with the limited dimensions getting larger up to 153um.

17) Similarly, a possible threshold of whisker length might exist in the deposition production. The maximum lengths of whiskers were observed and collected from specimens with different deposition parameters, which illustrated no clear correlation to thickness or grid dimensions.

Future Works

Though many works and studies have been made by researchers for decades, the growth mechanism of whiskers are still in vague. In this study, we proposed a new mechanism model which contributed whisker growth to the stress accumulation and relief process, established and calibrated algorithm for whisker predictions, trying to understand and illustrate the spontaneous whisker growth from metal surface. Basing on this mechanism, we applied areal limitation and volume limitation of depositions as stress-relief methods to study its suppression effect of whiskers, and gathered satisfying results. However, there are still multiple points which can improve the accuracy of whisker producing mechanism and helps minimize the threaten of them effectively in commercial applications. Multiple factors involved in the strain-accumulated model proposed in this study remain to be discussed, including the DRX process, the effect of erosion and corrosion due to the humidity, etc.

1) The DRX process has been proven as another major source of in-layer stress. In this study, the strain (stress) of the DRX process is primarily estimated,

which is comparable to thermal expansion strain of incubation environment. However, we cannot trace such strain back to statistics of the DRX process, such as the occurrence of the DRX process, the estimated expansion ratio of DRX grain, the micro-structure change of DRX grains during expansion process, etc. Most of them are still not in vague, and certain experiments are required to be conducted to measure or estimate them to acquire accurate parameters. With these statistics of the DRX process, we can improve the accuracy of the model and understand the growing mechanism of whiskering problem further.

2) The corrosion occurring on the surface of depositions can largely affect the whiskering process in both density and length. Multiple factors govern the corrosion process to minimize the incubation rate of corrosion-related whiskers, including choice of substrate-deposition materials combination, the deposition and incubation conditions, etc. The humidity plays an important role controlling the corrosion process, and studies have illustrated that calibrated incubation conditions (the humidity is the majority) can effectively reduce the threaten of whiskers to electronical components. However, in practical applications, the humidity can hardly be controlled within a suitable variation. Therefore, we need to further understand the relations between humidity variation and whiskering problem.

3) The suppression effect of deposition volume limitation requires application. We have observed concrete decrease in whisker production from limited

depositions, which can even be reduced to 0 with deposition volume limited below the threshold of 2.25um^3. However, comparing to the conventional deposition thickness of 2um to 300um adapted in commercial application, the accuracy of areal dimension needs to be limited below 1um^2, which requires much cost to achieved. A suitable balance between whisker suppressing effect of volume limitation and cost is required for commercial applications. As a result, further study should be conducted to depict the cost-suppression curve, associated with the commercial cost of different deposition methods and parameters, equipment and wastage cost, etc. With such curves and statistics, an efficient point would be achieved where suitable cost is consumed to reach maximum reliability.

4) Multiple methods have been applied for deposition, including metal evaporation, sputtering, electron plating, etc. Numerous studies concerning whiskering experiments applied different deposition methods, where similar and same incubation methods but different deposition methods would reach distinguished experimental results. We speculated that the deposition methods would govern the micro-structure of metal materials beneath the deposition surface, which would affect the atom expansion, multiple physical constants including but not limited to Young's Modules and conductivity, the in-layer stress and strain, etc. These influenced processes would finally govern the whisker production of such depositions. Further experiments could be conducted studying the differences between these deposition methods, and

might be helpful to reach the suitable balance mentioned in (3) associated with certain deposition volume limitation.

5) The DRX process was reported initialized by the strain exceeding the critical strain as a threshold. This critical strain is governed by several parameters, including the strain rate, environmental temperature, the initial grain size, etc., most of which are controllable: The initial grain size is adjustable from 0.6um to 3um for different specimen temperature during sputtering; the environmental temperature can be handled during incubation; the strain rate can be adjusted by the applied strain. With related parameters being calibrated, the DRX process, which is now recognized as one of the major source to whiskers, can be suppressed to occurring at a low rate. We can conduct a series of experiments on these parameters to establish the correlation between whiskering problems and these environmental conditions through governing the DRX process.